

Aus der Klinik für Zahn-, Mund- und Kiefergesundheit
der Universität Würzburg
Lehrstuhl für Funktionswerkstoffe der Medizin und der Zahnheilkunde
Lehrstuhlinhaber: Prof. Dr. rer. nat. Jürgen Groll

**Fabrication and characterization of NCO-sP(EO-stat-PO)-
crosslinked and functionalized electrospun gelatin scaffolds for
tissue engineering applications**

Inauguraldissertation
zur Erlangung der Doktorwürde der Medizinischen Fakultät
der Julius-Maximilians-Universität Würzburg

vorgelegt von
Christina Wiesbeck
aus Weiden in der Oberpfalz

Würzburg, Februar 2019

Referent: Prof. Dr. Jürgen Groll

Korreferent: Prof. Dr. Dr. Alexander Kübler

Dekan: Prof. Dr. Matthias Frosch

Tag der mündlichen Prüfung: 14. Oktober 2019

Die Promovendin ist Zahnärztin

Abbreviations

DCM	Dichloromethane
DMF	Dimethylformamide
DMSO	Dimethyl sulfoxide
ECM	Extracellular matrix
EDC	1-ethyl-3-(3-dimethyl-aminopropyl)-1-carbodiimide hydrochloride
GA	Glutaraldehyde
GEN	Genipin
Gt	Gelatin
HA	Hyaluronic acid
HDI	Hexamethylene diisocyanate
HFIP	Hexafluoroisopropanol, Hexafluoro-2-propanol
IPDI	Isophorone diisocyanate
NCO-sP(EO-stat-PO)	star-shaped NCO-end-functionalized statistical copolymer of ethylene oxide and propylene oxide
NHS	N-hydroxysuccinimide
NTA	Ni ²⁺ -nitrilacetic acid
PCL	Polycaprolactone
PDO	Polydioxanone
PEG	Poly(ethylene glycol)
PEO	Poly(ethylene oxide)
PGA	Poly(glycolic acid)
pI	Isoelectric point
PLLA	Poly(L-lactic-acid)
PPG	Poly(propylene glycol)
PPO	Poly(propylene oxide)
RGD	Arginine – glycine – aspartate peptide sequence
TE	Tissue engineering
TFA	Trifluoroacetic acid
TFE	2,2,2-trifluoroethanol
THF	Tetrahydrofuran

Table of contents

1. Introduction	1
2. Theoretical background	4
2.1 Electrospun nanofibers in tissue engineering.....	4
2.1.1 Principle and process of electrospinning	4
2.1.2 Electrospun TE materials.....	6
2.2 Gelatin in TE	9
2.2.1 Chemical and biological characteristics	9
2.2.2 Gelatin in tissue engineering	10
2.2.3 Gelatin crosslinking.....	11
2.3 Material functionalization via NCO-sP(EO-stat-PO)	14
2.3.1 Chemical structure of NCO-sP(EO-stat-PO).....	14
2.3.2 Functional properties of NCO-sP(EO-stat-PO)	15
3. Materials and methods.....	18
3.1 Materials and chemicals.....	18
3.2 Fiber fabrication	19
3.2.1 Spinning solutions.....	19
3.2.2 Solution Electrospinning	19
3.3 Fiber characterization.....	22
3.3.1 Scanning electron microscopy (SEM).....	22
3.3.2 Energy dispersive X-ray spectroscopy (EDX)	23
3.3.3 Image analysis.....	23
3.3.4 Water incubation and contact angle measurement.....	24
3.3.5 Tensile test	26
3.3.6 Fourier transform infrared spectroscopy (FT-IR)	28
3.3.7 Cell culture.....	29

4. Results.....	30
4.1 Fiber fabrication	30
4.1.1 Solvent choice	30
4.1.2 Spinning parameters.....	32
4.1.3 Mixing time	32
4.2 Fiber characterization	33
4.2.1 Fiber morphology.....	33
4.2.2 Hydrophilicity	38
4.2.3 Tensile properties	39
4.2.4 Weight loss	42
4.2.5 Fiber composition and stability.....	44
4.2.6 Cytocompatibility.....	49
5. Discussion	52
5.1 Fiber fabrication: impact of process and solution parameters	53
5.2 Fiber characterization	55
5.2.1 Fiber morphology: impact of polymer concentration and ratio	55
5.2.2 Fiber stability: tensile strength and water resistance	57
5.2.3 Fiber composition: chemical structure and reaction.....	60
5.2.4 Fiber biocompatibility: hydrophilicity and cell viability	61
6. Summary and outlook.....	64
7. References	66
8. Appendix.....	80

List of figures

Figure 1:	Schematic diagram of electrospinning apparatus setup in a) vertical and b) horizontal configuration. Reprinted from Bhardwaj & Kundu (2010) [13], with permission from Elsevier.	5
Figure 2:	Basic chemical structure of gelatin. Reprinted from Elzoghby (2013) [55], with permission from Elsevier.....	9
Figure 3:	Scheme of chemical structure and crosslinking reaction of the star polymer system. Partially reprinted from Heyes et al. (2007) [97], with permission from The Royal Society of Chemistry.	14
Figure 4:	Schematic display of surface grafting of a,b) star-shaped PEO, c) linear PEO, and d) intermolecularly crosslinked six-arm PEO. Reprinted from Gasteier et al. (2007) [103], with permission from Wiley.	15
Figure 5:	Collector drum covered with aluminum foil ready prepared for electrospinning of a NCO-sP(EO-stat-PO)/Gt mesh sheet.	20
Figure 6:	Image processing in FIJI. a) Measurement of fiber diameters. b) Determination of electrospun mesh thickness for later tensile testing.....	24
Figure 7:	a) Customized template for cardboard frame used for tensile testing of electrospun fiber scaffolds; b) cardboard frame with fixated electrospun fiber scaffold specimen; c) experimental setup for uniaxial tensile test with pulling jaws and 100N load cell; d) specimen fixated to cardboard frame with double sided tape, pulling jaws holding the frame, which is cut at the sides shortly before testing.	27
Figure 8:	Stress-strain curve of an electrospun NCO-sP(EO-stat-PO)/Gt scaffold with gradient triangle (schematic diagram). Young's moduli were calculated from the linear section of the curve.	28
Figure 9:	Fibers electrospun from a 5% Gt solution in a) DMSO and b) HFIP; c) electrospun hybrid fibers from a solution of 1:2 ratio of NCO-sP(EO-stat-PO)/Gt. Gt was dissolved in HFIP, NCO-sP(EO-stat-PO) in DMSO.....	31
Figure 10:	Mean diameter of fibers electrospun from different gelatin concentrations, determined via SEM image processing with FIJI software.	33
Figure 11:	Fibers electrospun from different concentrations of gelatin (w/v). a) 5%, b) 7.5%, c) 10%, d) 12.5%. A higher concentration (15%) of gelatin solution was not spinnable due to high solution viscosity.	34
Figure 12:	SEM images of electrospun pure Gt fibers and hybrid NCO-sP(EO-stat-PO)/Gt fibers of varying mixing ratios, relative fiber diameter distribution, mean fiber diameter, and cross section shape of fibers. o = rounded fiber shape, II = ribbon shape.....	37

Figure 13: a) Contact angles of all electrospun NCO-sP(EO-stat-PO)/Gt meshes and pure gelatin mesh (5 %); b) images and contact angles (θ) for hybrid ratios selected for further experiments.....	38
Figure 14: SEM measured average cross section of NCO-sP(EO-stat-PO)/Gt meshes utilized for tensile testing.....	40
Figure 15: Stress-strain response for electrospun meshes of selected NCO-sP(EO-stat-PO)/Gt ratios under uniaxial tension.	40
Figure 16: Tensile testing of electrospun hybrid meshes from different NCO-sP(EO-stat-PO)/Gt ratios. a) Ultimate tensile strength (UTS) measured as the maximum tensile stress a scaffold can withstand before breaking, represented in the highest point of the stress-strain curve; b) strain at UTS, describing the level of extension before breaking; c) Young's moduli calculated as the quotient of UTS and strain, describing the material's resistance to elastic deformation.....	41
Figure 17: Relative weight loss after 3 days of water incubation for selected NCO-sP(EO-stat-PO)/Gt ratios.....	42
Figure 18: Selected NCO-sP(EO-stat-PO)/Gt ratios after three days of incubation in H ₂ O and 1xPBS. Fiber stability seems to increase with rising NCO-sP(EO-stat-PO) content and was observed to be much higher after incubation in PBS than in water.	43
Figure 19: FT-IR spectra of pure NCO-sP(EO-stat-PO) (marked as "sPEG"), pure gelatin, and electrospun hybrid meshes of three selected NCO-sP(EO-stat-PO)/Gt ratios.....	45
Figure 20: FT-IR spectra of electrospun hybrid meshes of three selected NCO-sP(EO-stat-PO)/Gt ratios in dry state and after water incubation.	45
Figure 21: EDX spectra for assessment of water stability for NCO-sP(EO-stat-PO)/Gt ratio 3:2, 1:1, and 1:3 before and after water incubation for three days. Additionally the spectra for pure gelatin and NCO-sP(EO-stat-PO) are given.	46
Figure 22: Changes in element contents for NCO-sP(EO-stat-PO)/Gt ratios 3:2, 1:1, and 1:3 before and after three day water incubation.	47
Figure 23: RAW 264.7 cell viability on electrospun hybrid meshes as well as on pure gelatin crosslinked with glutaraldehyde (5%Gt(GA)) and control on tissue culture plate. Values were measured via WST-1 (testing the mitochondrial succinate dehydrogenase of viable cells) and PicoGreen DNA quantification. Due to a loss of material, PicoGreen could not be determined for day 7.....	50
Figure 24: SEM images of RAW 264.7 cells on electrospun meshes after 3 days of cell culture in close-up image and overview. a) control seeding on glass cover slips, b) 5% Gt crosslinked with GA, c) NCO-sP(EO-stat-PO)/Gt 1:3, d) NCO-sP(EO-stat-PO)/Gt 1:1, e) NCO-sP(EO-stat-PO)/Gt 3:2.	51
Figure 25: SEM images of RAW 264.7 cells after 7 days of cell culture on control cover glass, NCO-sP(EO-stat-PO)/Gt 1:1, and NCO-sP(EO-stat-PO)/Gt 3:2. Other ratios were contaminated.	51

1. Introduction

“A human embryo in its first eight weeks of life undergoes an extraordinary transformation from a single cell to a 3 cm long fetus with a beating heart, gut, nervous system, and limbs with fingers and toes. This progression involves massive growth, physical folds and twists, and myriad cellular and molecular events of breathtaking complexity; yet it is the ultimate goal of tissue engineering (TE) to recreate some of these processes in microcosm, to replace and regenerate lost tissue.” Place et al. 2009 [1]

As a response to exploding numbers of population and increasing life expectancy, the field of TE has emerged since the 1990s to meet this need for rehabilitation of failed organs and tissues. Researchers have pursued various attempts with much effort to produce replacement tissues by guided cell culture, hoping to find an addition and a possible future alternative to classical clinical treatments, i.e. autografts, allografts and xenografts. The final goal of TE products is to tackle current therapeutical issues such as lack of organ donors, rejection reactions, or poor biocompatibility [2]. As opposed to conventional transplants new tissue constructs aim to remodel natural tissue accurately customized to individual physiological needs by using a combination of mechanically supporting scaffolds, tissue-specific cells, and biochemical cues such as growth factors [3] as well as mechanical stimuli such as a certain material topography [4]. Additionally, the incorporation of bioactive molecules, such as drug delivery agents has gained importance [5].

A key factor to physiological tissue replacement is the understanding and imitation of extracellular matrix (ECM), the three-dimensional macromolecular network surrounding and embedding natural cells in all tissues and organs. It is built up by collagens, proteoglycans, glycosaminoglycans, fibronectin and numerous other glycoproteins. Matrix components adhere to each other and the resident cells via binding sites and cell adhesion receptors. Cellular functions, such as growth, migration, differentiation and survival are transmitted and regulated by ECM. A number of major pathological conditions, among them atherosclerosis and cancer, are associated with the degeneration of ECM elements [6]. This illustrates why the utilization of biomaterials as mere

architectural support for tissue growth and healing falls short. In order to mimic natural ECM, biofunctionalization is equally important to the fabrication of successful scaffolds as their mechanical properties.

The regeneration or neoformation of functional tissues further requires environmental conditions similar to those of native tissues to obtain the desired cell reactions. Biocompatibility of a scaffold, in the sense that no living tissue is negatively affected by the material, is fundamental. This also includes that the degradation of a biomaterial must occur within the same time frame of wound healing or tissue regeneration. Further, a complete degeneration of the scaffold without toxic residuals is obligatory [2]. For commercial success of tissue engineered materials the importance of cost-effectiveness has to be emphasized; this comes along with a need for simple techniques which are easy to use [1].

A number of synthetic and natural polymers have been used for tissue engineered scaffolds [7], but natural polymers offer distinct advantages such as chemical cues, hydrophilicity and degradability. In comparison to synthetic ones they induce natural cellular reactions, for example via contained integrins with binding affinity receptors on cellular surfaces. The natural polymer gelatin has a long tradition as material in TE applications. As a derivative of collagen gelatin is an attractive base material for TE due to its biological origin and similarity to native ECM. Nanofibers electrospun from gelatin display fiber diameters comparable to those found in natural collagen fibers, i.e. between 200 nm and 1 μm [8].

On the downside, most natural polymers, especially in nanofibrous scaffolds, show only poor mechanical properties, degrade rapidly and are more difficult to handle in fabrication processes. Therefore, scaffolds composed of polymer blends are able to bridge the gap by combining favorable properties of both polymer types, i.e. biocompatibility as well as strength and durability. Especially the construction of an ECM imitation can be enabled by manipulating natural polymers by addition of synthetics [9].

For ECM mimicry via fiber fabrication the technique of electrospinning has gained large attraction in the last 15 years. Originally conceived for the textile

industry, the method now offers a simple, versatile and economical way to produce fibers from all sorts of natural and synthetic polymers [10].

Accordingly, the aim of this study was the fabrication of ECM analog electrospun gelatin-blend fibers functionalized by adding different concentrations of an end-functionalized six-arm star-shaped polymer (NCO-sP(EO-stat-PO)) to the gelatin spinning solution, as well as the characterization and testing of the obtained scaffolds for applicability in TE purposes.

In the first part of the work a protocol for gelatin fiber fabrication from a solution in hexafluoroisopropanol (HFIP) is established. The obtained gelatin solutions are gradually mixed with different concentrations of NCO-sP(EO-stat-PO), and fibers of different ratios of NCO-sP(EO-stat-PO) to gelatin are electrospun. The second part deals with the characterization of the obtain scaffolds in dry state and after incubation in water and phosphate buffered saline (PBS). SEM imaging served as the main visualization method. By analyzing morphology and diameter fiber properties were assessed for further mechanical and biological testing. Water stability and hydrophilicity were examined via weight loss experiments and contact angle measurements. Changes in elemental composition were attempted to assess by EDX and FT-IR analyses. Uniaxial tensile tests were performed with dry scaffolds. Biocompatibility was studied in cell culture experiments with murine RAW 264.7 macrophages.

2. Theoretical background

2.1 Electrospun nanofibers in tissue engineering

2.1.1 Principle and process of electrospinning

Electrospinning is an electrostatic technique for producing micro- to nanosize fibers from all kinds of polymers. By creating randomly oriented fibers it is possible to mimic the geometrical composition of the natural cell environment.

Discovered in 1878 by Lord Rayleigh [11], the process was patented in the 1930s for the production of textile yarns [12]. Only since the 1990s and especially during the last years this technique has gained further attention thanks to developments in nanoscience and TE. Today it is utilized in a broad range of applications such as TE scaffolds, wound healing, drug delivery, immobilization of enzymes, membranes in biosensors, protective clothing, cosmetics, filtration and many more [13].

A typical electrospinning setup contains three elements: a high voltage power supply, a syringe pump, and a grounded collector [14]. For classic solution electrospinning, a polymer is dissolved and placed into a syringe fitted with a blunt tip needle (Figure 1). An electrical field is established between the needle and a grounded collector or target. The pumped solution builds up a pendant drop at the needle tip, when the liquid's surface tension is overcome by the field strength, a jet develops from the drop which is drawn towards the collector. Close to the needle the jet is linear but undergoes bending instabilities with increasing distance from the orifice. During the flight towards the collector the solvent evaporates from the solution and solid fibers are precipitated in random orientation on the collector, forming a three-dimensional network [15].

A number of alternative procedures have been developed, among them melt electrospinning, coaxial, needleless, side-by-side and wet electrospinning [16].

Fibers can be fabricated from both synthetic polymers, like poly(glycolic acid) (PGA), poly(lactic acid) (PLLA), poly(ethylene oxide) (PEO), polydioxanone (PDO), polycaprolactone (PCL) etc., and natural polymers (e.g. collagen, gelatin, silk fibroin, chitosan, alginate, hyaluronic acid (HA) and several others) as well as composites and ceramics. Blending of natural polymers and synthetic

2. Theoretical background

copolymers can enhance fiber properties such as thermal stability, mechanical strength or function as a biochemical barrier. For example in TE, hydrophobic polyesters usually show good structural properties but lack cell affinity. Co-electrospinning synthetic polymers with hydrophilic natural polymers can increase their biocompatibility [17].

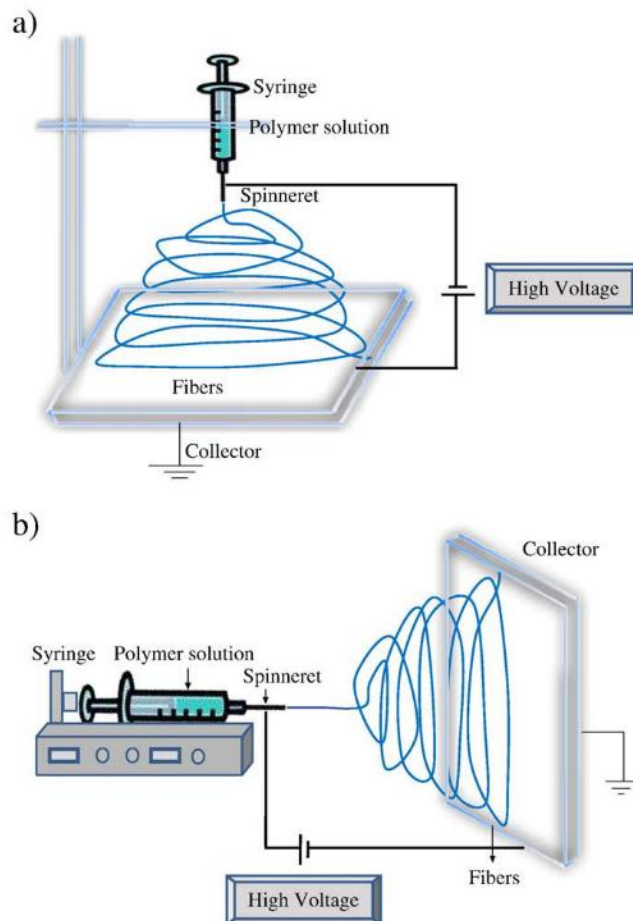


Figure 1: Schematic diagram of electrospinning apparatus setup in a) vertical and b) horizontal configuration. Reprinted from Bhardwaj & Kundu (2010) [13], with permission from Elsevier.

The process of electrospinning is governed by a broad number of parameters which have been classified by Doshi & Reneker [18, 17] under solution properties, controlled variables, and ambient parameters. Factors resulting from the polymer solution are viscosity, conductivity, surface tension, polymer molecular weight, polymer concentration, dipole moment, and dielectric constant. Effects from solution properties can be hard to isolate from each

other, as changing one parameter often affects others (e.g. changing molecular weight will also change the solution viscosity) [18]. Controlled variables include electric field strength, flow rate, needle tip to collector distance, needle tip design, needle and syringe diameter, as well as collector composition and geometry [19]. These factors can be manipulated individually to tune fiber morphology. Ambient parameters comprise temperature, humidity, and air velocity; their controllability is limited.

The variation of parameters significantly affects fiber morphology and properties, which makes the technique of electrospinning attractive for use in all sorts of applications with specific desired features. It shows great versatility as not only many parameters can be varied, but also a great variety of polymers and other materials can be utilized. Further, the process is easy to learn and establishment of the laboratory setup is simple. Also its economic affordability is advantageous. Disadvantages may result from a considerably small pore size of nanofibrous scaffolds often resulting in poor cellular infiltration and thus failing to imitate the native 3D tissue environment [13]. But efforts to overcome these porosity limitations have been made lately by design improvements through approaches like multilayering and combined application of laser ablation and mineralization [20, 14].

2.1.2 Electrospun TE materials

The highest priority in tissue engineering is the regeneration or replacement of lost tissues by reiteration of two components: native cells and their supporting environment, the extracellular matrix (ECM). Electrospinning can provide controllable fibrous structures of various compositions, dimensions and architectures [21]. The technique is naturally suitable for ECM mimicry as typical fiber diameters vary between 80 and 1500 nm, comprising the size range of natural ECM fibers (50 – 500 nm) [22]. Electrospun fibrous meshes display a very high surface-to-volume ratio and therefore offer a high porosity and active interface [23]. Both fiber diameter and pore space can be adjusted by manipulation of process parameters, a crucial potential for cellular infiltration into scaffolds. Creating a three-dimensional fiber construct provides

environments for cellular adhesion, migration, proliferation and differentiation [24]. Moreover, the orientation of fibers is tunable thanks to variation of collector compositions and geometries [25]. Mechanical but also electrostatic or magnetic fiber alignment is advantageous in mimicking specific tissues with perpendicular oriented fibers, e.g. cardiac or tendon tissue [26-28]. This affects mechanical properties on the one hand, but also allows control of cellular behavior, as it can be used to guide cellular adhesion, growth and alignment towards a desired direction. For example, nanotopographical cues created by electrospun fiber alignment have been shown to influence the differentiation of human neural crest stem cells [29]. Apart from topography, further biophysical cues, such as material stiffness or hydrophilicity, can be implemented in order to create *in vivo*-like conditions for cells [30]. By adequate composition of the spinning dope, changes in surface chemistry, e.g. suppression of non-specific protein adsorption, have been achieved [31, 32] and biochemical cues such as growth factors, adhesive peptide molecules or drug releasing agents could be included into the fibers [33, 34]. As opposed to this so called *in situ*-functionalization, modification and improvement of fiber properties via post-fabrication treatments have also been applied. These procedures comprise annealing, removal of residual solvent or various ways of surface coatings [35-37] and serve to increase mechanical stability, cytocompatibility, biofunctionalization, e.g. facilitating cell attachment, and hydrophilicity. For specific applications, electrospun fiber mats can be processed further into scaffolds of complex architectures, such as tubular conduits [38] or stacked multilayer arrays [39]. Not least, the choice of polymer determines the properties of an electrospun scaffold, often resulting in diverging effects *in vitro* and *in vivo* [40]. As many as 200 different polymers have been electrospun for various applications [41]. Altogether, electrospun nanofibers are highly convenient for mimicking the structural and functional properties of ECM, their variability makes them a versatile tool for tissue engineering purposes [42, 16]. Successful applications in the biomedical field have been in wound healing, drug delivery, enzyme immobilization, and for various sorts of tissue regeneration or substitution. Above all, skin replacement and wound dressing

2. Theoretical background

are fields with high potential for applying electrospun materials. The technique produces fibrous scaffolds which are highly conducive to cell infiltration and at the same time providing a temporary structural support during cell proliferation [43, 44]. The possibility to manipulate pore size and fiber diameters allows for control of cell infiltration. These properties may be promising for TE skin substitutes, which demand high degrees of cell differentiation and tissue stability. Also, the high surface area of electrospun fiber meshes allows oxygen permeability and prevents fluid accumulation, which makes them appropriate substrates for wound dressings [45]. Another field of application is the replacement of articular cartilage [46]. Various polymers such as collagen or PLLA have been electrospun to a three-dimensional network which has been seeded with chondrocytes in order to achieve *in vitro* chondrogenesis [47, 48]. Scaffolds electrospun from synthetic (PCL, phosphazenes) and natural polymers (silk fibroin, chitosan) have also been applied for bone regeneration and replacement [49, 50]. Further areas for use of electrospun tissue replacements are tendon and ligament [51], dura mater and nerves [52], vascular [53] and urological tissue [54].

2.2 Gelatin in TE

2.2.1 Chemical and biological characteristics

Gelatin (Gt) is a macromolecular protein, obtained from collagen via hydrolysis. It consists of 20 different amino acids and is therefore a polyampholyte, having both polar and non-polar side-chains. For that reason the molecule owns both hydrophobic and hydrophilic regions. Positive charges result from amino acids lysine and arginine, negative ones from glutamic and aspartic acid. Leucine, isoleucine, methionine, and valine convey hydrophobic properties [55]. Depending on the pre-treatment procedure, gelatin is commercially available as either Type A, which corresponds to acidic extraction from collagen, resulting in a higher isoelectric point ($pI = 7-9$); or as Type B of alkaline pre-treatment with a $pI = 4.8-5$.

The basic chemical structure of gelatin is presented in Figure 2. The most relevant functional end groups in the molecule for this study are amine ($R-NH_2$) and alcohol ($R-OH$) groups, which can react with isocyanates forming urea (amines) and urethane (alcohols) bonds (see chapter 2.3).

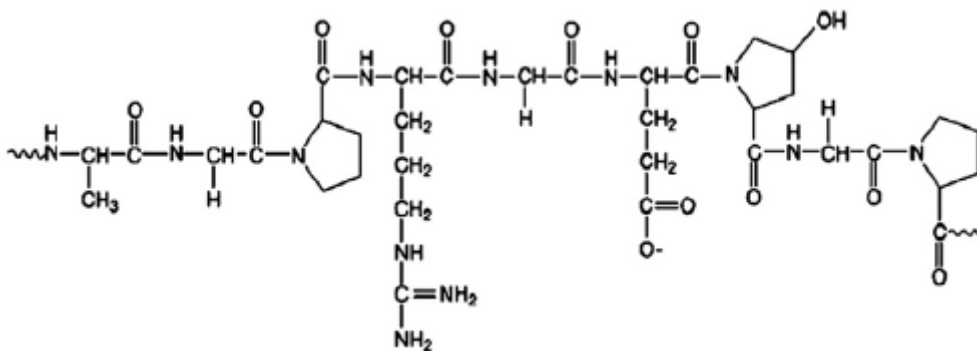


Figure 2: Basic chemical structure of gelatin. Reprinted from Elzoghby (2013) [55], with permission from Elsevier.

During extraction the initial alpha-helix conformation is lost by breaking of intermolecular bonds. However, primary structures of single gelatin molecules are preserved. This is especially important regarding the inherent RGD amino acid sequence (consisting of arginine, glycine, and aspartic acid), which is a recognition sequence for integrin-mediated cell adhesion [56].

From a biological point of view, gelatin as a natural polymer is therefore highly biocompatible. It even enhances infiltration, attachment, spreading and reproduction of cells [9]. In comparison to its source material, gelatin is much less antigenic in *in vivo*-applications than collagen [57]. Due to its natural origin and diverse and accessible functional groups, its physiological degradability is favorable. These properties are strongly directed by the collagen source the gelatin is derived from, as the amino acid composition and sequence differ from one origin to another [57]. For example porcine gelatin does not contain glycine (Gly), whereas it is present in fish scale and bone gelatin [58]. Also the age of an animal or the type of collagen are influencing factors.

2.2.2 Gelatin in tissue engineering

Due to several advantageous features, gelatin is highly interesting for TE purposes. A broad variety of functional end groups make the protein particularly attractive for chemical and biological modification and functionalization. Adding up to its biocompatibility, biodegradability, and low immunogenicity, it is widely available at low costs. Limitations are, above all, its solubility under physical conditions, lack in mechanical stability and a high chemical heterogeneity owing to production circumstances.

Regarding fields of application, gelatin has long been utilized safely in pharmaceuticals, cosmetics, and food products. In clinical use, it was applied in areas like wound dressing and as a carrier material in vaccines [59]. Since the emergence of TE, various new fields of use have opened up. In regenerative medicine, gelatin nanoparticles have been applied for drug release [60] or delivery systems for cytokines and other peptides [61]. It has further been employed as a surface coating in order to overcome material limitations such as inertness of a synthetic polymer [62]. As material porosity is a crucial factor in production of TE materials, gelatin has made a major contribution as a porogen to be leached from a scaffold post-fabrication in order to create larger pore space [63, 64]. As it is derived from natural collagen, gelatin is also an attractive substrate for nanofibrous scaffolds, which have the potential to substitute native ECM [65]. Due to mechanical limitations it has often been applied in blends with

other, mostly synthetic polymers (PLGA [66], PCL [67]), as well as mixed with mineral components, such as hydroxyapatite [68]. Both the gelatin-inherent cell affinity and hydrophilicity on the one hand, and mechanical stability of synthetic polymers on the other hand can provide scaffolds with very attractive properties for TE, due to synergistic effects.

Electrospinning of gelatin is only possible when gelatin adopts a random coil conformation in a solution [69]. This is not the case when gelation occurs at room temperature. Therefore, an aqueous gelatin solution must be heated during the electrospinning process to yield proper fibers [70]. However, Kwak et al. reported that fish gelatin can be spun at room temperature without additional heating due to low proline (Pro) contents [71]. Nevertheless, high surface tension of water solution and non-complete water evaporation make electrospinning of aqueous solutions complicated. Instead, toxic organic solvents such as 2,2,2-trifluoroethanol (TFE), trifluoroacetic acid (TFA), and 1,1,1,3,3,3-hexafluoro-2-propanol (HFIP) have been applied [9], as well as acidic solvents like acetic acid and formic acid aqueous solutions with and without addition of ethanol [72]. Apart from solvent selection, the stabilization of gelatin fiber structures is a crucial issue to deal with. This can be achieved basically by two major methods. One is blending gelatin with other polymers with more favorable mechanical properties, the second one is crosslinking of fibers.

2.2.3 *Gelatin crosslinking*

Despite the described advantages of gelatin as a biomaterial, several limitations restrict its use in biomedical applications. Under physiological conditions electrospun gelatin structures disintegrate at high humidity or in aqueous solutions due to their high surface area and fine structure [73]. This limitation can be overcome by use of crosslinking methods, which interconnect molecules, enhance molecular weight, and generally provide more mechanical stability. Crosslinking can be achieved either by chemical or physical mechanisms [74, 75]; while the chemical method establishes covalent bonds between molecules, physical crosslinking produces non-covalently bonded

ionic, hydrophobic or hydrogen bridge bonds [76]. Regarding processing, the crosslinking agent can be included in the spinning dope during fiber formation (so-called *in situ*-crosslinking) or applied in post-fabrication treatments. One general problem of chemical gelatin crosslinking are morphology modifications with inherent changes in material properties, decreasing the electrospinnability [77]. Furthermore, the toxicity of unreacted crosslinkers has been discussed controversially [78-80].

Despite its possible cytotoxic effect on cells, the most widely used chemical crosslinker for gelatin is glutaraldehyde (GA) vapor; favorable results in preserving fiber diameter and porosity, as well as mechanical stabilization and fibroblast adhesion were achieved [81, 82]. Further, carbodiimides (e.g. EDC), succinimides (e.g. NHS), glyceraldehyde, genipin (GEN), hexamethylene diisocyanate (HDI), and oxidized phenolic compounds have also been applied. EDC and NHS were described to have low cytotoxicity, but this crosslinking method leads to agglutination and therefore an increase in fiber diameter, accompanied by a decrease in porosity [83, 84]. Glyceraldehyde and GEN were considered good crosslinking options, as they yield low toxicity and dissolution stability in cell culture medium at 37 °C [85]. GEN, a naturally occurring crosslinker extracted from gardenia fruits, has been shown to strongly improve Young's modulus and stress at break of electrospun gelatin fibers [86]; further it has been applied successfully in a cost-effective *in situ*-crosslinking approach for gelatin fibers in a coaxial electrospinning setup [87]. HDI was employed as a crosslinker for *in situ*-crosslinked coelectrospun gelatin-methacrylate fibers in studies including investigation of drug release dynamics. It has been shown that the use of HDI enables modifying and preprogramming the release kinetics of gelatin meshes via crosslinking density [88, 89]. Oxidized phenolic compounds of vegetable origin from tannic, gallic, ferulic, and caffeic acids have been successfully employed as crosslinkers for gelatin fibers, with slight increase in fiber diameter and an increase in water stability by 30 % [90].

In applications of physical crosslinking methods, gelatin nanofibers were submitted to dehydrothermal treatment. However, thus crosslinked scaffolds tended to lose their fibrous structure during cell culture and were also shown –

2. Theoretical background

although less toxic – to be less biocompatible than GA crosslinked fibers [81]. Blends of gelatin and other polymers (e.g. poly(acrylic acid) or PEG) have been demonstrated to be effectively crosslinked by UV radiation [91] and supramolecular hydrogen bonding ureido-pyrimidinone (UPy) moieties [92].

2.3 Material functionalization via NCO-sP(EO-stat-PO)

2.3.1 Chemical structure of NCO-sP(EO-stat-PO)

Poly(ethylene oxide) (PEO) is a polymer widely used for fabrication of tissue engineering scaffolds, thanks to its cytocompatibility and various available molecular weights [93]. The macromolecule used in this study for functionalization of gelatin nanofibers is a six-arm star-shaped statistical copolymer of ethylene oxide (80 %) and propylene oxide (20 %) [94]. The molecular mass is approximately 12 kDa [95]. Initially, the arms are OH-terminated and can be functionalized with various reagents to obtain reactivities adapted to a specific application. In this present case, isophorone diisocyanate (IPDI) had been attached during production, in order to obtain isocyanate (NCO)-functionalized reactive termini [96]. The primary, less reactive aliphatic isocyanate groups of IPDI remain as free functional groups at the distal ends of the arms. In contact with water, carbaminic acid is formed by hydrolysis of the isocyanate groups, and immediately decarboxylates forming amine groups. The latter can form urea bridges with unreacted isocyanate groups, building a three-dimensional hydrogel matrix by intermolecular crosslinking [97] (Figure 3). In general, NCO groups show a high reactivity with alcohol (R-OH), amine (R-NH₂), and thiol groups (R-SH), with reaction rates rising in that order. This affinity leads up to a great versatility in applications [98].

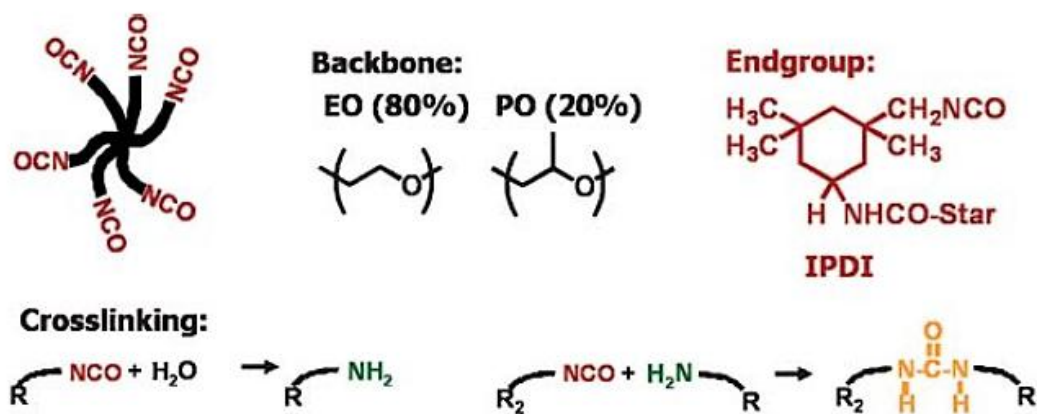


Figure 3: Scheme of chemical structure and crosslinking reaction of the star polymer system. Partially reprinted from Heyes et al. (2007) [97], with permission from The Royal Society of Chemistry.

2.3.2 Functional properties of NCO-sP(EO-stat-PO)

In previous studies, the NCO-sP(EO-stat-PO) system was used to create non-adhesive surfaces on polymer substrates [94, 99, 100] and, in addition, to improve specific cell adhesion by biofunctionalization of these surfaces [101-103].

PEO was found to be particularly efficient in fabrication of protein-resistant surfaces [104], while most authors grafted linear polymer chains on substrates [105]. Repelling of proteins by PEOs functions by forming a steric barrier on the grafted surfaces [106]. Groll et al. demonstrated that star-shaped polymers are beneficial in achieving a higher grafting density due to their molecular architecture [107, 108]. Owing to the situation of the functional groups at the periphery of each molecule, PEO-surface interactions, i.e. binding to a substrate, are more likely to occur. Packing density of the molecules increases with decreasing star-molecule diameter. End-functionalization of the arms, e.g. with NCO, further leads to a higher intermolecular crosslinking (Figure 4), leading to a higher surface coverage, thicker layers, and a better control of thickness variation [109].

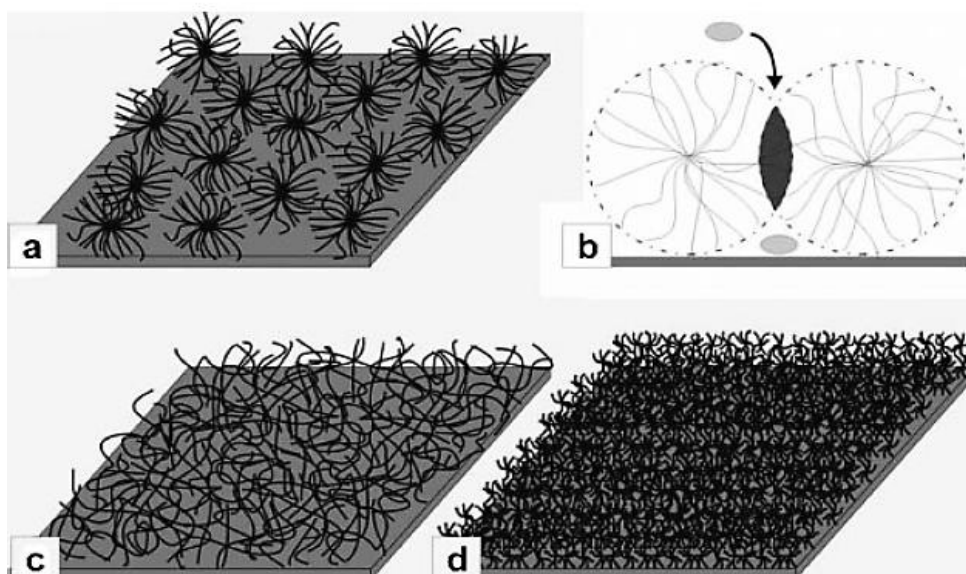


Figure 4: Schematic display of surface grafting of a,b) star-shaped PEO, c) linear PEO, and d) intermolecularly crosslinked six-arm PEO. Reprinted from Gasteier et al. (2007) [103], with permission from Wiley.

2. Theoretical background

In order to create an ultrathin surface coating on silicon wafers, Groll et al. [94] produced a film of variable thickness (3 to 500 nm) via spinning the polymer, dissolved in aqueous THF, onto the substrates. Activated by water, crosslinking of the star-shaped molecules resulted in a dense network of NCO-sP(EO-stat-PO) with protein repellent properties. In a specific medical application, Hoffmann et al. were able to show a distinct reduction of blood component-biomaterial interaction after spin coating with the polymer [100]. Also, NCO-sP(EO-stat-PO) converts hydrophobic into hydrophilic surfaces by the same mechanism, as the free terminal NCO groups at the distal arms are highly reactive with water [110]. Dalton et al. demonstrated that the system is able to provide a broad spectrum of tissue engineering materials, from nanoparticles up to complex channeled hydrogels, depending on the molecular mass of the macromer [111]. Recently, the applicability of NCO-sP(EO-stat-PO) has also been described in a bone TE application [112], however, its use in surface modification and specific bioactivation was mainly employed with flat glass, silicon, or titanium surfaces [99, 113] and electrospun fiber scaffolds [114-116].

In preparation of biofunctional surfaces, reactive termini of NCO-sP(EO-stat-PO) offer various reaction possibilities, thanks to a high reactivity of isocyanates with amines, alcohols and thiols. Functionalization can be realized either by adding functional compounds to the solution before coating, or after coating by reaction with isocyanates in freshly prepared or with amines (reacted from isocyanates) in readily crosslinked layers. Bioactive compounds can thus be statistically distributed or patterned by stamping onto the surface [103]. Components used in this context are, among others, DNA and oligonucleotides [101], streptavidin and NTA-receptors [102], RGD for cell adhesion [117], collagen and fibronectin fragments [118, 119], and growth factors and therapeutics with controlled release regimes [120]. Biocompatibility of NCO-sP(EO-stat-PO) hydrogel coatings with protein immobilization of RGD and a surface bound growth factor (BMP-4 = bone morphogenetic protein-4) has been tested successfully in vivo [121].

Recently, NCO-sP(EO-stat-PO) has been applied with success as a crosslinker for hyaluronic acid (HA) based hydrogels. In this case, terminal -OH groups of

2. Theoretical background

HA react with NCO at the distal arms of the star-polymers, forming urethane bonds. In parallel, the described intermolecular crosslinking by urea bridges occurs during hydrolysis of NCO in an aqueous environment [122-124].

As described above, the macromolecular structure of gelatin displays free nucleophilic groups such as alcohols and free amines. Therefore, we expect that NCO-functionalized sP(EO-stat-PO) has the potential to crosslink and functionalize gelatin-based electrospun fiber scaffolds.

3. Materials and methods

3.1 Materials and chemicals

All materials and chemicals were used as received unless otherwise stated.

The gelatin used in this study is a Type A kind (acidic extraction) of porcine origin with a gel strength of ~300 g Bloom obtained from Sigma Aldrich GmbH (Steinheim, Germany, Lot# SLBT6921).

For the dissolution of gelatin HFIP (1,1,1,3,3,3-Hexafluoro-2-propanol, $C_3H_2F_6O$) of $\geq 99\%$ purity was applied. It was acquired from Sigma Aldrich GmbH (Steinheim, Germany, Lot# WXBC5954V).

NCO end functionalized 6-armed sP(EO-stat-PO) (NCO-sP(EO-stat-PO)) has a molecular weight of approximately 12 kDa and was received by DWI-Leibniz Institute for Interactive Materials (Aachen, Germany, Lot## SS_CHT_7 and SS_CHT_8). Dissolution of NCO-sP(EO-stat-PO) was conducted with dried Tetrahydrofuran (THF, C_4H_8O , max. 0.005 % H_2O), obtained from Merck KGaA (Darmstadt, Germany, Lot# I806407618).

NCO-sP(EO-stat-PO) and THF were kept under a protective gas atmosphere (Ar) in a glovebox and in all cases unloaded shortly before dissolving and mixing with the other reagents to keep the reaction with atmospheric water and oxygen as small as possible.

Cell studies were conducted with RAW 264.7 murine macrophages, transformed by Abelson murine leukemia virus. This cell line is commercially produced and distributed, therefore no ethics committee vote had to be sought. The cells were obtained from the American Type Culture Collection ATCC® (Manassas, VA, USA, TIB71™).

Cell culture was performed in Dulbecco's Modified Eagles Medium (DMEM, 500 ml, ATCC®, Manassas, VA, USA, Cat.No. 30-2002). 10 % Fetal Calf Serum (FCS) and 1 % penicillin/streptomycin (both Thermo Fisher Scientific, Waltham, MA, USA) were added to the medium.

Cultivation of the cells was accomplished in T75 tissue culture flasks (Greiner Bio-One GmbH, Frickenhausen, Germany) and non-treated 24-well plates (Corning®Costar®, Corning Inc., Corning, NY, USA). For experimental

purposes treated transparent and black 96-well plates were used (Greiner Bio-One GmbH, Frickenhausen, Germany).

The WST-1 assay for assessment of cell viability was conducted with Cell Proliferation Agent WST-1 (Roche Diagnostics GmbH, Mannheim, Germany). DNA quantification was performed with a PicoGreen® assay (PicoGreen dsDNA Quantitation Reagent (Lot ## 1915834 & 1942213, Thermo Fisher Scientific, Waltham, MA, USA).

3.2 Fiber fabrication

3.2.1 *Spinning solutions*

Gelatin was dissolved in HFIP stirring under a fume hood in 10 ml glass beakers. This basic gelatin solution had a constant concentration of 5 % (w/v). About four hours of stirring time were needed for complete solution.

NCO-sP(EO-stat-PO) was freshly taken out of the glovebox and dissolved in THF for three minutes right when the gelatin was fully dissolved. The two solutions were subsequently mixed for a defined time span, which was varied between 30 s and 24 hrs, as this factor was assumed to greatly influence the properties of the obtained meshes. After that the solution was electrospun immediately.

In pre-experiments NCO-sP(EO-stat-PO) and gelatin were mixed at different ratios ranging from 1:10 to 1:1 as well as 3:2 and 3:1. According to their spinnability, obtained fibrous morphology and mechanical handling, three ratios (1:1, 1:3, 3:2) were chosen for further investigation.

3.2.2 *Solution Electrospinning*

In pre-experiments fibers were spun from solutions of varying amounts of PCL, an easy to spin polymer, in a mixture (1:1) of DMF (Dimethylformamide) and DCM (Dichloromethane) to get accustomed to the technique and the appliance setup. Later on, a protocol for the fabrication of gelatin fibers was established. Once a suitable method was applicable, another protocol for mixed NCO-

3. Materials and methods

sP(EO-stat-PO)/Gt fibers was constituted with varying ratios of NCO-sP(EO-stat-PO) and gelatin.

The solution of gelatin and NCO-sP(EO-stat-PO) was filled into a 1 ml plastic syringe (Norm-Ject, Henke-Sass, Wolf GmbH, Tuttlingen, Germany, Lot# 15H24C8) and furnished with a 27G blunt metal needle (B. Braun Melsungen AG, Melsungen, Germany, Lot# 16M18G8811). Both were single-use products. The electrospinning apparatus was designed in-house at the Department for Functional Materials in Medicine and Dentistry at the University of Würzburg. Its three main components are a syringe pump (Model '11' Plus, Harvard Apparatus, Holliston, MA, USA), an adjustable high voltage source (Conrad Electronic, Hirschau, Germany) and a stainless steel cylindrical collector (\varnothing 6 cm, width 10 cm) which can be rotated at varying speeds. In the present study a rotation speed of approx. 68 rpm was applied. A slide underneath also allows translational motion, although it was kept stationary in this case. The needle tip with the high voltage electrode and the grounded collector are located within an acrylic glass encasing.

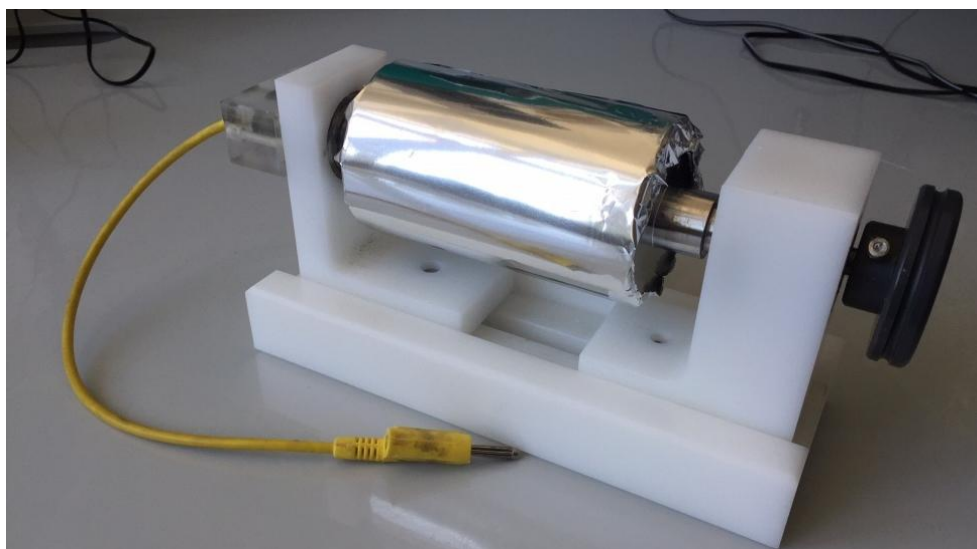


Figure 5: Collector drum covered with aluminum foil ready prepared for electrospinning of a NCO-sP(EO-stat-PO)/Gt mesh sheet.

The syringe was placed and fixated in the pump, which was operated at a flowing rate of 0.5 ml/hr. A high voltage was applied via an electrode directly clamped to the needle, whereas a constant voltage of 14 kV was found to be

3. Materials and methods

best in order to achieve an ideal spinning process for the given material. The needle tip to collector distance was 15 cm. Depending on the desired application the fibers were collected either on aluminum foil (obtaining a wide compact sheet useful for most study purposes, e.g. tensile testing, see Figure 5) or on round glass cover slips (\varnothing 10 mm resp. 12 mm, for cell culture purposes and contact angle measurement).

3.3 Fiber characterization

3.3.1 Scanning electron microscopy (SEM)

Scanning electron microscopy represents a high resolution imaging method for analyzing morphological and topographical features on solid state surfaces. A focused electron beam is moving in a high vacuum across the sample surface according to a defined scanning scheme. Accelerated electrons interact with surface atoms, generating X-ray fluorescence as well as secondary and backscattered electrons, which are eventually used to produce images of the object [125].

For fiber characterization in this study round specimens of the electrospun meshes were cut with a 12 mm \varnothing biopsy punch from the center of each mesh, to avoid fabrication irregularities close to the edge. The samples were placed on conductive double sided carbon tape onto 12 mm \varnothing aluminum holders (Plano GmbH, Wetzlar, Germany) and coated with a 2 nm thick layer of platinum using a sputter coating device (Leica EM ACE600, Leica Microsystems, Wetzlar, Germany). Images were taken at 2.00 kV acceleration voltage with a scanning electron microscope (Zeiss Crossbeam 340, Jena, Germany).

Characterization of water incubated fibers was performed by punching 12 mm \varnothing round specimens from the central parts of the meshes and fixating them onto 14 mm \varnothing plastic rings (Minucells & Minutissue Vertriebs GmbH, Bad Abbach, Germany). The samples were then immersed in purified water (aurium® pro VF TOC, Sartorius Weighing Technology GmbH, Göttingen, Germany) in a Petri dish and stored at room temperature. After defined time intervals (15, 30, 45, 60 min, 5 h, 1, 2, 4 d) they were removed and left to dry in a fume hood overnight, prior to platinum sputter coating and characterization under SEM as described above.

For cross section measurements samples were cut into 2x2 mm squares and mounted with conductive carbon tape to a 45° angled aluminum holder. By further inclining the sample table of the microscope by 45° a vertical view at the mesh cross section was enabled. Image analysis with thickness measuring was conducted with FIJI image processing software [126].

3.3.2 *Energy dispersive X-ray spectroscopy (EDX)*

Energy dispersive X-Ray spectroscopy (EDX) is an analytical method to assess the elemental composition of a specimen by using the characteristic X-ray radiation of the material surface induced by the incident electron beam of an SEM. The difference in energy is emitted as a characteristic number and energy of X-rays, which can be detected by an energy-dispersive spectrometer. The results are displayed as peaks in a spectrogram and/or as an overlaying sample topography electron image. By this technique detection of extremely small amounts of an element (< 0.1 pg) is possible [125].

In this study electrospun meshes of three different ratios of NCO-sP(EO-stat-PO) and gelatin were measured with an EDX detector (X-Max 50, Oxford Instruments, Abingdon, England) before and after incubation in water for three days, to assess first the presence of either component and second to determine the changes in composition in an aqueous environment.

NCO-sP(EO-stat-PO)/Gt ratios 1:3, 1:1 and 3:2 were electrospun on aluminum foil. Round specimens of the resulting mesh were cut with a 12 mm Ø biopsy punch. Half of the samples were mounted with carbon double sided tape onto aluminum SEM specimen holders and measured with EDX. The other half were fixated and weighted down with plastic rings and immersed in purified water for three days. After that they were dried under a fume hood overnight and subsequently also measured in the SEM.

3.3.3 *Image analysis*

In order to assess and measure different features of the electrospun fibers a comprehensive image analysis was conducted with FIJI (ImageJ) image processing software [126] and its associated plugin DiameterJ [127]. SEM images of 10,000x magnification were used for this purpose. Fiber diameters were measured by placing a grid on each image, and ~100 fiber diameters were established with a measuring tool, set to the respective scale bar. Averages and standard deviations for each image were calculated to assess mean diameters and variation of fiber thickness.

SEM images were also examined qualitatively regarding the fiber morphology, i.e. the shape of diameter (rounded or ribbon-shaped) and the homogeneity of the fiber surface. The latter was necessary because an improper spinning process usually leads to bead-like structures on the fibers. Specimens with these properties were excluded from the study.

A further application of SEM images and FIJI was to measure the cross section thickness of the electrospun meshes. These values were needed for calculation of the stress parameter in tensile testing. Conventional measurements with a thickness gauge or digital caliper were not reliable so this rather inconvenient way had to be taken. Of each sample a minimum of three images were taken, and for each image at least 50 cross sections were quantified with the measuring tool (Figure 6) yielding a total number of 150 measuring points per sample. For practical aspects cf. chapter 3.3.1.

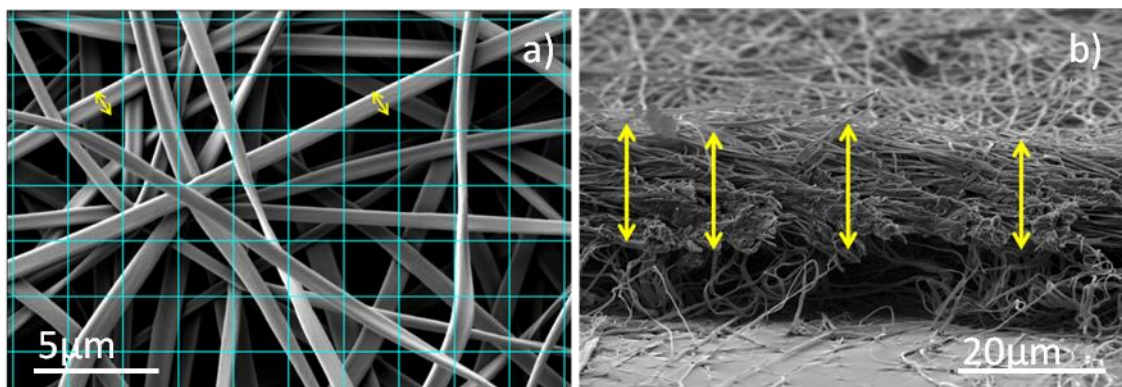


Figure 6: Image processing in FIJI. a) Measurement of fiber diameters. b) Determination of electrospun mesh thickness for later tensile testing.

3.3.4 Water incubation and contact angle measurement

The water stability of the electrospun fibers was analyzed on the one hand by weight loss experiments; on the other hand with further imaging under SEM. In order to assess the weight loss of the material, three selected NCO-sP(EO-stat-PO)/Gt ratios (1:3, 1:1, 3:2) were cut into squares of 3x3 mm (n=3). The dry weight of the samples and their containing Petri dishes was determined with the help of an analytical balance ABT 100-5M (Kern&Sohn GmbH, Balingen-Frommern, Germany) with a readability of 0.01 mg. The specimens were

3. Materials and methods

subsequently immersed in purified water and incubated for three days covered with a lid at room temperature. After that they were taken out and left to dry under a fume hood over night and weighed out again to measure the weight loss after incubation. The weight difference was calculated and averaged. In order to test the reproducibility, these experiments were performed in three repetitions. Further water stability assessment was implemented by SEM imaging of different NCO-sP(EO-stat-PO)/Gt ratios before and after incubation of the material in purified water and under physiological conditions in 1xPBS (phosphate buffered saline) at 37 °C for defined time spans of 10 min, 30 min, 1 h, 3 hrs, 24 hrs and 3 days.

Fiber hydrophilicity was assessed by contact angle measurements. Therefore, the mixed NCO-sP(EO-stat-PO)/Gt solutions at different ratios were electrospun onto glass cover slips ($\varnothing=10$ mm) which were attached to the surface of the stationary collector. In order to avoid interference of the glass surface during measurement, spinning was conducted for 1 h to provide sufficient thickness of the meshes. This spinning time was kept consistent for all samples. Measurements were performed with purified water at room temperature using a contact angle system OCA 20 and its associated software SCA 20 (both Dataphysics Instruments GmbH, Filderstadt, Germany). During measuring a live camera image allows to track the adsorption or infiltration of a pending water drop onto or into the surface to be examined. In this case, one mesh covered cover slip was placed on the sample table and moved upwards to catch the pending drop. When infiltration had ceased and the drop surface was steady a picture was taken, which was subsequently analyzed with the software.

$$\cos\theta = \frac{\sigma_{SG} - \sigma_{SL}}{\sigma_{LG}} \quad \text{E 1}$$

A baseline detection tool enables to distinguish the borderline between sample and water drop, while a drop surface profile is detected by another extraction tool. The contact angle is then calculated by the software using Young's equation (E 1). θ is defined as the angle at the phase boundary of gaseous,

liquid and solid surfaces, while σ represents the interfacial tension between the respective aggregation states. The measured values were averaged at $n=4$.

3.3.5 Tensile test

Tensile testing of the electrospun scaffolds was performed with a universal testing machine (Zwick Z010, Zwick/Roell, Ulm, Germany) furnished with a 100 N load cell and two pulling clamps, arranged in a uniaxial setting (Figure 7). For determining tensile strength the material was cut into rectangular test specimens of 15x1.5 mm. The thickness h of the specimens was established under SEM (as described in chapters 3.3.1 and 3.3.3) and arithmetically averaged. The initial length of each specimen was measured before testing. Because the material is rather sensitive, standardized cardboard frames were created to hold and stabilize the meshes during the measurement. Their sides were cut shortly before starting the test.

Tensile testing itself was performed at a constant speed of 2.5 mm/min and a pre-load of 0.1 N. The resulting parameters of elongation [mm] and standard force [N] are registered and plotted in the corresponding software testXpert II V 3.1 (Zwick/Roell, Ulm, Germany). From these data a stress-strain curve and Young's modulus were calculated. Strain ε is defined as the proportional deformation, i.e. the change in length along the tensile distance with reference to the initial length of the sample. Hereby Δl represents the distance covered and l_0 the initial length (E 2):

$$\varepsilon = \frac{\Delta l}{l_0} \quad \text{E 2}$$

Stress σ is the relationship between standard measured force F and the specimen's cross section A , i.e. the width b multiplied by its height h (E 3):

3. Materials and methods

$$\sigma = \frac{F}{A} = \frac{F}{b * h} \quad \text{E 3}$$

Young's modulus E is a measure to describe the stiffness of a material and is displayed by the relationship between stress σ and strain ε (E 4) in a linear system:

$$E = \frac{\sigma}{\varepsilon} \quad \text{E 4}$$

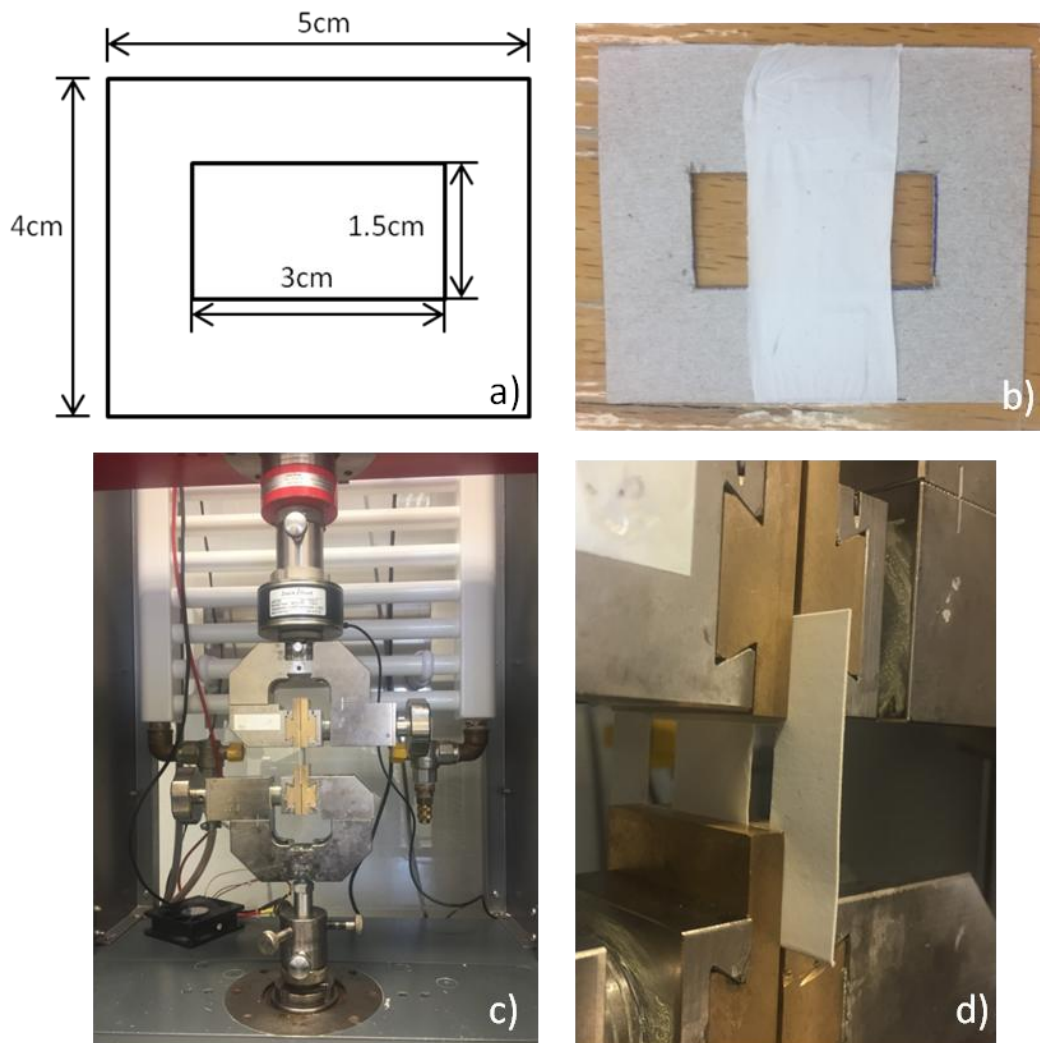


Figure 7: a) Customized template for cardboard frame used for tensile testing of electrospun fiber scaffolds; b) cardboard frame with fixated electrospun fiber scaffold specimen; c) experimental setup for uniaxial tensile test with pulling jaws and 100N load cell; d) specimen fixated to cardboard frame with double sided tape, pulling jaws holding the frame, which is cut at the sides shortly before testing.

3. Materials and methods

As this parameter is not linear along the entire tensile distance, it was calculated in the quasi linear strain range between 0.01 and 0.05 and arithmetically averaged (Figure 8).

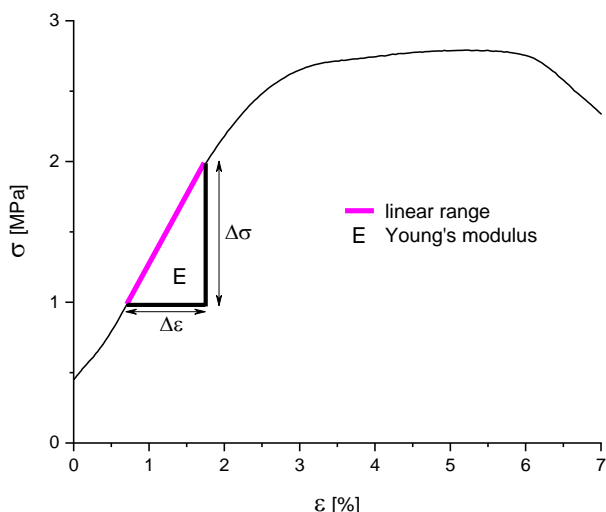


Figure 8: Stress-strain curve of an electrospun NCO-sP(EO-stat-PO)/Gt scaffold with gradient triangle (schematic diagram). Young's moduli were calculated from the linear section of the curve.

3.3.6 Fourier transform infrared spectroscopy (FT-IR)

The principle of FT-IR is to expose the respective sample to infrared radiation, whereas the molecules interact with the electromagnetic wave and start to vibrate. Thereby the frequency is strongly depending on the type of chemical bonding which allows drawing conclusions on the atoms and molecules involved [128]. In measuring FT-IR an absorption spectrum is generated, where the absorption bands are characterized by their wave number $\tilde{\nu}$, which equals the reciprocal wave length λ (E 5).

$$\tilde{\nu} = \frac{1}{\lambda}$$

E 5

In this study a Nicolet is10 ATR spectrometer (Thermo Fisher Scientific Inc., Waltham, MA, USA) was used.

ATR FT-IR spectroscopy (ATR = *attenuated total reflection*) investigates the interactions at the interface between a sample surface and an internal reflection

element i.e. a prism, in this case made of diamond. Total reflection takes place and a standing wave reflected from the sample surface interferes with the IR beam and thereby attenuates it [129].

The resulting interferogram is matched with a reference spectrum and the sample spectrum is calculated via Fourier transform. For all generated spectra the transmission [%] was recorded within wave numbers ranging from 4000 to 650 cm^{-1} . Imaging was conducted with OMNIC™ Spectra software (Thermo Fisher Scientific Inc., Waltham, MA, USA).

3.3.7 Cell culture

For the cell tests murine RAW 264.7 macrophages were chosen. This cell line has become popular in recent research for assessing the biocompatibility and bioactivity of natural materials, and is commonly utilized to predict *in vivo* effects. The RAW cellular response is described to reflect the human *de novo* immune response to implanted materials [130]. Therefore, these cells were considered to give information on the bio- and immunological compatibility of the electrospun hybrid meshes in this study.

The cells were seeded on the fiber scaffolds electrospun on 12 mm Ø glass cover slips, placed in a non-treated 24-well tissue culture plate. As a comparative control, cells were also seeded on pure gelatin electrospun scaffolds, which had been crosslinked with 25 % glutaraldehyde vapor for 24 hrs. The seeding scheme was 50,000 cells per well in 50 μl DMEM with 10 % FCS and 1 % penicillin/streptomycin. Cells were incubated at 37° and a 5 % CO_2 atmosphere for 7 days. On days 1, 4 and 7 cell growth on the meshes was analyzed using a WST-1 viability assay and a PicoGreen™ DNA quantification assay. The assays were analyzed with a multichannel absorbance plate reader (Tecan™, Tecan Life Sciences, Zurich, Switzerland). On days 4 and 7 samples assigned for microscopy analysis were fixated using 25 % glutaraldehyde and dried following a protocol with increasing concentrations of ethanol. These samples were examined under the SEM for assessment of cell morphology, proliferation, and adhesion.

4. Results

The process of electrospinning natural polymers is governed by numerous factors (cf. chapter 2), which are in many cases hard to assess independently from each other. Therefore the first result chapter on the fabrication of electrospun NCO-sP(EO-stat-PO)/Gt fibers describes qualitative observations, mostly obtained in pre-experiments but nevertheless worth mentioning. The second results chapter eventually presents characterization of the NCO-sP(EO-stat-PO)/Gt scaffolds with quantitative experimental approaches, such as mechanical, chemical and biological analyses.

4.1 Fiber fabrication

4.1.1 Solvent choice

For the solution of gelatin different organic solvents were tested for their dissolving properties. 50 mg of gelatin were mixed with 1 ml of the respective solvent and the dissolution time was measured. Gelatin was not soluble in DMF, DCM, acetone and chloroform, but was dissolved in H₂O, DMSO and HFIP. Solution in water takes approximately 30 min at 50 °C. The aqueous solution tends to solidify quickly at room temperature; therefore an electrospinning process was not feasible without further heating appliances. Attempts to heat up the solution during spinning with a heating cable were unsuccessful in the present apparatus configuration. Gelatin was dissolved in DMSO within 1 h, but the solution was not applicable for spinning either. Low gelatin concentrations in DMSO prevent the complete establishment of a polymer jet, while higher concentrations only yield poor fiber qualities. HFIP dissolves gelatin completely in approximately 4 hrs. It yields a solution of low viscosity, which is easy to handle with a syringe and thin needles such as 27G. Of all solvents, HFIP is the one resulting in the most favorable fiber quality (Figure 9).

Also the solvent for NCO-sP(EO-stat-PO) further influences spinning process and fiber quality. In pre-experiments 25 mg of NCO-sP(EO-stat-PO) were dissolved in DMSO, HFIP, and THF respectively, and were mixed subsequently with a 5 % gelatin solution in HFIP. DMSO causes a suboptimal spinning

4. Results

process with visible fibers, drop formation at the needle tip, and poor jet development. Additionally, not one single broad sheet of electrospun mesh was obtained but two narrow stripes of about 1 cm in width. This mesh was very fragile, sticky and hard to detach from the collector, therefore, it was not possible to handle the mesh for further experiments (e.g. tensile test). SEM imaging of these samples reveals an insufficient fiber formation (Figure 9). HFIP was ruled out as a solvent for NCO-sP(EO-stat-PO) in order to prevent early reactions between its hydroxyl groups and the highly reactive NCO end groups of NCO-sP(EO-stat-PO) before mixing with the gelatin solution. Instead dry THF was chosen as a solvent.

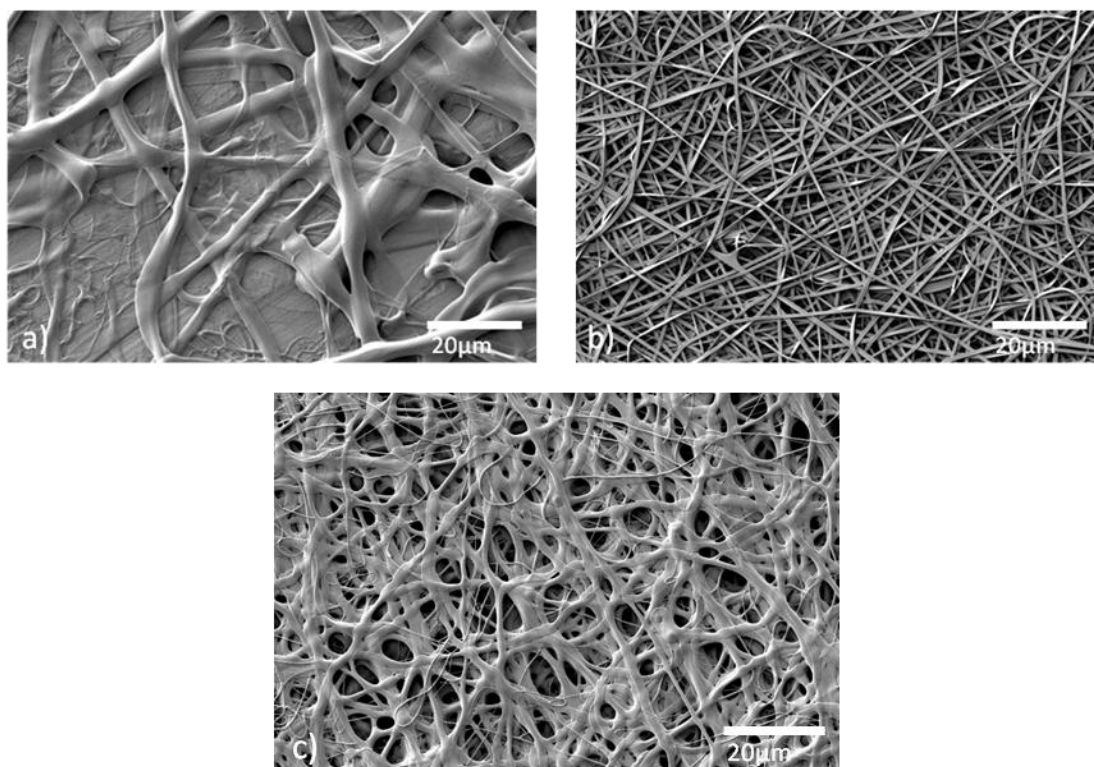


Figure 9: Fibers electrospun from a 5% Gt solution in a) DMSO and b) HFIP; c) electrospun hybrid fibers from a solution of 1:2 ratio of NCO-sP(EO-stat-PO)/Gt. Gt was dissolved in HFIP, NCO-sP(EO-stat-PO) in DMSO.

4.1.2 *Spinning parameters*

In the electrospinning process are the following parameters are crucial: high voltage, needle-collector distance, solution feeding rate, needle diameter and collector movement. For an optimal spinning process, voltage has to be adapted to form a stable but invisible polymer jet and spitting or dropping of the spinning dope should be avoided. In the present case, a constant voltage of 14 kV was found to be ideal. Needle-collector distance (collection distance) influences the covering width of the spun meshes on the collector and also the quality of process and fibers. The collector width of 10 cm was best exploited at a distance of 15 cm. The solution was fed at a constant rate of 0.5 ml/hr, while higher rates lead to considerable spitting and lower rates decrease the ability to form a jet. The rather thin needle diameter (27G = 0.4 mm) was selected according to the viscosity of the solution. Thicker test solutions were spun with 21G needles. For creating long sheets, the collector drum was rotated, when only small amounts of material were needed or for spinning on cover slips it remained stationary.

4.1.3 *Mixing time*

The reaction time of the gelatin solution with NCO-sP(EO-stat-PO) was expected to greatly influence the stability and the extent of crosslinking inside the meshes. Mixing time of the two solutions was therefore varied between 30 min, 1 h, 4 hrs, 18 hrs and 24 hrs. Also the option of the shortest possible mixing time was tested. For this purpose, the NCO-sP(EO-stat-PO) solution in THF was added to the dissolved gelatin. Both solutions are clear initially, whereas they turn cloudy upon mixing. After approximately 1-2 minutes of agitation, the precipitate disappeared, and the solution was electrospun immediately. The effect of mixing time on fiber stability will be described and discussed further below.

4.2 Fiber characterization

4.2.1 Fiber morphology

4.2.1.1 Gelatin concentration and fiber diameter

Different concentrations of gelatin in HFIP (5 %, 7 %, 10 %, 12.5 %, 15 % w/v) were electrospun for 1h at constant spinning parameters as described above. Figure 11 displays the different results obtained from varying gelatin concentrations. 15 % gelatin solution could not be used eventually in the spinning process due to its high viscosity. It is clearly visible that the fiber diameter increases strongly with increased gelatin concentration. A concentration of 5 % gelatin yields fibers of 500 nm to 1.0 μm in diameter. 7.5 % fibers vary in thickness between 1.0 and 2.0 μm , whereas fibers spun of 10 % gelatin solution show a width of 2.5 to 4.5 μm . A concentration of 12.5 % gelatin leads to an increasing loss of fiber structure, as the single strands converge and produce mostly a closed sheet, which makes a measurement of single fibers highly unreliable (Figure 10). The standard deviation therefore increases with increasing gelatin content. Based on fiber quality the 5 % gelatin solution was selected as a base solution for further spinning experiments combining gelatin with different amounts of NCO-sP(EO-stat-PO).

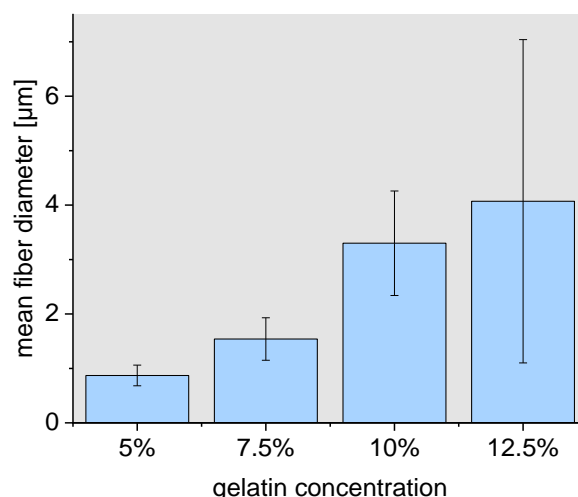


Figure 10: Mean diameter of fibers electrospun from different gelatin concentrations, determined via SEM image processing with FIJI software.

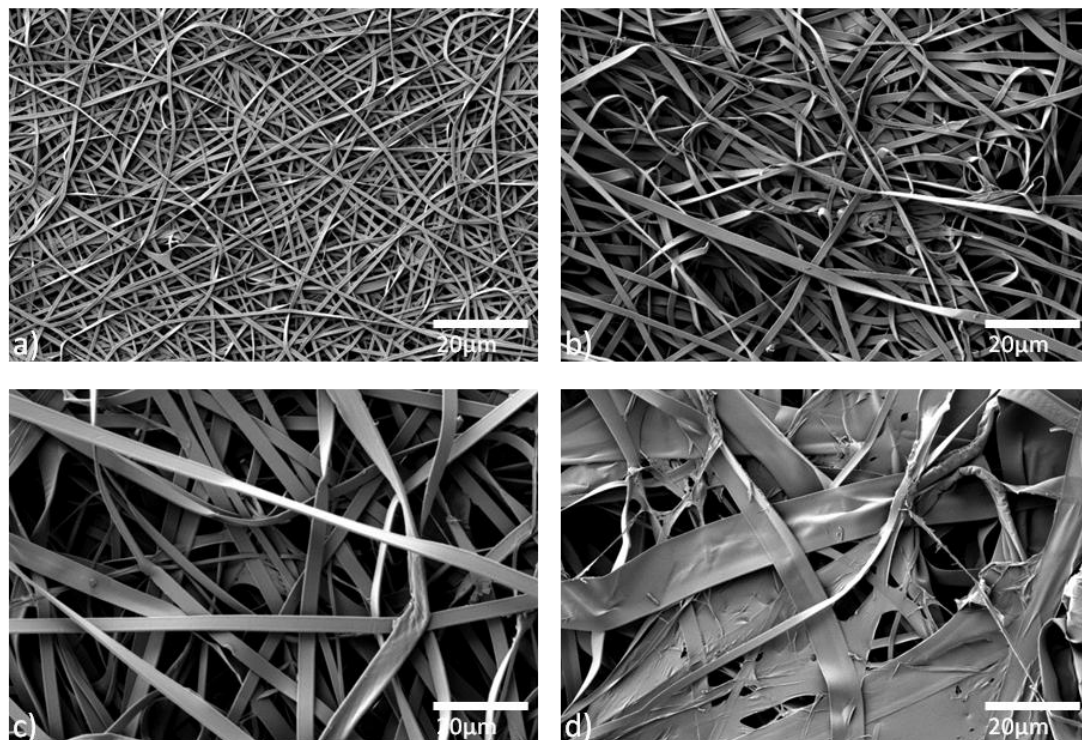


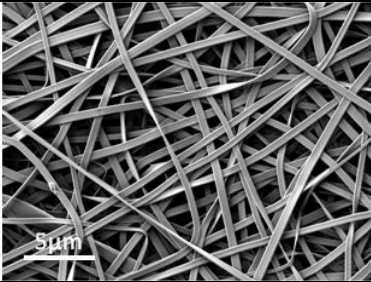
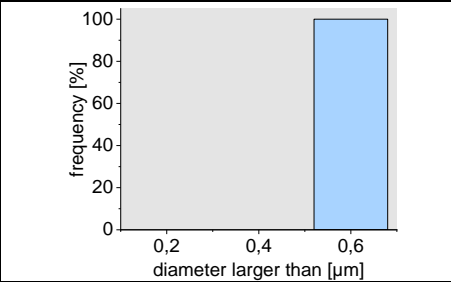
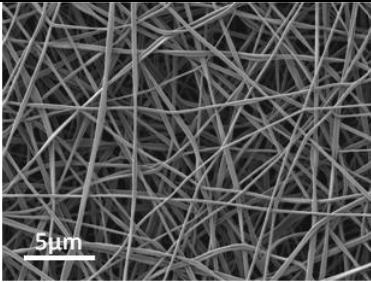
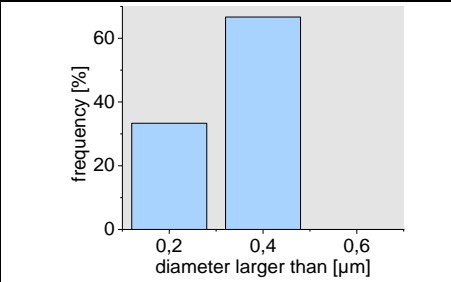
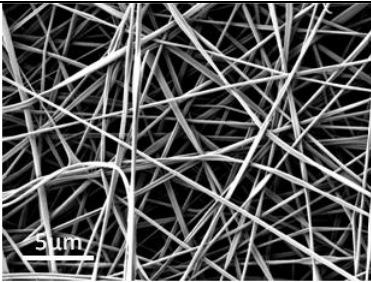
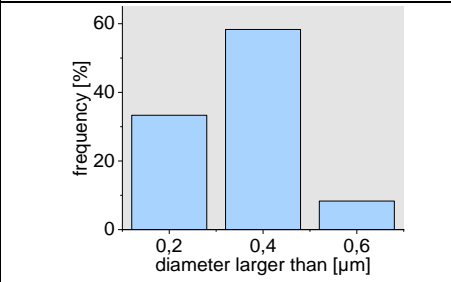
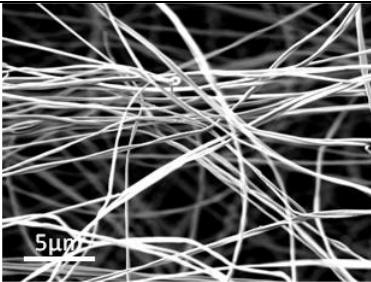
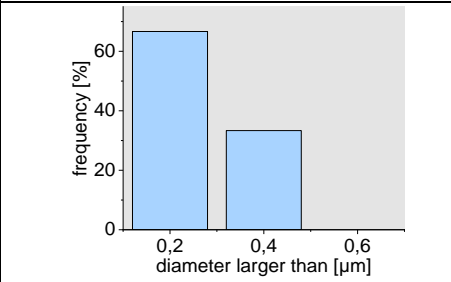
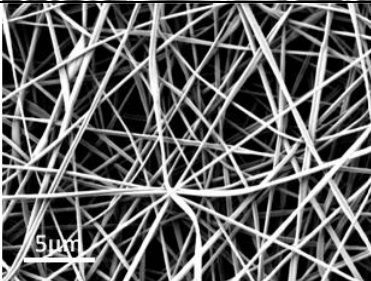
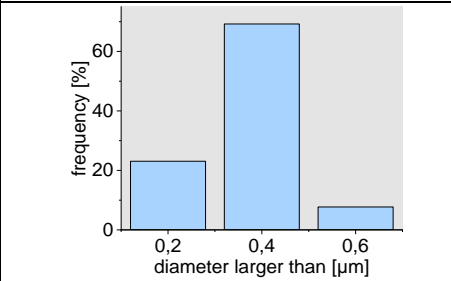
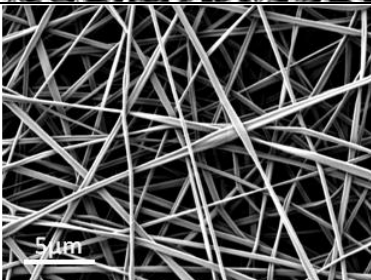
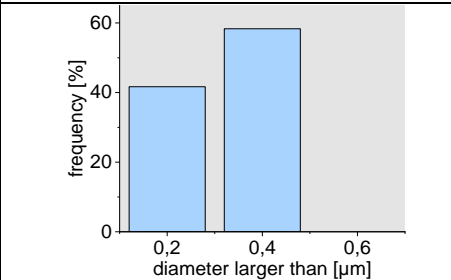
Figure 11: Fibers electrospun from different concentrations of gelatin (w/v). a) 5%, b) 7.5%, c) 10%, d) 12.5%. A higher concentration (15%) of gelatin solution was not spinnable due to high solution viscosity.

4.2.1.2 NCO-sP(EO-stat-PO)/Gt ratio and fiber morphology

To the basic 5 % gelatin solution, increasing amounts of NCO-sP(EO-stat-PO) were added systematically. NCO-sP(EO-stat-PO)/Gt weight ratio was varied from 1:10 up to 1:1. The maximum ratio for which a reasonable spinning process was applicable was three parts NCO-sP(EO-stat-PO) to two parts gelatin (3:2 = 1.5:1). Parameters assessed by means of SEM imaging were distribution of fiber diameter, mean diameter and shape of fiber cross section. Electrospun fiber shape and texture can occur in various forms, such as uniform, beaded, branched, porous, core-shell, Janus, hollow and flat/ribbon [131]. In this study it was achieved to produce uniform, non-beaded fibers. Single-strand fibers were formed throughout all NCO-sP(EO-stat-PO)/Gt ratios, only when NCO-sP(EO-stat-PO) content exceeded the amount of gelatin (in 3:2 samples) branching of fibers was noticeable. All fibers show smooth and non-porous surfaces. The prevailing fiber cross section shape was either ribbon shaped, rounded or a combination of both types.

Figure 12 gives an overview of the obtained results. It presents SEM images of electrospun gelatin nanofibers with increasing amounts of NCO-sP(EO-stat-PO) from pure gelatin to 3:2 NCO-sP(EO-stat-PO)/Gt. Regarding fiber diameter SEM analysis revealed that thickest fibers occurred in pure gelatin samples (concentration of 5 %) with an average of 0.87 μm . NCO-sP(EO-stat-PO)/Gt ratio 1:10 shows the smallest fiber cross section of 0.25 μm . 1:1 and 1:2 ratios show an average thickness of around 0.67 μm . A general increase in mean diameter with increasing NCO-sP(EO-stat-PO) content can be stated. 3:2 samples with highest contents of NCO-sP(EO-stat-PO), again, show a thickness alike the one for lowest ratio 1:10 (0.24 μm). Concerning homogeneity of fiber diameters it is noticeable that pure gelatin fibers yield the most uniform fiber diameter, unlike mixed samples. Fiber shape varies from ribbon-shaped to rounded cross-sections. The ribbon shape is visible most prominently in pure gelatin samples; while lowest NCO-sP(EO-stat-PO) amounts (1:10) develop thin round fibers. A general shift from rounded to ribbon is noticeable with increasing NCO-sP(EO-stat-PO) contents. A pronounced change back to rounded fibers is noted in the 3:2 batch. Regarding diameter and fiber shape, these samples where NCO-sP(EO-stat-PO) exceeds the gelatin content deviate strongly from all others. Visible fiber crosslinking is only present in this ratio.

4. Results

mixing ratio	SEM (5000x)	distribution	$\langle D \rangle$ [μm]	shape
pure gelatin			0.87	
1:10			0.25	o
1:9			0.43	o>
1:8			0.36	o
1:7			0.47	o
1:6			0.35	o>

4. Results

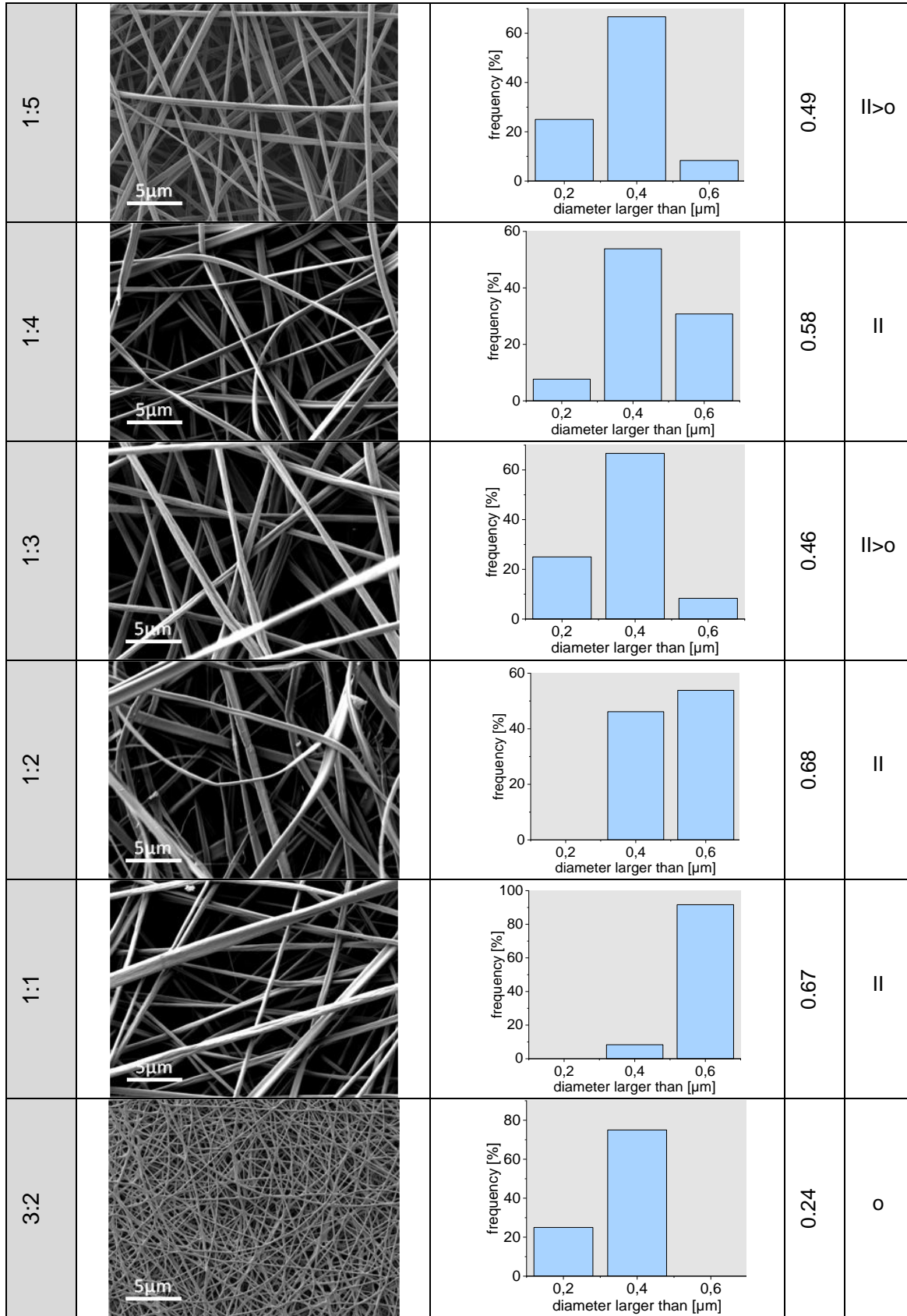


Figure 12: SEM images of electrospun pure Gt fibers and hybrid NCO-sP(EO-stat-PO)/Gt fibers of varying mixing ratios, relative fiber diameter distribution, mean fiber diameter, and cross section shape of fibers. ∅ = rounded fiber shape, || = ribbon shape.

4.2.2 Hydrophilicity

Data of contact angle measurements for electrospun meshes with different ratios of NCO-sP(EO-stat-PO)/Gt and also for pure gelatin are given in Figure 13. Highest contact angles of around 50° , equivalent to lowest hydrophilicity, were found in pure gelatin (5 %) as well as in ratio 1:10. With increasing NCO-sP(EO-stat-PO) content an almost linear increase in infiltration capability, reflected by smaller angles, and therefore hydrophilicity can be stated. A general property of all analyzed samples is that infiltration of water takes place very quickly in NCO-sP(EO-stat-PO)/Gt samples, compared to test samples electrospun from PCL. A convex drop shape only remains stable for a few seconds before infiltration starts.

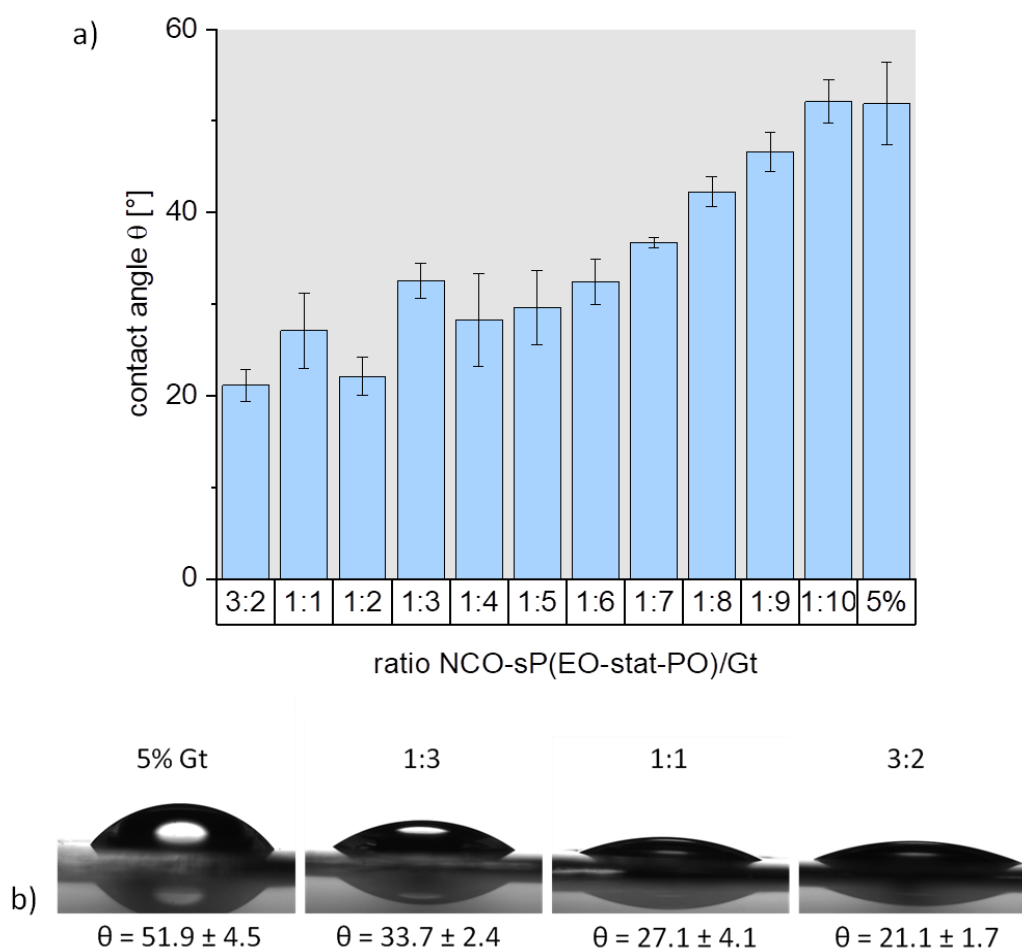


Figure 13: a) Contact angles of all electrospun NCO-sP(EO-stat-PO)/Gt meshes and pure gelatin mesh (5 %); b) images and contact angles (θ) for hybrid ratios selected for further experiments.

4.2.3 Tensile properties

Basic parameters measured by the Zwick device during tensile strength analyses are elongation [mm] and standard force [N]. In order to calculate true stress and strain the cross sectional area of the specimens has to be calculated. Therefore, the initial length l_0 and the width b of the specimen, as well as the mesh thickness were measured before testing. The first two parameters could be established with a caliper, whereas measuring mesh cross section (thickness) was performed with the aid of SEM imaging (see chapter 3.3.1.).

Figure 14 shows the averaged cross sections of meshes analyzed in tensile testing. All specimens were electrospun under consistent conditions and parameters. Spinning time was 60 min for each mesh. Highest thickness values were measured for 1:1 and 1:2 at about 20 μm . A general trend towards thinner cross sections with lower NCO-sP(EO-stat-PO) contents can be observed.

Results of tensile testing are given in Figures 14-16. NCO-sP(EO-stat-PO) content was varied while gelatin concentration remained constant at 5 % (w/v). Measured ratios of NCO-sP(EO-stat-PO)/Gt were 1:1, 1:2, 1:3, 1:5 and 1:9; Unfortunately, meshes of other electrospun ratios and pure gelatin meshes could not be utilized for tensile specimens due to their fragility and difficult handling. Figure 15 shows the stress-strain behavior of the electrospun hybrid meshes. The overall tensile strength of the samples ranges between 1.0 and 8.5 MPa. NCO-sP(EO-stat-PO)/Gt ratio 1:1 reaches the highest strength at more than 8.5 MPa. 1:2, 1:3 and 1:9 showed stress values between 2 and 4 MPa, while the lowest tensile strength was achieved by 1:5 at around 1 MPa. It becomes clear that an equal amount of gelatin and NCO-sP(EO-stat-PO) gives rise to very high levels of tensile strength compared to lower ratios. For instance, 1:2 mesh with half the amount of NCO-sP(EO-stat-PO) only shows about a third of the maximum strength of 1:1. The lowest tensile strength is not in accordance with the lowest amount of NCO-sP(EO-stat-PO), it was measured in ratio 1:5. Altogether a linear relation of tensile strength and NCO-sP(EO-stat-PO) content cannot be observed.

4. Results

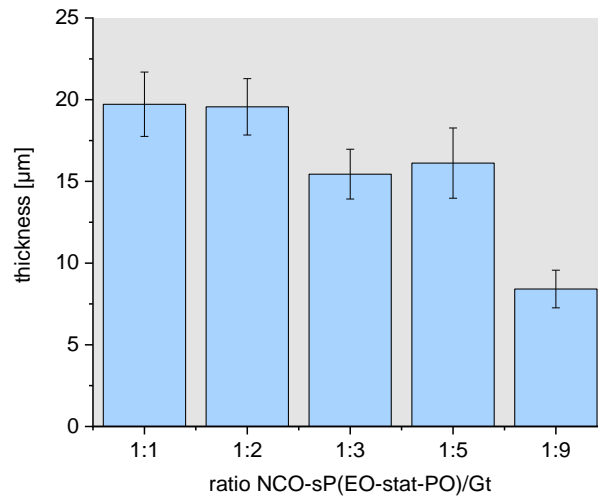


Figure 14: SEM measured average cross section of NCO-sP(EO-stat-PO)/Gt meshes utilized for tensile testing.

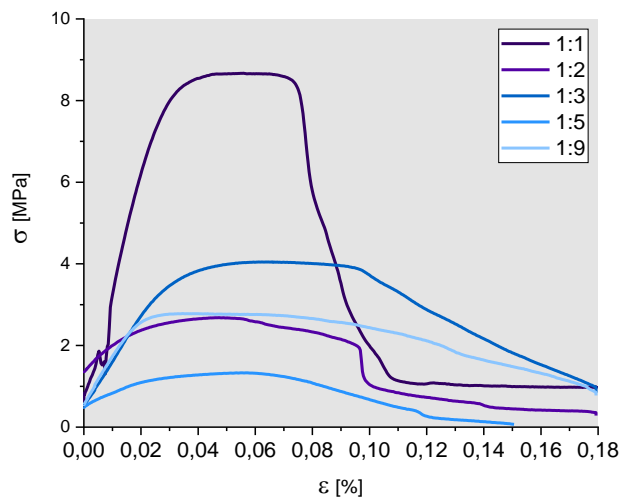


Figure 15: Stress-strain response for electrospun meshes of selected NCO-sP(EO-stat-PO)/Gt ratios under uniaxial tension.

Ultimate tensile strength (UTS), strain at UTS and Young's moduli are displayed in Figure 16. Corresponding to the stress-strain diagram, the highest ultimate strength is measured with ratio 1:1 at 8.75 MPa, however, a great variability in the data has to be taken into account. Nevertheless, all other ratios range at very low values around 0.2 MPa. It can be stated further that 1:1 ratio shows an exceptionally low ductility by contrast with lower ratios, as the strain at UTS was measured as 0.1 % while other ratios reach elongations up to 3 % and more.

4. Results

Also Young's modulus, which represents a measure of a material's resistance to elastic deformation, was measured at 300 MPa for 1:1, other samples with lower NCO-sP(EO-stat-PO) content showed at least 50 % lower values between 50 and 150 MPa. Therefore, equal amounts of NCO-sP(EO-stat-PO) and gelatin seem to enhance not only the tensile strength but also the stiffness of the meshes.

Overall the measured data indicate that an increase in NCO-sP(EO-stat-PO) gives rise to a distinct growth of tensile strength and Young's modulus, i.e. an increase in stability and stiffness. However, no linear correlation of NCO-sP(EO-stat-PO) content and stability could be determined. A decrease in NCO-sP(EO-stat-PO) content on the other hand seems to weaken the material, but may also promote its flexibility.

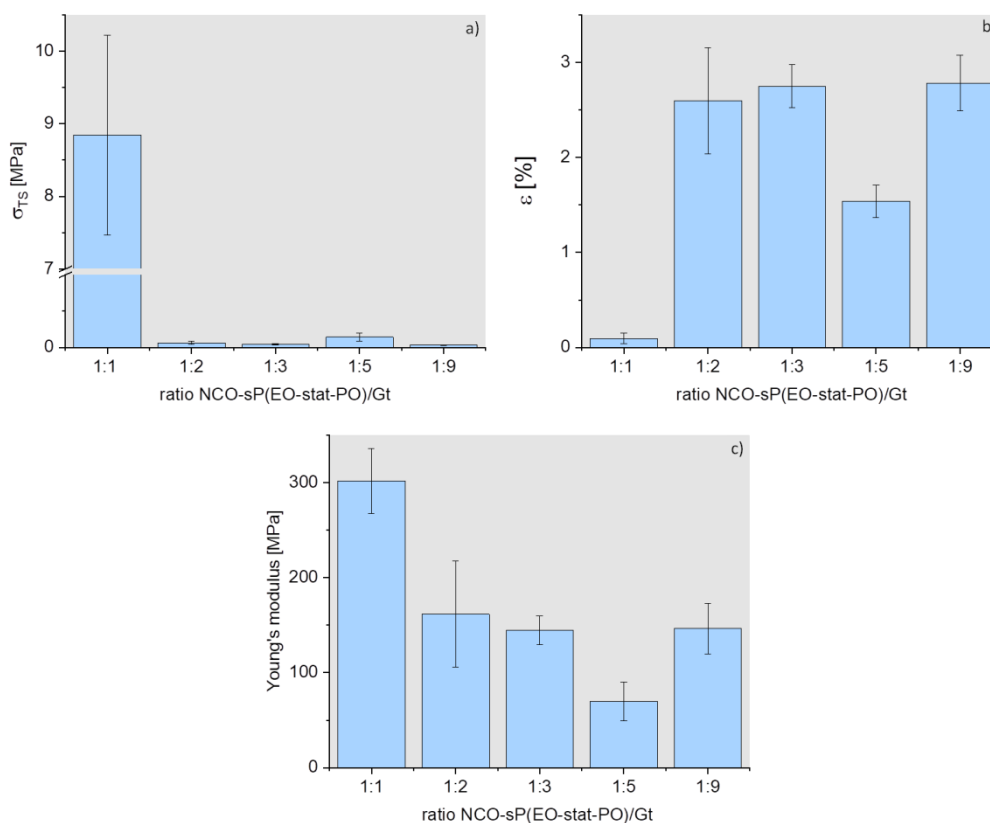


Figure 16: Tensile testing of electrospun hybrid meshes from different NCO-sP(EO-stat-PO)/Gt ratios. a) Ultimate tensile strength (UTS) measured as the maximum tensile stress a scaffold can withstand before breaking, represented in the highest point of the stress-strain curve; b) strain at UTS, describing the level of extension before breaking; c) Young's moduli calculated as the quotient of UTS and strain, describing the material's resistance to elastic deformation.

4.2.4 Weight loss

Weight loss analyses were conducted with three selected NCO-sP(EO-stat-PO)/Gt ratios which yielded promising potential during previous experiments, i.e. ratios 1:3, 1:1 and 3:2. Experiments were carried out in triplicates and subsequently measured values were averaged.

Figure 17 shows the results of analyzing weight loss of electrospun NCO-sP(EO-stat-PO)/Gt meshes after water incubation for three days. It can be determined clearly that ratio 1:3 is the least stable throughout with weight losses around 5 % (w/w). 1:1 lost on average 2.5 %, whereas 3:2 reaches an even higher stability than 1:1, losing about 2 % of its dry weight. Taking into account the standard deviation, ratios 1:1 and 3:2 show a similar loss.

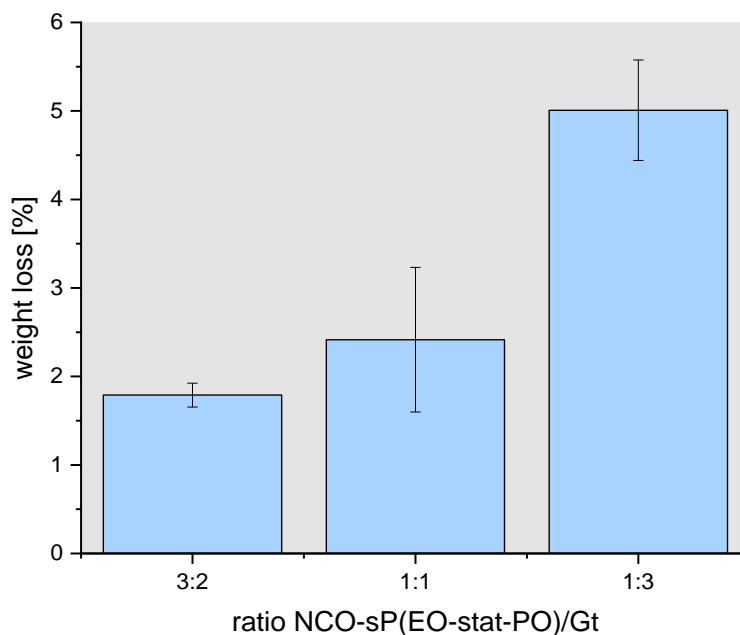


Figure 17: Relative weight loss after 3 days of water incubation for selected NCO-sP(EO-stat-PO)/Gt ratios.

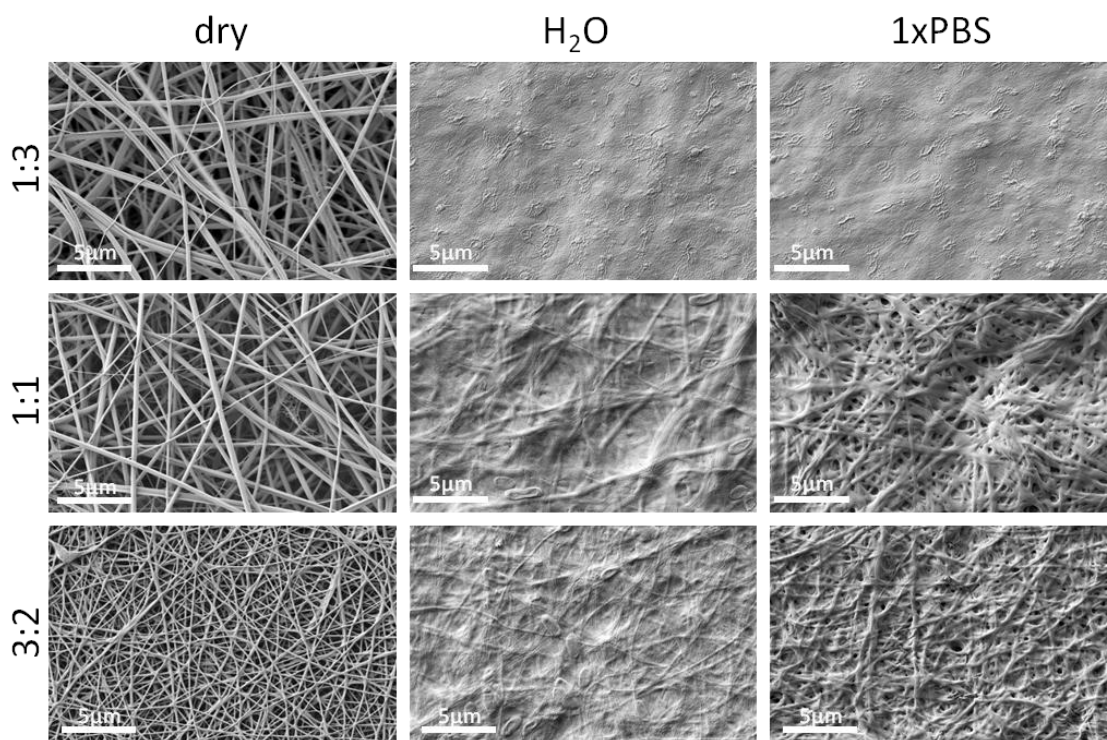


Figure 18: Selected NCO-sP(EO-stat-PO)/Gt ratios after three days of incubation in H₂O and 1xPBS. Fiber stability seems to increase with rising NCO-sP(EO-stat-PO) content and was observed to be much higher after incubation in PBS than in water.

Weight loss experiments were accompanied by SEM imaging of the analyzed samples (ratios 1:3, 1:1, 3:2) before and after incubation in water (Figure 18). Additionally the same samples were immersed in 1xPBS at 37 °C to imitate physiological conditions more closely.

SEM imaging illustrates that the fiber structure in mesh 1:3 is lost completely after three days in H₂O as well as in 1xPBS. The sample surface shows a flat topography with only small patches of material left over in all cases. In group 1:1 the fibers are preserved but show strong swelling in water, associated with a loss of pore space between fibers. This is not the case in 1xPBS where fiber structure is preserved better and pores remain open. The results for 3:2 meshes are similar, but the fiber structure appears more pronounced and shows less swelling than mesh 1:1.

4.2.5 Fiber composition and stability

With the aim at assessing first the reaction of gelatin and NCO-sP(EO-stat-PO), second to compare NCO-sP(EO-stat-PO)/Gt meshes to their base materials, and third to evaluate changes after water incubation, FT-IR spectras were produced within the wavelength range of 500 cm^{-1} and 3500 cm^{-1} of bare porcine gelatin, dry NCO-sP(EO-stat-PO), and NCO-sP(EO-stat-PO)/Gt hybrid meshes in ratios 1:3, 1:1, and 3:2.

Figure 19 presents FT-IR spectra of bare gelatin, dry NCO-sP(EO-stat-PO) and electrospun NCO-sP(EO-stat-PO)/Gt hybrid fibers. Pure gelatin samples show characteristic bands of C=O stretching at 1630 cm^{-1} (amide I), C-N stretching and N-H bending at 1530 cm^{-1} (amide II), CH_2 wagging at 1235 cm^{-1} (Amide III) and N-H stretching of peptide bond at around 3288 cm^{-1} (Amide A).

The dry NCO-sP(EO-stat-PO) samples display a distinct band for N=C=O stretching at 2266 cm^{-1} . In addition, C-O-C stretching and bending of ether at 1105 cm^{-1} and 1240 cm^{-1} , and C-H symmetric vibration at 2868 cm^{-1} could be identified for the NCO-sP(EO-stat-PO) compound.

Spectra of hybrid fibers basically show a blending of both base materials, in that they combine the evident C-O-C stretching band at 1105 cm^{-1} from NCO-sP(EO-stat-PO) and the Amide I, II, III, and A bands of gelatin. Comparing between different ratios of NCO-sP(EO-stat-PO)/Gt meshes, it can clearly be detected that the bands at 2868 cm^{-1} and 1105 cm^{-1} become more pronounced with the increasing amount of NCO-sP(EO-stat-PO). Changes in the spectra after water incubation as displayed in Figure 20 cannot be stated.

4. Results

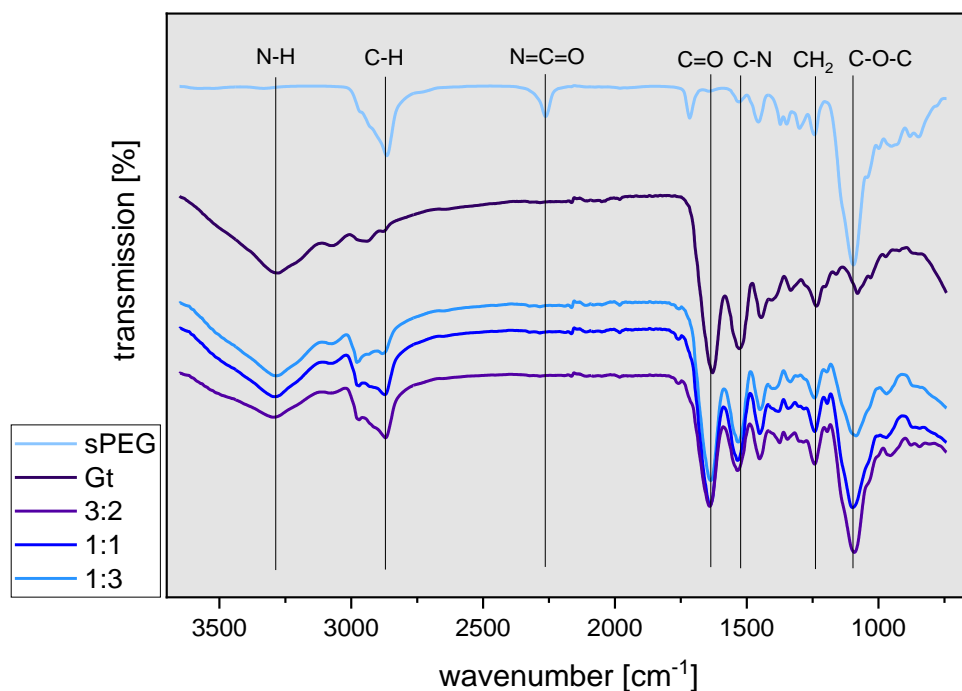


Figure 19: FT-IR spectra of pure NCO-sP(EO-stat-PO) (marked as “sPEG”), pure gelatin, and electrospun hybrid meshes of three selected NCO-sP(EO-stat-PO)/Gt ratios.

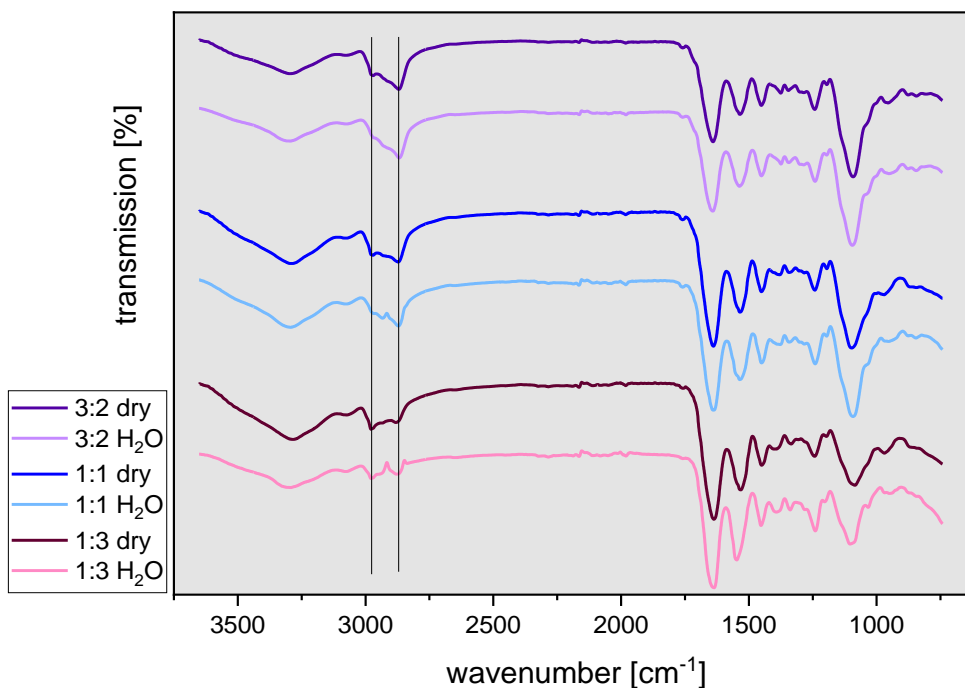


Figure 20: FT-IR spectra of electrospun hybrid meshes of three selected NCO-sP(EO-stat-PO)/Gt ratios in dry state and after water incubation.

4. Results

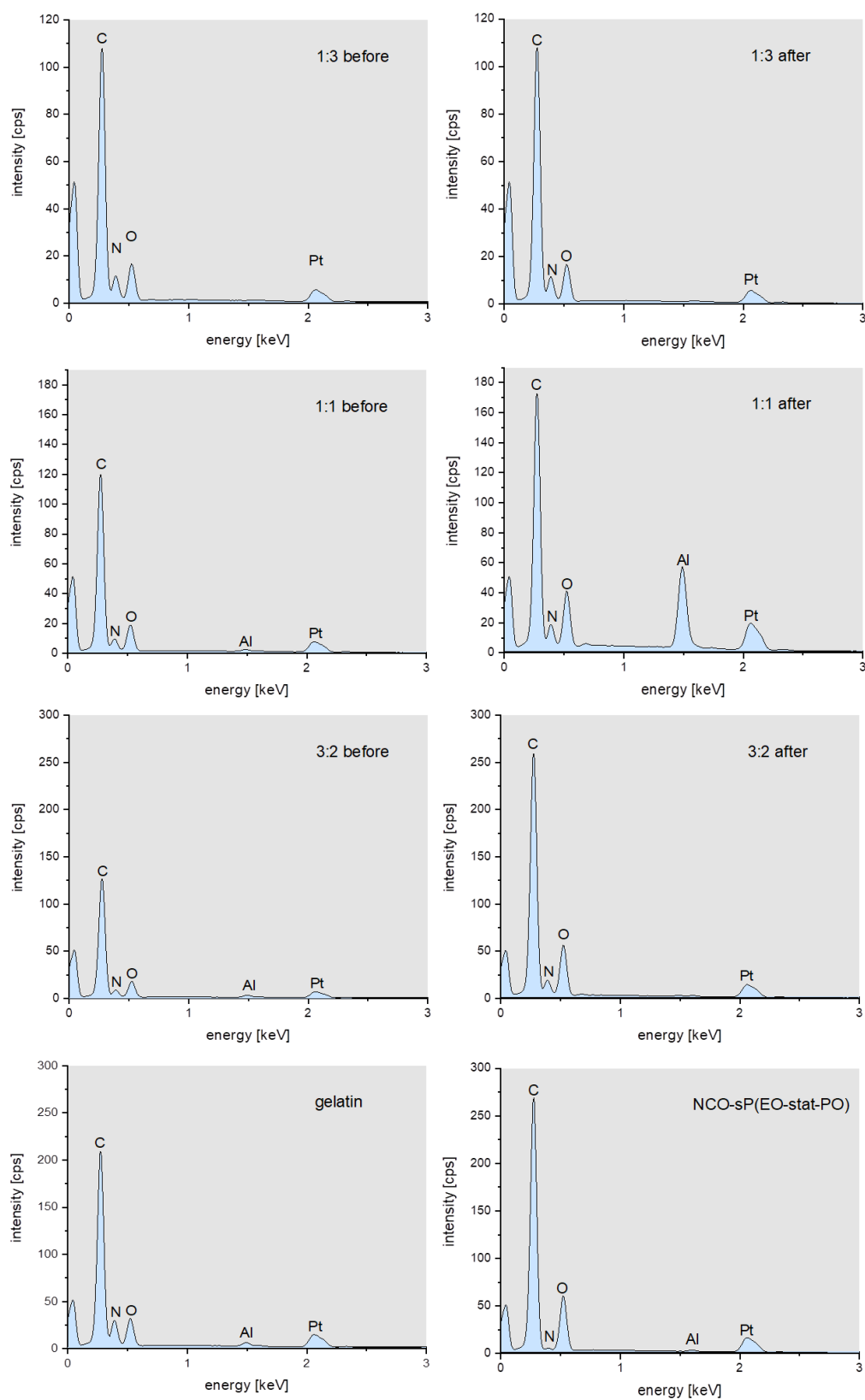


Figure 21: EDX spectra for assessment of water stability for NCO-sP(EO-stat-PO)/Gt ratio 3:2, 1:1, and 1:3 before and after water incubation for three days. Additionally the spectra for pure gelatin and NCO-sP(EO-stat-PO) are given.

4. Results

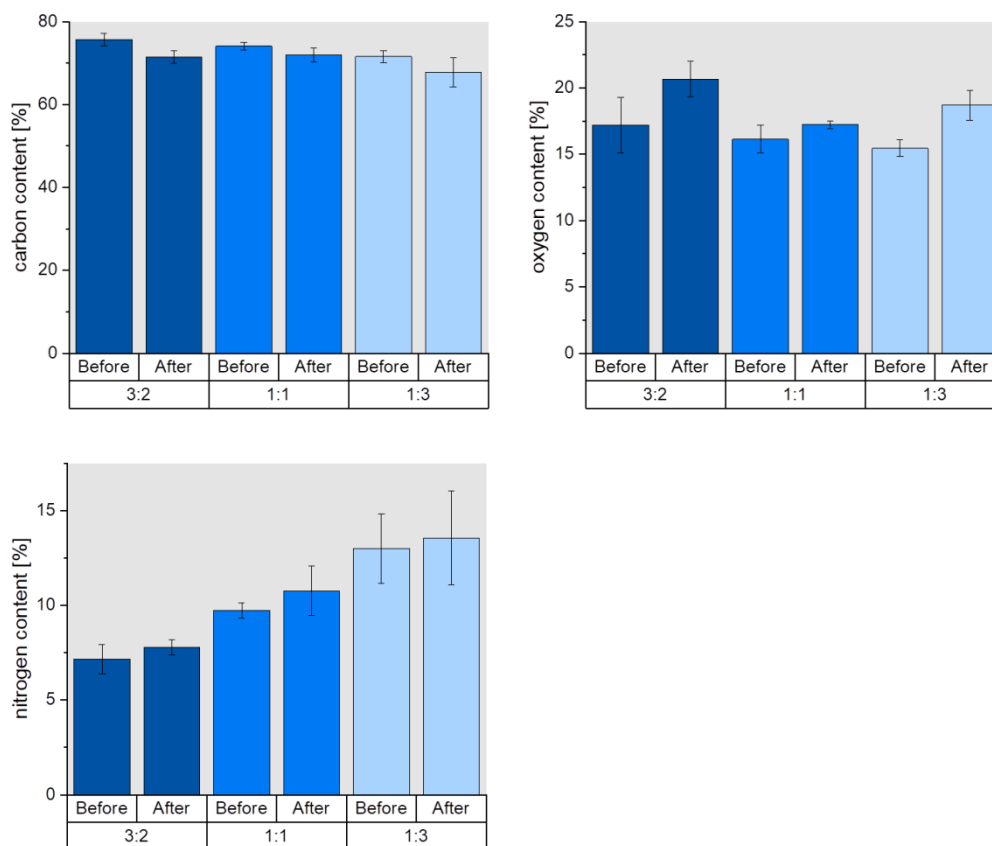


Figure 22: Changes in element contents for NCO-sP(EO-stat-PO)/Gt ratios 3:2, 1:1, and 1:3 before and after three day water incubation.

For EDX measurements samples were analyzed before and after three days of water incubation in order to assess a possible loss of the components gelatin and/or NCO-sP(EO-stat-PO) within the crosslinked meshes in an aqueous environment. The method was set to detect only the elements of interest; therefore measured values were extrapolated to 100 %. Measuring standard deviation was kept constant at 0.1.

An overview of the carbon, oxygen, and nitrogen contents for pure gelatin meshes and NCO-sP(EO-stat-PO) films measured with EDX is given in Table 1 (Appendix). For both gelatin and NCO-sP(EO-stat-PO) carbon makes up for more than two thirds of total measured elements. Gelatin contains comparably high amounts of oxygen and nitrogen, whereas for NCO-sP(EO-stat-PO) no nitrogen could be detected, remarkably as the six-armed molecule is NCO-end-functionalized and should contain a certain amount. However, in the EDX

spectrum for pure NCO-sP(EO-stat-PO) a minor nitrogen peak is visible (Figure 21).

Figure 22 shows the measured changes in element contents for carbon, oxygen, and nitrogen before and after water incubation for three days. A decrease in carbon content was quantifiable for all three ratios at hand, although only for around 5 %. However, the oxygen and nitrogen contents show a rise in both elements after water incubation. Table 2 additionally gives the raw data measured for all batches. Overall, a broad variation in measured values between samples of the same composition is clearly visible. The reliability and significance of trends in element changes measured with EDX will be discussed in chapters 5.2.2 and 5.2.3.

4.2.6 Cytocompatibility

In order to assess cytocompatibility of the hybrid scaffolds electrospun from gelatin and NCO-sP(EO-stat-PO) the meshes were examined in culture with RAW 264.7 cells. SEM images show the cells after 3 days (Figure 24) and after 7 days (Figure 25) of culture on meshes of different NCO-sP(EO-stat-PO)/gelatin ratios, on glutaraldehyde (GA) crosslinked 5 % gelatin meshes for comparison, as well as glass cover slips as a control. Results of the WST-1 viability assay and PicoGreen™ DNA quantification assay are displayed in Figure 23.

SEM imaging revealed that cells adhere and proliferate on all three hybrid meshes, and also on the control slips. On pure gelatin meshes crosslinked with GA the number of attached cells is comparably smaller; cells show smaller diameters, and a high degree of rounding. On hybrid meshes 1:3 and 1:1 a clear loss of fiber structure (especially of ratio 1:3) in accordance with our water incubation experiments is observed, whereas 3:2 fibers retained their original configuration. However, in some samples the fiber structure was surprisingly preserved. Throughout, some cells show rounded shapes, but the degree of rounding appears to be reduced with increasing NCO-sP(EO-stat-PO) amounts in fibers. Also spreading of individual cells seems to be most pronounced in the 3:2 mesh, and in any case it is more distinct than in the GA gelatin scaffolds. Images after 7 days of cell culture display that cell proliferation continues on the control and on the meshes alike; however, a beginning monolayer formation is visible on all scaffolds. But still, cells on mesh 3:2 seem to stretch more and do not cling to each other as much as on other scaffolds. Nevertheless, it is noted that a considerable infiltration into the fibers is lacking.

Cell viability as determined by WST-1 and PicoGreen assays is within an equal range for all three NCO-sP(EO-stat-PO)/Gt ratios. A single optimum ratio cannot be distinguished. However, cell viability as measured by WST-1 is higher on all three electrospun hybrid meshes than on the tissue culture plate (control) and higher than on the GA crosslinked gelatin meshes. PicoGreen yields highest viability values for the control group, but still viability is higher for

4. Results

all electrospun NCO-sP(EO-stat-PO) hybrid meshes than for the conventionally crosslinked gelatin.

Overall, it is obvious that RAW 264.7 cells can attach and grow on all three NCO-sP(EO-stat-PO)/Gt scaffolds. They appear to spread and interact better with the meshes with increasing NCO-sP(EO-stat-PO) contents.

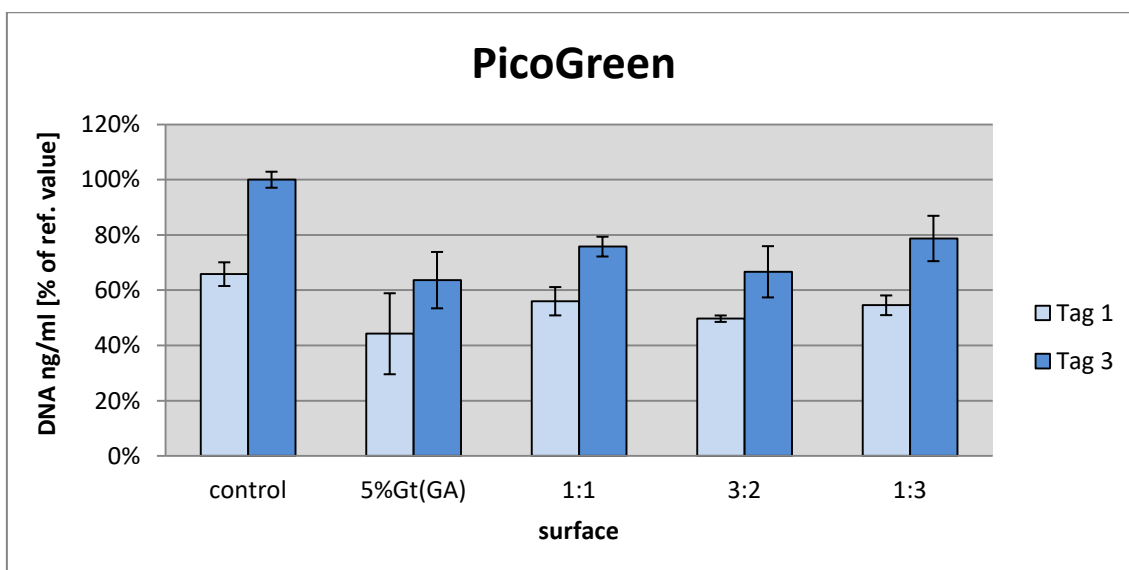
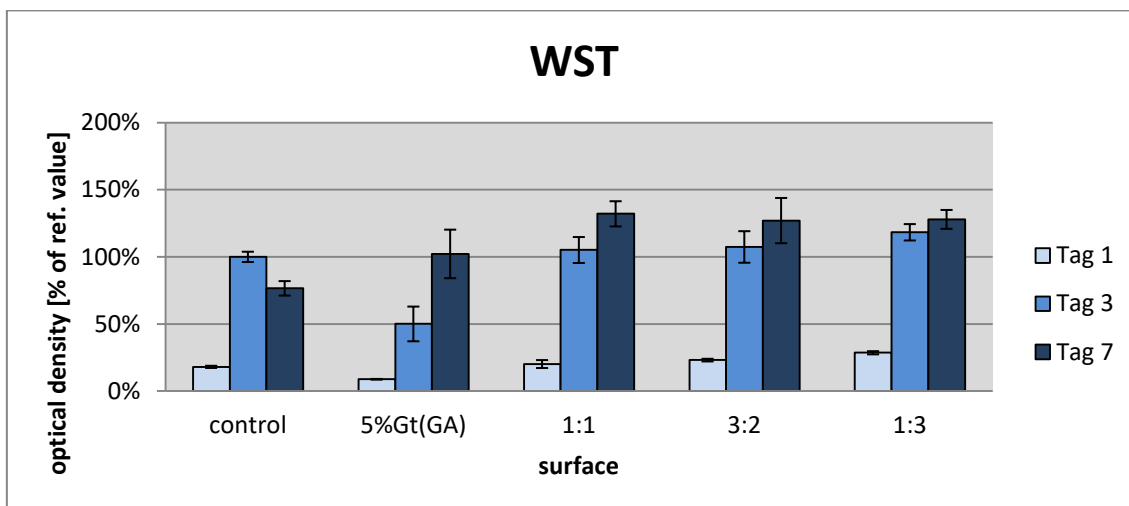


Figure 23: RAW 264.7 cell viability on electrospun hybrid meshes as well as on pure gelatin crosslinked with glutaraldehyde (5%Gt(GA)) and control on tissue culture plate. Values were measured via WST-1 (testing the mitochondrial succinate dehydrogenase of viable cells) and PicoGreen DNA quantification. Due to a loss of material, PicoGreen could not be determined for day 7.

4. Results

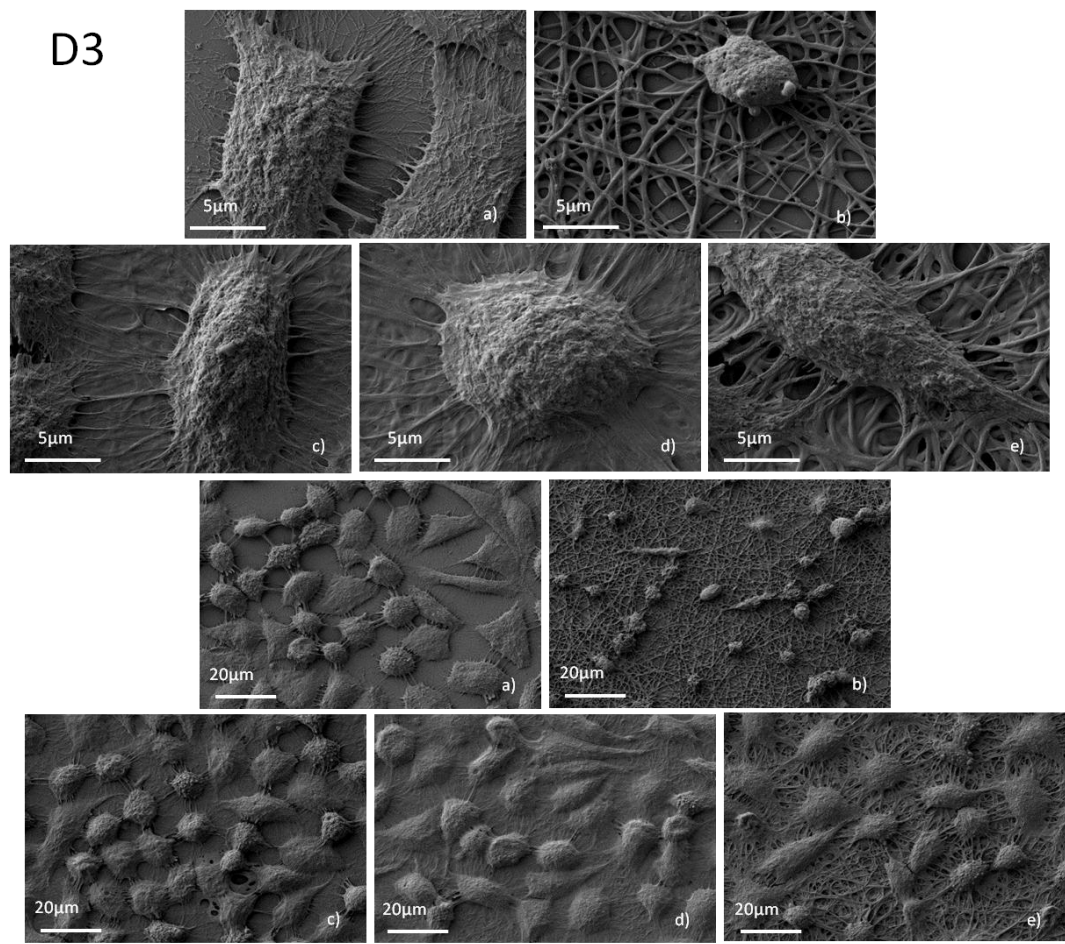


Figure 24: SEM images of RAW 264.7 cells on electrospun meshes after 3 days of cell culture in close-up image and overview. a) control seeding on glass cover slips, b) 5% Gt crosslinked with GA, c) NCO-sP(EO-stat-PO)/Gt 1:3, d) NCO-sP(EO-stat-PO)/Gt 1:1, e) NCO-sP(EO-stat-PO)/Gt 3:2.

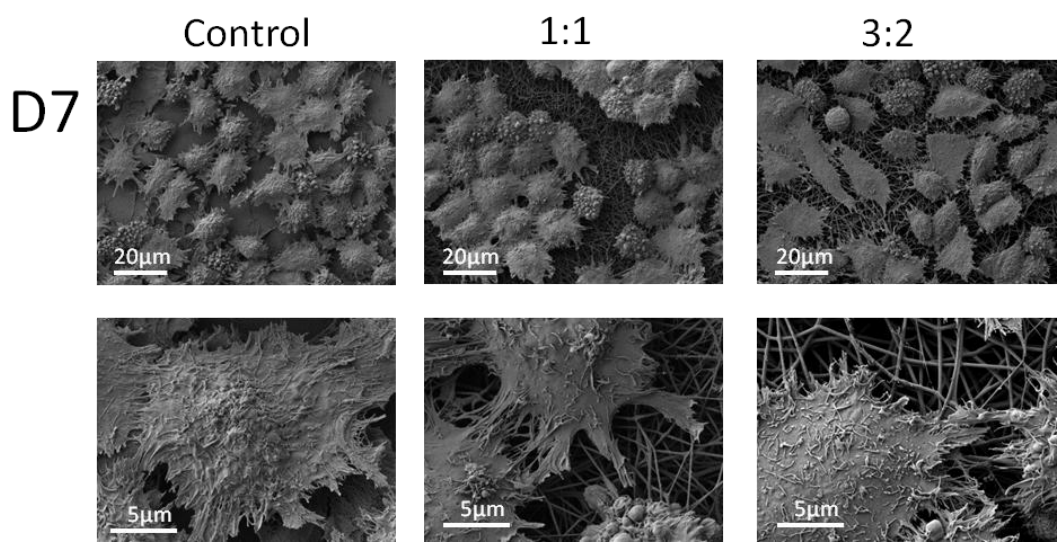


Figure 25: SEM images of RAW 264.7 cells after 7 days of cell culture on control cover glass, NCO-sP(EO-stat-PO)/Gt 1:1, and NCO-sP(EO-stat-PO)/Gt 3:2. Other ratios were contaminated.

5. Discussion

The aim of this study was to establish an electrospinning protocol for NCO-sP(EO-stat-PO)-stabilized and functionalized gelatin fibers, in order to produce water stable, non-cytotoxic tissue engineering scaffolds. It was attempted to achieve this by adding the highly reactive copolymer NCO-sP(EO-stat-PO) to a spinning dope based on gelatin dissolved in HFIP. Thanks to its functional NCO groups, the molecule contains a broad variety of reactivities, which should enable it to form covalent bonds with functional end groups (amines, alcohols) of the gelatin macromolecule. A crosslinking and functionalizing effect of NCO-functionalized components in electrospun polymer fiber scaffolds has been shown for other materials such as PCL [132] and PLGA [116]. However, synthetic polymers in TE materials are known to possibly lead up to inflammation processes during degradation, for example by reducing the local pH in a tissue [133]. Further, aligning degradation time of synthetic materials with wound healing often causes difficulties, as the duration of degradation can strongly deviate from native tissue recovery [134]. Therefore, the application of a natural polymer such as gelatin can yield desirable results in terms of biocompatibility (see chapter 2.2). Combining the favorable properties of gelatin with the stabilizing and functionalizing effects of NCO-sP(EO-stat-PO) appears as an attractive and simple solution to overcome typical limitations of electrospun natural polymers, such as lack in mechanical stability and water resistance, and, at the same time, meet the needs for native ECM mimicry. During fiber production, solution, process, and ambient parameters were varied and assessed, in order to constitute a reproducible fabrication protocol (chapter 4.1). Electrospun fibers were subsequently characterized according to their morphology, hydrophilicity, tensile mechanical properties, weight loss in an aqueous environment, chemical structure, and changes in the very same (chapter 4.2). Finally, cytocompatibility was evaluated in cell culture with murine RAW 264.7 cells (chapter 4.2.7).

5.1 Fiber fabrication: impact of process and solution parameters

The process of electrospinning is governed by numerous parameters, classified roughly into solution, process and ambient parameters [13]. Ambient parameters can hardly be manipulated in the spinning process, despite this fact it was attempted to hold room temperature and humidity constant as far as possible. Further, temperature and humidity were monitored during each spinning process. It has to be taken into account that these parameters could strongly influence fiber morphology and diameter [26]. However, reproducibly homogeneous fibers were successfully produced in the course of this study; it is therefore assumed that variation of ambient parameters did not have a major influence on fiber properties in our case. Deviations within single batches can nevertheless be attributed to temperature and humidity changes. In establishing a spinning protocol, process and solution parameters are the controllable features. Process parameters such as feeding rate, nozzle diameter, applied voltage, needle tip to collector distance, and spinning time in this study were again subject to solution properties. Above all, the process had to be adapted to the low viscosity of the spinning dope. Therefore, a rather slow feeding rate of 0.5ml/hr and a thin 27G needle, as well as a fairly high voltage of 14 kV were necessary to obtain usable gelatin fiber meshes. Spinning time was extended to 1 h for yielding a 20 μm thick mesh at a gelatin concentration of 5 % (w/v). The solution properties in this case are assumed to be mainly governed by the high molecular weight and low solubility of gelatin in an organic solvent like HFIP. It was shown that fiber diameters are clearly proportional to gelatin concentration, whereas the best fiber results were obtained with the lowest concentration of gelatin (5 %). Fiber formation with higher concentrations was possible, but only at the expense of fiber homogeneity, diameter, and porosity. Higher gelatin concentrations (7.5 %, 10 %, 12.5 %) yielded thicker and more irregular fibers, while the pore space was diminishing with increasing gelatin concentration. Therefore, low solution viscosity is obviously a consequence of low gelatin concentration, and does not affect process or fiber quality in a negative way. Further, fiber diameters were shown to correlate with solution viscosity and

gelatin concentration. 5 % Gt concentration yielded fiber diameters of 500 to 1000 nm, which are most convenient for mimicry of natural ECM.

Regarding the choice of solvent, it has to be stated, that water is generally the chemically most suitable and most biocompatible solvent for gelatin. The natural polymer is practically insoluble in most organic solvents, such as alcohol, chloroform, carbon disulfide, ether, benzene, and acetone [135]. In the present case, water as a solvent is only a potential option for pure gelatin solutions, and has been attempted with minor success (ch. 4.1.1). Due to the described high reactivity of NCO-functionalized NCO-sP(EO-stat-PO), an aqueous gelatin solution mixed with NCO-sP(EO-stat-PO) forms a hydrogel within less than three minutes; with loss of all desired functionalities of the star-polymer.

Therefore a different solvent had to be chosen. In past studies, numerous different possibilities have been discussed, such as TFE [70], TFA [9], DMSO, ethylene glycol [136], hyaluronic acid [137], acetic acid [138], formic acid [139], and their aqueous solutions, as well as HFIP [140]. Acidic solvents, such as acetic or formic acid, have been applied with success for pure gelatin fibers or blended fibers with cellulose and have turned out as biocompatible options [141]. However, due to the sensitivity of the gelatin molecule, which is prone to degradation by acids, application of acidic solvents is limited to dilutions in water. For NCO-sP(EO-stat-PO)/gelatin hybrid fibers in the present study an aqueous solution of any chemical must be excluded, in order to avoid premature reactions of NCO-sP(EO-stat-PO) and H₂O, which could negatively interfere with the desired crosslinking of gelatin fibers by NCO-sP(EO-stat-PO) NCO-functional groups.

In the present study, HFIP was chosen as a solvent, as it showed best results in dissolving gelatin, yielding a clear, homogeneous solution after mixing with NCO-sP(EO-stat-PO) dissolved in THF, as well as producing successfully reproducible gelatin and NCO-sP(EO-stat-PO)/gelatin hybrid fibers. HFIP promotes gelatin solubility due to strong hydrogen-bonding properties and its potential to inhibit hydrophobic interactions [142]. Nevertheless, it has to be taken into account that HFIP, just as TFE, TFA, and DMSO, is highly toxic to cells, and its residual amounts may leak from an implanted scaffold into the

body [143]. It has further been demonstrated that HFIP induces protein denaturation, specifically in increasing the percentage of α -helical secondary structures [144]. All of these substances can therefore never be seen as an ideal solution for native tissue engineering [145]. However, this drawback was accepted in the present *in vitro* study in order to investigate primarily the *in situ*-crosslinking properties of NCO-sP(EO-stat-PO) in hybrid NCO-sP(EO-stat-PO)/gelatin fibers. The aim of the described experiments was not to establish a more biologically compatible solvent, which evidently is an issue of great relevance. On the other hand, the aggressive potential of HFIP may also have been responsible for limitations detected during the experiments described in the present study in our electrospun meshes.

5.2 Fiber characterization

5.2.1 Fiber morphology: impact of polymer concentration and ratio

Pure gelatin fibers were fabricated in polymer concentrations of 5 %, 7.5 %, 10 %, and 12.5 %, whereas a 15 % solution was not spinnable due to its high viscosity (see ch. 5.1). An effect of variation in gelatin concentration was clearly detectable during SEM imaging of the electrospun fibers regarding fiber morphology, homogeneity, and mesh porosity. As described above, fiber diameters were shown to increase with growing gelatin concentrations, while porosity and structural homogeneity decrease analogously. During pre-experiments, these fiber properties could be successfully reproduced and therefore provided tunable fiber morphology. This may be potentially useful in adapting fiber morphology to suit a specific application, and may further be interesting for so-called gradient electrospinning, where variable fiber diameters are produced within a single mesh, resulting in scaffolds of superior material properties as opposed to scaffolds using only one concentration of polymer [146].

Compared to all ratios of NCO-sP(EO-stat-PO)/Gt hybrid fibers, pure gelatin always yielded fibers of larger diameters. Within hybrid fibers, an increase in diameter with increasing NCO-sP(EO-stat-PO) content was observed. Fiber diameters are known to be the product of a complex interaction of applied

voltage, strength of the electrical field, polymer concentration, conductivity of the solvent, and evaporation speed of the solvent [147]. As there is a multitude of interconnected influencing factors, it is impossible to make a statement on what is the exact causality of hybrid fibers being thinner than pure Gt fibers. Process parameters such as applied voltage and resulting field strength remained unchanged in both cases. It is clear, however, that a reaction must be taking place during hybrid fiber fabrication, resulting in a change of physical, in particular rheological, solution properties. Two major factors determining fiber size and shape are jet ejection from the needle tip and whipping of the jet due to bending instabilities [148]. Jet ejection at a critical voltage is linked to solution viscosity as well as to electric conductivity. It can therefore be assumed that the reaction of NCO-sP(EO-stat-PO) and gelatin leads to a change in these parameters. The same may be true for jet whipping in the electrical field.

Fiber diameters increase with increasing NCO-sP(EO-stat-PO) content, but are always thinner than the pure Gt fibers. They reach a maximum thickness at NCO-sP(EO-stat-PO)/Gt ratio 1:1; once the NCO-sP(EO-stat-PO) content exceeded the amount of Gt (in ratio 3:2), very thin fibers again were observed. This can easily be explained by total polymer concentration (Gt+NCO-sP(EO-stat-PO)) in the solution, which had to be reduced by 50 % in the latter solution due to its high viscosity and in order to fabricate a spinnable solution. The total polymer concentration in this solution was obviously lower than in all batches before, which explains smaller diameters of these fibers.

Apart from variation in fiber diameters, a shift in fiber shapes from ribbon (in pure Gt) to rounded (in 1:10 NCO-sP(EO-stat-PO)/Gt) was observed. The ribbon shape is most prominently realized in pure Gt fibers, whereas 1:1 and 1:2 ratios show similar appearance. Lowest NCO-sP(EO-stat-PO) contents (1:10) lead to almost exclusively rounded fibers. From our point of view it may be possible that the round fiber shape occurs via a sort of longitudinal folding of the previous ribbon structure. Topuz & Uyar [131] attribute flat ribbon shapes to higher polymer concentrations and fast evaporation of the solvent from the mesh structure, as opposed to rounded shapes, where solvent evaporates more slowly, combined with a lower polymer concentration and fibers are given more

time to slowly roll up. This corresponds to our observations when higher NCO-sP(EO-stat-PO)/Gt ratios lead to more flattened structures, and lower ones to round fibers.

Next to fiber shapes, the investigation of crosslinking effects in the hybrid fibers was a major aim of the study. Visibly crosslinked fibers were exclusively recognized under SEM imaging in 3:2 ratio. It was demonstrated in the present study, that hybridization of gelatin fibers with NCO-sP(EO-stat-PO) induces stabilization in comparison to pure gelatin fibers, with increasing effects proportional to the applied amount of NCO-sP(EO-stat-PO). However, fibers did not show a crosslinked appearance apart from ratio 3:2. It has to be considered that a visible crosslinking only takes place when NCO-sP(EO-stat-PO) content exceeds that of gelatin. As a possible reason it is assumed that NCO groups of NCO-sP(EO-stat-PO) may react with OH groups of the solvent HFIP rather than with functional end groups (NH₂, OH) of gelatin to a certain extent. Nevertheless, a stabilizing effect is measurable regardless the visibility.

5.2.2 Fiber stability: tensile strength and water resistance

Mechanical performance of a scaffold is an important parameter in both cell culture and tissue engineering, as tensile properties reflect on the strain and stress resistance of the material [149]. The NCO-sP(EO-stat-PO)/Gt hybrid meshes tested in this study represented ratios 1:1, 1:2, 1:3, 1:5, and 1:9, and give insight into the variation of mechanical properties along increasing NCO-sP(EO-stat-PO) contents. However, testing of pure gelatin meshes failed, as their fragility did not allow utilizing them in the testing setup. Electrospun bare gelatin scaffolds in other studies reached ultimate tensile strengths of 0.7 MPa (uncrosslinked) [150], 2.5 MPa [151, 152], 9.1 MPa (both crosslinked with glutaraldehyde) [153], and 22 MPa (crosslinked with genipin) [154].

Regarding hybrid scaffolds, the highest tensile strength achieved in this study was measured for 1:1 NCO-sP(EO-stat-PO)/Gt ratio at an average 8.5 MPa and a maximum 10.2 MPa. All other ratios of hybrid meshes remained below this value, ranging between 2 and 4 MPa. A rise in tensile strength with increasing

NCO-sP(EO-stat-PO) content can be stated. Hybrid scaffolds in similar studies were mostly fabricated by blending gelatin with PCL, which individually taken was reported to have a tensile strength between 3.8 MPa [155] and 12 MPa [156]. Blended PCL/gelatin fiber scaffolds displayed values of 3.7 MPa in a 2:1 PCL/Gt ratio [157]. Other researchers blended 70 % gelatin with 30 % PLLA and reached a tensile strength of 14 MPa [154].

Regarding elasticity the hybrid meshes show comparably high Young's moduli of approximately 300 MPa for 1:1, around 150 MPa for 1:2, 1:3, and 1:9, and 60 MPa for ratio 1:5. This may be partially attributed to the gelatin component, which by itself shows high rigidity. Zhang et al. [151] report a modulus of 105 MPa for pure gelatin, whereas a PCL/gelatin hybrid mesh was measured with 30.8 MPa. This decrease is ascribed to the influence of PCL's high elasticity. Young's moduli for hybrid fibers of 1:1 PLLA/Gt were measured at around 300 MPa [154]. In future research on NCO-sP(EO-stat-PO)/Gt fibers it might be interesting to further investigate the tensile moduli of pure NCO-sP(EO-stat-PO) and its influence on rigidity. It is assumed that by forming a chemically crosslinked layer, the stiffness of, for example, an NCO-sP(EO-stat-PO) film will be very high. Therefore, also the electrospinnability of pure NCO-sP(EO-stat-PO) might be interesting to be looked into. In our scaffolds the resistance against deformation is highest with the highest NCO-sP(EO-stat-PO) content, and diminishes with decreasing amounts. An increase in NCO-sP(EO-stat-PO) makes the material more stable, but also more rigid. A requirement for tissue engineering materials is stability on the one hand, but also a certain flexibility and resilience.

In the context of tissue engineering materials, the tensile strength and Young's moduli results of in situ crosslinked fibers fabricated in our study are within the range of other comparable materials. However, mechanical properties of electrospun fibers are highly dependent on process parameters. Polymer composition, fiber diameter and orientation influence strongly tensile strength and modulus [158]. It has been shown in the previous chapters, that NCO-sP(EO-stat-PO)/Gt fibers offer a broad range of possibilities to adapt and customize several parameters.

Next to mechanical stability, water stability of electrospun NCO-sP(EO-stat-PO)/Gt fibers was determined. Fibers were immersed in deionized water for the duration of three days. Overall, weight loss did not exceed 6 % of the original weight for all tested meshes; specifically, 3:2 meshes lost 2 wt%, 1:1 2.5 wt%, and 1:3 showed a loss of around 5 wt%.

It was reported that in hybrid gelatin/shellac composites an increasing amount of gelatin gives rise to more swelling, and therefore a loss of water stability [159]. This is in accordance with our results, where weight loss experiments and SEM imaging confirm a higher stability for higher ratios of NCO-sP(EO-stat-PO), which corresponds to relatively lower amounts of gelatin. SEM images further show that superficial fiber structure is completely lost for ratio 1:3, distinctly worn out for ratio 1:1, and still negatively affected for 3:2 after three days in water. Fiber stability appears to be higher after same time incubation in 1xPBS. It is assumed that mineral components in PBS help to support the preservation of fiber structures. Yu et al. [160] illustrate that mineral coatings containing calcium and phosphate can help stabilize protein conformational structures thanks to organizing nanoscale surface features which prohibit aggregation and loss of conformation in protein molecules.

Weight loss experiments showed that material loss in the scaffolds is minor; however, there is a clear loss in fibrous structure. It was interesting to see which component is lost, as it may allow concluding which parameter failed to react in the crosslinking reaction, and further what prevents higher fiber stability. In order to evaluate closer reaction and change in components after water incubation, FT-IR and EDX measurements were carried out. FT-IR confirmed that fiber composition does not change strongly by water (see chapter 5.2.3). In EDX a change in elemental contents before and after water was discernible; carbon is lost, whereas a general increase in nitrogen and oxygen was noted. The spectrum for gelatin is in accordance with other reported measurements [161]. Nevertheless, the fact that the nitrogen content in NCO-sP(EO-stat-PO) could not be detected, although each of the molecule's six arms is isocyanate functionalized, gives reason to doubt the reliability of the method. The position of the nitrogen peak within the spectrum, partly overlapped by C and O peaks,

might be partly responsible for difficulties in detecting it. To the best of our knowledge, EDX analyses of different gelatin/crosslinking agent ratios in the context of element loss have not been performed by other researchers yet. Therefore, the choice of method may have to be questioned overall. These results can be seen as preliminary information and require further investigation with a more specific methodology. However, elemental composition of the examined samples shifts after water incubation. This at least indicates that water incubation is responsible for a certain loss of material. A possible explanation for this might be a preliminary reaction of isocyanates with hydroxyl groups of the solvent HFIP, inhibiting full reaction of NCO-sP(EO-stat-PO) and gelatin. Concluding from this argumentation the lost component must be gelatin.

5.2.3 Fiber composition: chemical structure and reaction

With the aim of assessing the chemical structure and thus the reaction of gelatin and NCO-sP(EO-stat-PO), FT-IR spectra were produced within the wavelength range of 3500 cm^{-1} and 500 cm^{-1} from all involved base materials and their hybrid meshes of different ratios. In general, infrared spectra of proteins exhibit 5 characteristic bands, three of which are referred to as amide bands [129]. Strongest infrared absorption takes place in the Amide I band between 1600 and 1700 cm^{-1} . It is mostly evoked by C=O stretching vibrations. In the present study a band at 1630 cm^{-1} was related to this (Figure 19). The Amide II band is generally found at 1500 to 1600 cm^{-1} , caused mainly by C-N stretching and is expressed in our gelatin at 1530 cm^{-1} . Lastly, Amide III band is represented at 1235 cm^{-1} and therefore within with the general range of 1200 - 1300 cm^{-1} . The exact position of the bands is strongly influenced by the molecule backbone conformation and hydrogen bonds [162]. Therefore, the chemical structure of gelatin used for our experiments is in general accordance with proteins FT-IRs in literature [163].

Comparing the dry NCO-sP(EO-stat-PO) samples with hybrid NCO-sP(EO-stat-PO)/Gt meshes an obvious band for N=C=O stretching at 2266 cm^{-1} is found in NCO-sP(EO-stat-PO), which is not visible in the hybrid samples. This may

indicate that NCO groups were fully reacted during mixing with gelatin. Looking at the hybrid samples, the more pronounced bands at 2868 cm^{-1} and 1105 cm^{-1} with the increasing amount of NCO-sP(EO-stat-PO) clearly imply a successful incorporation of hybrid samples.

As expected, the FT-IR analysis of hybrid samples 1:3, 1:1, and 3:2 before and after water incubation did not result in significantly different bands, since weight loss analysis also showed only a minimum amount of mass loss (see chapter 4.2.4). However, a close look at the regions of 2868 cm^{-1} and 2960 cm^{-1} corresponding to C-H symmetric vibration and C-H asymmetric vibrations indicate, that the 2868 cm^{-1} band is more dominant compared to the small shoulder at 2960 cm^{-1} , although both bands are present in NCO-sP(EO-stat-PO). Since pure gelatin omits a band at 2868 cm^{-1} but presents a small band at 2960 cm^{-1} , a comparison of those bands before and after water incubation may suggest which material is preferentially lost during water incubation. As all water treated spectra show a smaller band/shoulder at 2960 cm^{-1} compared to their dry counterparts, gelatin might be the component which was washed out more than NCO-sP(EO-stat-PO). This would also coincide with conclusions drawn in chapter 5.2.2.

5.2.4 Fiber biocompatibility: hydrophilicity and cell viability

For implantation, cell growth, attachment, infiltration, differentiation, and biocompatibility in general, hydrophilicity of a scaffold is a crucial parameter. Cell attachment behavior can strongly be influenced by surface wettability [164]. It is reported that hydrophilicity of a fiber surface can be altered by blending polymers with different properties [165, 166]. In adding NCO-sP(EO-stat-PO) to pure gelatin fibers, the hydrophilicity and wettability should certainly be increased, regarding the high reactivity of its NCO-functionalized end groups with water. In the present study changes in hydrophilicity were determined by water contact angle measurements. Lowest wettability was found in pure 5 % gelatin fibers as well as in NCO-sP(EO-stat-PO)/Gt ratio 1:10 with contact angles around 50° . This value is still in a range to be described as very

hydrophilic [167]. Increasing NCO-sP(EO-stat-PO) contents induced an almost linear increase in infiltration capacity, indicating rising hydrophilicity. The smallest contact angles were measured for NCO-sP(EO-stat-PO)/Gt ratio 3:2 at 21°, reflecting the highest amount of NCO-sP(EO-stat-PO). Contact angles measured in comparable studies were between 10 and 35° for PCL/Gt fibers [168], 45° for PCL/Gt fibers crosslinked with polyglycerol sebacate [169] and 74° for gelatin fibers crosslinked with bisvinyl sulfonemethyl [170]. All of these scaffolds were tested successfully in *in vitro* cell culture or *in vivo*, indicating that our own fibers may also be promising for *in vitro* cell culture in terms of wettability.

In culture with RAW 264.7 cells it was shown that cells are able to attach and grow on the electrospun NCO-sP(EO-stat-PO)/Gt fibers. In comparison with 5 % Gt crosslinked with glutaraldehyde, the most common crosslinking method for gelatin fibers, cells showed better adhesion, proliferation, and spreading. Enzymatic and DNA quantification assays demonstrated up to 20 % higher cell viability on the electrospun hybrid meshes than on GA crosslinked gelatin. The extent of cell rounding, indicating suboptimal and proinflammatory living conditions [171], seems to decrease with increasing NCO-sP(EO-stat-PO) content of the meshes. Overall, a general cytocompatibility of the material can be stated, which is in any case better than on conventionally crosslinked gelatin fibers.

Regarding stability of the fiber structure, it was noted that 3:2 fibers were preserved, whereas fibers are either lost or swollen in ratio 1:3 and 1:1. In some samples, however, the fibers surprisingly were perfectly preserved. This may be attributed to sterilization of the meshes before starting cell culture with UV light. It has been reported that *in situ* UV crosslinking during the spinning process can enhance mechanical strength and water stability of electrospun gelatin fibers and also hybrid fibers of polyacrylic acids and gelatin [91, 172]. An effective post-process crosslinking with UV light has also been demonstrated [173].

Despite cell adhesion and proliferation a lack in infiltration into the fibers was noted. It has been demonstrated that low porosity of a fiber scaffold can limit cell infiltration [174]. Pores in our electrospun hybrid meshes are not generally

5. Discussion

assumed to be too small; however, in lower NCO-sP(EO-stat-PO)/Gt ratios, fiber swelling was observed. Obviously, this is also associated with a loss of pore space. This may explain the lack of infiltration especially on the swollen meshes, while infiltration was found more distinct in 3:2 meshes with better preserved fibers. If fiber stability in culture could be improved, it is likely that infiltration could also increase.

6. Summary and outlook

The present study was carried out with the aim of fabricating electrospun gelatin nanofibers, *in situ* functionalized and stabilized during the spinning process with highly reactive NCO-sP(EO-stat-PO). Scaffolds were required to be reproducible, homogeneous, stable, flexible, and biocompatible, aiming at mimicking natural ECM structures as closely as possible. In the first part of our experiments the main focus was placed on establishing a spinning protocol in order to fabricate bead-free fibers with suitable handling properties and stability to perform further investigations such as mechanical testing, water contact angle determination, water and PBS incubation, FT-IR, and EDX measurements. Fiber morphology was extensively analyzed via SEM imaging. Finally, the scaffolds were examined in terms of their biocompatibility in cell culture with murine RAW 264.7 macrophages.

Regarding fabrication it was found that gelatin concentration sets the baseline for fiber quality. A concentration of 5 % (w/v) gelatin yielded fibers with diameters in the range of native ECM (250 – 900 nm), and was therefore chosen as basic solution to be mixed with NCO-sP(EO-stat-PO). Electrospinning of homogeneous, bead-free hybrid NCO-sP(EO-stat-PO)/gelatin fibers in ratios varying from 1:10 up to 3:2, was successfully accomplished. High NCO-sP(EO-stat-PO) amounts, as applied in ratios 1:2 and 1:1, produced broad fiber diameters similar to pure gelatin, between 700 and 900 nm, whereas this was not found possible in lower NCO-sP(EO-stat-PO) contents and 3:2 meshes, which only allow for diameters between 250 and 600 nm. A general increase in fiber diameter with increasing NCO-sP(EO-stat-PO) content was detected. In accordance with literature fiber shape was flat and ribbon shaped for high polymer concentrations, e.g. 1:1 and pure gelatin, whereas in lower NCO-sP(EO-stat-PO)/Gt ratios rounded fibers occurred.

Mechanical properties of the scaffolds were evaluated with uniaxial tensile tests. Ultimate tensile strength of 8.5 MPa and Young's moduli between 150 and 300 MPa can stand comparison with other fibers in comparable studies. Water stability of the meshes was further assessed in water incubation experiments. Ratio 3:2 proved to be most water stable, but in all three ratios selected for

testing, fiber structure was either entirely lost (1:3) or fibers showed distinct swelling (1:1, 3:2). Much better structural preservation was observed after incubation in 1xPBS. It is assumed that minerals in the solution support fiber stability. Fiber composition was investigated via FT-IR, EDX, and weight loss measurements. The desired crosslinking reaction between NCO-sP(EO-stat-PO) and gelatin was found to be successful to a substantial extent. However, it requires further investigation. It was observed in weight loss experiments that a loss of material, although minor (<6 %), is discernible. EDX results hint at a shift in element composition towards higher nitrogen and oxygen (+5-10 %), and lower carbon contents (-5 %) after water incubation. This is in accordance with weight loss, so it is likely that a component is partially lost. FT-IR spectra indicated further that NCO-sP(EO-stat-PO) had fully reacted, whereas hybrid meshes show smaller gelatin bands after incubation, which was interpreted as washing out of gelatin. In order to further investigate how to stabilize this composition, it remains to be evaluated what amount of reactivity may possibly exist between NCO-sP(EO-stat-PO) and solvent components. We suspect that hydroxyl groups of HFIP might react with NCO groups of NCO-sP(EO-stat-PO), disturbing the desired reaction of NCO-sP(EO-stat-PO) and gelatin to a certain extent, although the reaction is not fully inhibited.

In terms of biocompatibility, it was shown that hydrophilicity of the already hydrophilic pure gelatin could be further increased with addition of NCO-sP(EO-stat-PO), and a linear progression of wettability with rising contents could be stated. During cell culture it was found that RAW 264.7 cells can successfully adhere and proliferate on the electrospun hybrid meshes. Cell growth and attachment was observed to be better on the NCO-sP(EO-stat-PO) stabilized scaffolds than on the same gelatin meshes conventionally crosslinked with glutaraldehyde. However, if higher fiber stability was achieved, cell infiltration could be improved even further.

It was shown that the natural polymer gelatin can be effectively co-electrospun with NCO-sP(EO-stat-PO) to fabricate biocompatible and stable fiber scaffolds. Future research should primarily aim at perfecting the crosslinking reaction, with a special focus on the solvent component.

7. References

1. Place, E.S., N.D. Evans, and M.M. Stevens. *Complexity in biomaterials for tissue engineering*. Nature Materials, 2009. **8**(6): p. 457-470.
2. Seal, B., T. Otero, and A. Panitch. *Polymeric biomaterials for tissue and organ regeneration*. Materials Science and Engineering: R: Reports 2001. **34**(4): p. 147-230.
3. Dvir, T., B.P. Timko, D.S. Kohane, and R. Langer. *Nanotechnological Strategies fro Engineering Complex Tissues*. Nature Nanotechnology, 2011. **6**: p. 13-22.
4. Hollister, S.J. *Porous scaffold design for tissue engineering*. Nature Materials, 2005. **4**(7): p. 518-524.
5. Puppi, D., X. Zhang, L. Yang, F. Chiellini, X. Sun, and E. Chiellini. *Nano/microfibrous polymeric constructs loaded with bioactive agents and designed for tissue engineering applications: a review*. Journal of Biomedical Materials Research. Part B, Applied Biomaterials, 2014. **102**(7): p. 1562-1579.
6. Theocharis, A.D., S.S. Skandalis, C. Gialeli, and N.K. Karamanos. *Extracellular matrix structure*. Advanced Drug Delivery Reviews, 2016. **97**: p. 4-27.
7. Ma, P.X. *Scaffolds for tissue fabrication*. Materials Today, 2004. **7**(5): p. 30-40.
8. Li, M., M.J. Mondrinos, M.R. Gandhi, F.K. Ko, A.S. Weiss, and P.I. Lelkes. *Electrospun protein fibers as matrices for tissue engineering*. Biomaterials, 2005. **26**(30): p. 5999-6008.
9. Aldana, A.A. and G.A. Abraham. *Current advances in electrospun gelatin-based scaffolds for tissue engineering applications*. International Journal of Pharmaceutics, 2017. **523**(2): p. 441-453.
10. Sell, S.A., M.J. McClure, K. Garg, P.S. Wolfe, and G.L. Bowlin. *Electrospinning of collagen/biopolymers for regenerative medicine and cardiovascular tissue engineering*. Advanced Drug Delivery Reviews, 2009. **61**(12): p. 1007-1019.
11. Lord Rayleigh, F.R.S. *On The Instability Of Jets*. Proceedings of the London Mathematical Society, 1878. **s1-10**(1): p. 4-13.
12. Formhals, A. *Process and apparatus for preparing artificial treads*. United States Patent Office, 1934. **Patent No. 1975504**.
13. Bhardwaj, N. and S.C. Kundu. *Electrospinning: a fascinating fiber fabrication technique*. Biotechnology Advances, 2010. **28**(3): p. 325-347.
14. Jin, G., R. He, B. Sha, W. Li, H. Qing, R. Teng, and F. Xu. *Electrospun three-dimensional aligned nanofibrous scaffolds for tissue engineering*. Materials Science & Engineering C, Materials for Biological Applications, 2018. **92**: p. 995-1005.
15. Sell, S., C.P. Barnes, M. Smith, M.J. McClure, P. Madurantakam, J. Grant, M. McManus, and G.L. Bowlin. *Extracellular matrix regenerated: tissue engineering via electrospun biomimetic nanofibers*. Polymer International, 2007. **56**(11): p. 1349-1360.

7. References

16. Taskin, M.B. *Functional Electrospun Fibers for Extracellular Matrix Mimicry*. Interdisciplinary Nanoscience (INANO) Center. 2016. Aarhus. 171pp.
17. Sridhar, R., R. Lakshminarayanan, K. Madhaiyan, V. Amutha Barathi, K.H. Lim, and S. Ramakrishna. *Electrosprayed nanoparticles and electrospun nanofibers based on natural materials: applications in tissue regeneration, drug delivery and pharmaceuticals*. Chemical Society Reviews, 2015. **44**(3): p. 790-814.
18. Doshi, J. and D.H. Reneker. *Electrospinning process and applications of electrospun fibers*. Journal of Electrostatics, 1995. **35**: p. 151-160.
19. Pham, Q.P., U. Sharma, and A.G. Mikos. *Electrospinning of polymeric nanofibers for tissue engineering applications: a review*. Tissue Engineering, 2006. **12**(5): p. 1197-1211.
20. Rodriguez, K., J. Sundberg, P. Gatenholm, and S. Renneckar. *Electrospun nanofibrous cellulose scaffolds with controlled microarchitecture*. Carbohydrate Polymers, 2014. **100**: p. 143-149.
21. Pelipenko, J., P. Kocbek, and J. Kristl. *Critical attributes of nanofibers: Preparation, drug loading, and tissue regeneration*. International Journal of Pharmaceutics, 2015. **484**(1): p. 57-74.
22. Wang, X., B. Ding, and B. Li. *Biomimetic electrospun nanofibrous structures for tissue engineering*. Materials Today, 2013. **16**(6): p. 229-241.
23. Ramakrishna, S., K. Fujihara, W. Teo, T. Yong, Z. Ma, and R. Ramaseshan. *Electrospun nanofibers: solving global issues*. Materials Today, 2006. **9**: p. 40-50.
24. Telemeco, T.A., C. Ayres, G.L. Bowlin, G.E. Wnek, E.D. Boland, N. Cohen, C.M. Baumgarten, J. Mathews, and D.G. Simpson. *Regulation of cellular infiltration into tissue engineering scaffolds composed of submicron diameter fibrils produced by electrospinning*. Acta Biomaterialia, 2005. **1**(4): p. 377-385.
25. Sill, T.J. and H.A. von Recum. *Electrospinning: applications in drug delivery and tissue engineering*. Biomaterials, 2008. **29**(13): p. 1989-2006.
26. Li, D. and Y. Xia. *Electrospinning of Nanofibers: Reinventing the Wheel?* Advanced Materials, 2004. **16**(14): p. 1151-1170.
27. Barnes, C.P., S.A. Sell, E.D. Boland, D.G. Simpson, and G.L. Bowlin. *Nanofiber technology: designing the next generation of tissue engineering scaffolds*. Advanced Drug Delivery Reviews, 2007. **59**(14): p. 1413-1433.
28. Yang, D., B. Lu, Y. Zhao, and X. Jiang. *Fabrication of Aligned Fibrous Arrays by Magnetic Electrospinning*. Advanced Materials, 2007. **19**(21): p. 3702-3706.
29. Ren, Y.-J., S. Zhang, R. Mi, Q. Liu, X. Zeng, M. Rao, A. Hoke, and H.-Q. Mao. *Enhanced differentiation of human neural crest stem cells towards the Schwann cell lineage by aligned electrospun fiber matrix*. Acta Biomaterialia, 2013. **9**(8): p. 7727-7736.
30. Doyle, A.D., N. Carvajal, A. Jin, K. Matsumoto, and K.M. Yamada. *Local 3D matrix microenvironment regulates cell migration through*

7. References

- spatiotemporal dynamics of contractility-dependent adhesions*. Nature Communications, 2015. **6**: p. 8720-8735.
31. Grafahrend, D., K.H. Heffels, M. Moller, D. Klee, and J. Groll. *Electrospun, biofunctionalized fibers as tailored in vitro substrates for keratinocyte cell culture*. Macromolecular Bioscience, 2010. **10**(9): p. 1022-1027.
 32. Grafahrend, D., K.H. Heffels, M.V. Beer, P. Gasteier, M. Moller, G. Boehm, P.D. Dalton, and J. Groll. *Degradable polyester scaffolds with controlled surface chemistry combining minimal protein adsorption with specific bioactivation*. Nature Materials, 2011. **10**(1): p. 67-73.
 33. Huang, G., F. Li, X. Zhao, Y. Ma, Y. Li, M. Lin, G. Jin, T.J. Lu, G.M. Genin, and F. Xu. *Functional and Biomimetic Materials for Engineering of the Three-Dimensional Cell Microenvironment*. Chemical Reviews, 2017. **117**(20): p. 12764-12850.
 34. Wei, G., Z. Su, N.P. Reynolds, P. Arosio, I.W. Hamley, E. Gazit, and R. Mezzenga. *Self-assembling peptide and protein amyloids: from structure to tailored function in nanotechnology*. Chemical Society Reviews, 2017. **46**(15): p. 4661-4708.
 35. Kalra, V., J.H. Lee, J.H. Park, M. Marquez, and Y.L. Joo. *Confined assembly of asymmetric block-copolymer nanofibers via multi-axial jet electrospinning*. Small, 2009. **5**(20): p. 2323-2332.
 36. D'Amato, A.R., N.J. Schaub, J.M. Cardenas, A.S. Fiumara, P.M. Troiano, A. Fischetti, and R.J. Gilbert. *Removal of Retained Electrospinning Solvent Prolongs Drug Release from Electrospun PLLA Fibers*. Polymer (Guildford), 2017. **123**: p. 121-127.
 37. Wang, S., Y. Li, R. Zhao, T. Jin, L. Zhang, and X. Li. *Chitosan surface modified electrospun poly(epsilon-caprolactone)/carbon nanotube composite fibers with enhanced mechanical, cell proliferation and antibacterial properties*. International Journal of Biological Macromolecules, 2017. **104**(Pt A): p. 708-715.
 38. Teo, W.E. and S. Ramakrishna. *A review on electrospinning design and nanofibre assemblies*. Nanotechnology, 2006. **17**(14): p. 89-106.
 39. Salifu, A.A., C. Lekakou, and F. Labeed. *Multilayer cellular stacks of gelatin-hydroxyapatite fiber scaffolds for bone tissue engineering*. Journal of Biomedical Materials Research. Part A, 2017. **105**(3): p. 779-789.
 40. Gomes, S.R., G. Rodrigues, G.G. Martins, M.A. Roberto, M. Mafra, C.M. Henriques, and J.C. Silva. *In vitro and in vivo evaluation of electrospun nanofibers of PCL, chitosan and gelatin: a comparative study*. Materials Science & Engineering. C, Materials for Biological Applications, 2015. **46**: p. 348-358.
 41. Shabafrooz, V., M. Mozafari, D. Vashaei, and L. Tayebi. *Electrospun nanofibers: from filtration membranes to highly specialized tissue engineering scaffolds*. Journal of Nanoscience and Nanotechnology, 2014. **14**(1): p. 522-534.
 42. Agarwal, S., J.H. Wendorff, and A. Greiner. *Progress in the field of electrospinning for tissue engineering applications*. Advanced Materials, 2009. **21**(32-33): p. 3343-3351.

7. References

43. Huang, C., X. Fu, J. Liu, Y. Qi, S. Li, and H. Wang. *The involvement of integrin beta1 signaling in the migration and myofibroblastic differentiation of skin fibroblasts on anisotropic collagen-containing nanofibers*. *Biomaterials*, 2012. **33**(6): p. 1791-1800.
44. Abrigo, M., S.L. McArthur, and P. Kingshott. *Electrospun Nanofibers as Dressings for Chronic Wound Care: Advances, Challenges, and Future Prospects*. *Macromolecular Bioscience*, 2014. **14**(6): p. 772-792.
45. Miguel, S.P., D. Simoes, A.F. Moreira, R.S. Sequeira, and I.J. Correia. *Production and characterization of electrospun silk fibroin based asymmetric membranes for wound dressing applications*. *International Journal of Biological Macromolecules*, 2018. **121**: p. 524-535.
46. Hutmacher, D.W. *Scaffolds in tissue engineering bone and cartilage*. *Biomaterials*, 2000. **21**(24): p. 2529-2543.
47. Matthews, J.A., E.D. Boland, G.E. Wnek, D.G. Simpson, and G.L. Bowlin. *Electrospinning of Collagen Type II: A Feasibility Study*. *Journal of Bioactive and Compatible Polymers*, 2003. **18**(2): p. 125-134.
48. Li, Z., P. Liu, T. Yang, Y. Sun, Q. You, J. Li, Z. Wang, and B. Han. *Composite poly(l-lactic-acid)/silk fibroin scaffold prepared by electrospinning promotes chondrogenesis for cartilage tissue engineering*. *Journal of Biomaterials Applications*, 2016. **30**(10): p. 1552-1565.
49. Kundu, B. and S.C. Kundu. *Osteogenesis of human stem cells in silk biomaterial for regenerative therapy*. *Progress in Polymer Science*, 2010. **35**(9): p. 1116-1127.
50. Costa-Pinto, A.R., R.L. Reis, and N.M. Neves. *Scaffolds based bone tissue engineering: the role of chitosan*. *Tissue Engineering. Part B, Reviews*, 2011. **17**(5): p. 331-347.
51. Sensini, A. and L. Cristofolini. *Biofabrication of Electrospun Scaffolds for the Regeneration of Tendons and Ligaments*. *Materials (Basel)*, 2018. **11**(10): p. 1-43.
52. Liu, C., Y. Huang, M. Pang, Y. Yang, S. Li, L. Liu, T. Shu, W. Zhou, X. Wang, L. Rong, and B. Liu. *Tissue-engineered regeneration of completely transected spinal cord using induced neural stem cells and gelatin-electrospun poly (lactide-co-glycolide)/polyethylene glycol scaffolds*. *PLoS One*, 2015. **10**(3): p. 1-19.
53. Ju, Y.M., H. Ahn, J. Arenas-Herrera, C. Kim, M. Abolbashari, A. Atala, J.J. Yoo, and S.J. Lee. *Electrospun vascular scaffold for cellularized small diameter blood vessels: A preclinical large animal study*. *Acta Biomaterialia*, 2017. **59**: p. 58-67.
54. Wei, G., C. Li, Q. Fu, Y. Xu, and H. Li. *Preparation of PCL/silk fibroin/collagen electrospun fiber for urethral reconstruction*. *International Urology and Nephrology*, 2015. **47**(1): p. 95-99.
55. Elzoghby, A.O. *Gelatin-based nanoparticles as drug and gene delivery systems: Reviewing three decades of research*. *Journal of Controlled Release*, 2013. **172**(3): p. 1075-1091.
56. Zhou, P., B. Yin, R. Zhang, Z. Xu, Y. Liu, Y. Yan, X. Zhang, S. Zhang, Y. Li, H. Liu, Y.A. Yuan, and S. Wei. *Molecular basis for RGD-containing peptides supporting adhesion and self-renewal of human pluripotent*

7. References

- stem cells on synthetic surface*. Colloids and Surfaces. B, Biointerfaces, 2018. **171**: p. 451-460.
57. Su, K. and C. Wang. *Recent advances in the use of gelatin in biomedical research*. Biotechnology Letters, 2015. **37**(11): p. 2139-2145.
58. Zhang, F., S. Xu, and Z. Wang. *Pre-treatment optimization and properties of gelatin from freshwater fish scales*. Food and Bioprocess Processing, 2011. **89**(3): p. 185-193.
59. Sahoo, N., R.K. Sahoo, N. Biswas, A. Guha, and K. Kuotsu. *Recent advancement of gelatin nanoparticles in drug and vaccine delivery*. International Journal of Biological Macromolecules, 2015. **81**: p. 317-331.
60. Farbod, K., M. Diba, T. Zinkevich, S. Schmidt, M.J. Harrington, A.P. Kentgens, and S.C. Leeuwenburgh. *Gelatin Nanoparticles with Enhanced Affinity for Calcium Phosphate*. Macromolecular Bioscience, 2016. **16**(5): p. 717-729.
61. Attarwala, H., V. Clausen, P. Chaturvedi, and M.M. Amiji. *Cosilencing Intestinal Transglutaminase-2 and Interleukin-15 Using Gelatin-Based Nanoparticles in an in Vitro Model of Celiac Disease*. Molecular Pharmaceutics, 2017. **14**(9): p. 3036-3044.
62. Pezzoli, D., E. Cauli, P. Chevallier, S. Fare, and D. Mantovani. *Biomimetic coating of cross-linked gelatin to improve mechanical and biological properties of electrospun PET: A promising approach for small caliber vascular graft applications*. Journal of Biomedical Materials Research. Part A, 2017. **105**(9): p. 2405-2415.
63. Prieto, E.M. and S.A. Guelcher. *5 - Tailoring properties of polymeric biomedical foams*, in Netti, P.A. (Ed.). *Biomedical Foams for Tissue Engineering Applications*, 2014, Woodhead Publishing (Sawston, Cambridge). p. 129-162.
64. Hong, Y. *19 - Electrospun fibrous polyurethane scaffolds in tissue engineering*, in Cooper, S.L. and J. Guan (Ed.). *Advances in Polyurethane Biomaterials*, 2016, Woodhead Publishing (Sawston, Cambridge). p. 543-559.
65. Jiang, Q., H. Xu, S. Cai, and Y. Yang. *Ultrafine fibrous gelatin scaffolds with deep cell infiltration mimicking 3D ECMs for soft tissue repair*. Journal of Materials Science. Materials in Medicine, 2014. **25**(7): p. 1789-1800.
66. Ozkizilcik, A. and K. Tuzlakoglu. *A new method for the production of gelatin microparticles for controlled protein release from porous polymeric scaffolds*. Journal of Tissue Engineering and Regenerative Medicine, 2014. **8**(3): p. 242-247.
67. Ren, K., Y. Wang, T. Sun, W. Yue, and H. Zhang. *Electrospun PCL/gelatin composite nanofiber structures for effective guided bone regeneration membranes*. Materials Science & Engineering. C, Materials for Biological Applications, 2017. **78**: p. 324-332.
68. Salifu, A.A., B.D. Nury, and C. Lekakou. *Electrospinning of nanocomposite fibrillar tubular and flat scaffolds with controlled fiber orientation*. Annals of Biomedical Engineering, 2011. **39**(10): p. 2510-2520.

7. References

69. Sajkiewicz, P. and D. Kolbuk. *Electrospinning of gelatin for tissue engineering--molecular conformation as one of the overlooked problems*. Journal of Biomaterials Science, Polymer Edition, 2014. **25**(18): p. 2009-2022.
70. Huang, Z.-M., Y.Z. Zhang, S. Ramakrishna, and C.T. Lim. *Electrospinning and mechanical characterization of gelatin nanofibers*. Polymer, 2004. **45**(15): p. 5361-5368.
71. Kwak, H.W., M. Shin, J.Y. Lee, H. Yun, D.W. Song, Y. Yang, B.S. Shin, Y.H. Park, and K.H. Lee. *Fabrication of an ultrafine fish gelatin nanofibrous web from an aqueous solution by electrospinning*. International Journal of Biological Macromolecules, 2017. **102**: p. 1092-1103.
72. Gonen, S.O., M. Erol Taygun, and S. Kucukbayrak. *Evaluation of the factors influencing the resultant diameter of the electrospun gelatin/sodium alginate nanofibers via Box-Behnken design*. Materials Science & Engineering. C, Materials for Biological Applications, 2016. **58**: p. 709-723.
73. Hennink, W.E. and C.F. van Nostrum. *Novel crosslinking methods to design hydrogels*. Advanced Drug Delivery Reviews, 2002. **54**(1): p. 13-36.
74. Sung, H.-W., D.-M. Huang, W.-H. Chang, R.-N. Huang, and J.-C. Hsu. *Evaluation of gelatin hydrogel crosslinked with various crosslinking agents as bioadhesives: In vitro study*. Journal of Biomedical Materials Research, 1999. **46**(4): p. 520-530.
75. Mo, X.M., C.Y. Xu, M. Kotaki, and S. Ramakrishna. *Electrospun P(LLA-CL) nanofiber: a biomimetic extracellular matrix for smooth muscle cell and endothelial cell proliferation*. Biomaterials, 2004. **25**(10): p. 1883-1890.
76. Reddy, N., R. Reddy, and Q. Jiang. *Crosslinking biopolymers for biomedical applications*. Trends in Biotechnology, 2015. **33**(6): p. 362-369.
77. Khorshidi, S., A. Solouk, H. Mirzadeh, S. Mazinani, J.M. Lagaron, S. Sharifi, and S. Ramakrishna. *A review of key challenges of electrospun scaffolds for tissue-engineering applications*. Journal of Tissue Engineering and Regenerative Medicine, 2016. **10**(9): p. 715-738.
78. Meng, L., O. Arnoult, M. Smith, and G.E. Wnek. *Electrospinning of in situ crosslinked collagen nanofibers*. Journal of Materials Chemistry, 2012. **22**(37): p. 19412-19417.
79. Umashankar, P.R., P.V. Mohanan, and T.V. Kumari. *Glutaraldehyde treatment elicits toxic response compared to decellularization in bovine pericardium*. Toxicology International, 2012. **19**(1): p. 51-58.
80. Lai, J.-Y. *Interrelationship between cross-linking structure, molecular stability, and cytocompatibility of amniotic membranes cross-linked with glutaraldehyde of varying concentrations*. RSC Advances, 2014. **4**(36): p. 18871-18880.
81. Gomes, S.R., G. Rodrigues, G.G. Martins, C.M.R. Henriques, and J.C. Silva. *In vitro evaluation of crosslinked electrospun fish gelatin scaffolds*. Materials Science and Engineering: C, 2013. **33**(3): p. 1219-1227.

7. References

82. Furuike, T., T. Chaochai, T. Okubo, T. Mori, and H. Tamura. *Fabrication of nonwoven fabrics consisting of gelatin nanofibers cross-linked by glutaraldehyde or N-acetyl-d-glucosamine by aqueous method*. International Journal of Biological Macromolecules, 2016. **93**: p. 1530-1538.
83. Kuijpers, A.J., G.H. Engbers, J. Krijgsveld, S.A. Zaat, J. Dankert, and J. Feijen. *Cross-linking and characterisation of gelatin matrices for biomedical applications*. Journal of Biomaterials Science. Polymer Edition, 2000. **11**(3): p. 225-243.
84. Zhang, Y.Z., J. Venugopal, Z.M. Huang, C.T. Lim, and S. Ramakrishna. *Crosslinking of the electrospun gelatin nanofibers*. Polymer, 2006. **47**(8): p. 2911-2917.
85. Sisson, K. *Evaluation of cross-linking methods for electrospun gelatin on cell growth and viability*. Biomacromolecules, 2009. **10**(7): p. 1675–1680.
86. Panzavolta, S., M. Gioffre, M.L. Focarete, C. Gualandi, L. Foroni, and A. Bigi. *Electrospun gelatin nanofibers: optimization of genipin cross-linking to preserve fiber morphology after exposure to water*. Acta Biomaterialia, 2011. **7**(4): p. 1702-1709.
87. Gualandi, C., P. Torricelli, S. Panzavolta, S. Pagani, M.L. Focarete, and A. Bigi. *An innovative co-axial system to electrospin in situ crosslinked gelatin nanofibers*. Biomedical Materials, 2016. **11**(2): p. 025007.
88. Kishan, A.P., R.M. Nezarati, C.M. Radzicki, A.L. Renfro, J.L. Robinson, M.E. Whitely, and E.M. Cosgriff-Hernandez. *In situ crosslinking of electrospun gelatin for improved fiber morphology retention and tunable degradation*. Journal of Materials Chemistry B, 2015. **3**(40): p. 7930-7938.
89. Kishan, A., T. Walker, N. Sears, T. Wilems, and E. Cosgriff-Hernandez. *Development of a bimodal, in situ crosslinking method to achieve multifactor release from electrospun gelatin*. Journal of Biomedical Materials Research. Part A, 2018. **106**(5): p. 1155-1164.
90. Tavassoli-Kafrani, E., S.A.H. Goli, and M. Fathi. *Fabrication and characterization of electrospun gelatin nanofibers crosslinked with oxidized phenolic compounds*. International Journal of Biological Macromolecules, 2017. **103**: p. 1062-1068.
91. Lin, W.H. and W.B. Tsai. *In situ UV-crosslinking gelatin electrospun fibers for tissue engineering applications*. Biofabrication, 2013. **5**(3): p. 035008.
92. Mollet, B.B., S. Spaans, P.G. Fard, N.A.M. Bax, C.V.C. Bouten, and P.Y.W. Dankers. *Mechanically Robust Electrospun Hydrogel Scaffolds Crosslinked via Supramolecular Interactions*. Macromolecular Bioscience, 2017. **17**(9): p. 1700053-1700061.
93. Harris, J.M. *Poly(Ethylene Glycol) Chemistry: Biotechnical and Biomedical Applications*. 2013. Springer (Berlin, Heidelberg). 385pp.
94. Groll, J., T. Ameringer, J.P. Spatz, and M. Moeller. *Ultrathin coatings from isocyanate-terminated star PEG prepolymers: layer formation and characterization*. Langmuir, 2005. **21**(5): p. 1991-1999.
95. Köhler, J., *Analyse der s-PEG-NCO (12kDa), Charge SSCHT-7*. 2017, DWI Leibniz-Institut für Interaktive Materialien. p. 1-2.

7. References

96. Götz, H., U. Beginn, C.F. Bartelink, H.J.M. Grünbauer, and M. Möller. *Preparation of Isophorone Diisocyanate Terminated Star Polyethers*. *Macromolecular Materials and Engineering*, 2002. **287**(4): p. 223-230.
97. Heyes, C.D., J. Groll, M. Moller, and G.U. Nienhaus. *Synthesis, patterning and applications of star-shaped poly(ethylene glycol) biofunctionalized surfaces*. *Molecular BioSystems*, 2007. **3**(6): p. 419-430.
98. Hildebrandt, H., O. Paloheimo, E. Mäntylä, S. Willman, S. Hakanen, K. Albrecht, J. Groll, M. Möller, and M. Vihinen-Ranta. *Reactive Self-Assembly and Specific Cellular Delivery of NCO-sP(EO-stat-PO)-Derived Nanogels*. *Macromolecular Bioscience*, 2018. **18**(10): p. 1800094.
99. Groll, J., J. Fiedler, E. Engelhard, T. Ameringer, S. Tugulu, H.A. Klok, R.E. Brenner, and M. Moeller. *A novel star PEG-derived surface coating for specific cell adhesion*. *Journal of Biomedical Materials Research Part A*, 2005. **74**(4): p. 607-617.
100. Hoffmann, J., J. Groll, J. Heuts, H. Rong, D. Klee, G. Ziemer, M. Moeller, and H.P. Wendel. *Blood cell and plasma protein repellent properties of star-PEG-modified surfaces*. *Journal of Biomaterials Science. Polymer Edition*, 2006. **17**(9): p. 985-996.
101. Ameringer, T., M. Hinz, C. Mourran, H. Seliger, J. Groll, and M. Moeller. *Ultrathin functional star PEG coatings for DNA microarrays*. *Biomacromolecules*, 2005. **6**(4): p. 1819-1823.
102. Groll, J., W. Haubensak, T. Ameringer, and M. Moeller. *Ultrathin coatings from isocyanate terminated star PEG prepolymers: patterning of proteins on the layers*. *Langmuir*, 2005. **21**(7): p. 3076-3083.
103. Gasteier, P., A. Reska, P. Schulte, J. Salber, A. Offenhausser, M. Moeller, and J. Groll. *Surface grafting of PEO-based star-shaped molecules for bioanalytical and biomedical applications*. *Macromolecular Bioscience*, 2007. **7**(8): p. 1010-1023.
104. Zalipsky, S. and J.M. Harris. *Introduction to Chemistry and Biological Applications of Poly(ethylene glycol)*, in Zalipsky, S. and J.M. Harris (Ed.). *Poly(ethylene glycol)*, 1997, American Chemical Society (Washington, D.C.). p. 1-13.
105. Sofia, S.J. and E.W. Merrill. *Grafting of PEO to polymer surfaces using electron beam irradiation*. *Journal of Biomedical Materials Research*, 1998. **40**(1): p. 153-163.
106. Szleifer, I. and M.A. Carignano. *Tethered polymer layers: phase transitions and reduction of protein adsorption*. *Macromolecular Rapid Communications*, 2000. **21**(8): p. 423-448.
107. Groll, J., E.V. Amirgoulova, T. Ameringer, C.D. Heyes, C. Röcker, G.U. Nienhaus, and M. Möller. *Biofunctionalized, Ultrathin Coatings of Cross-Linked Star-Shaped Poly(ethylene oxide) Allow Reversible Folding of Immobilized Proteins*. *Journal of the American Chemical Society*, 2004. **126**(13): p. 4234-4239.
108. Groll, J., Z. Ademovic, T. Ameringer, D. Klee, and M. Moeller. *Comparison of coatings from reactive star shaped PEG-stat-PPG prepolymers and grafted linear PEG for biological and medical applications*. *Biomacromolecules*, 2005. **6**(2): p. 956-962.

7. References

109. Groll, J. and M. Moeller. *Star Polymer Surface Passivation for Single-Molecule Detection*, in Walter, N.G. (Ed.). *Methods in Enzymology*, 2010, Academic Press (Cambridge, MA). p. 1-18.
110. Grafahrend, D., J.L. Calvet, K. Klinkhammer, J. Salber, P.D. Dalton, M. Moller, and D. Klee. *Control of protein adsorption on functionalized electrospun fibers*. *Biotechnology and Bioengineering*, 2008. **101**(3): p. 609-621.
111. Dalton, P.D., C. Hostert, K. Albrecht, M. Moeller, and J. Groll. *Structure and properties of urea-crosslinked star poly[(ethylene oxide)-ran-(propylene oxide)] hydrogels*. *Macromolecular Bioscience*, 2008. **8**(10): p. 923-931.
112. Schamel, M., J. Groll, and U. Gbureck. *Simultaneous formation and mineralization of star-P(EO-stat-PO) hydrogels*. *Materials Science & Engineering C, Materials for Biological Applications*, 2017. **75**: p. 471-477.
113. Fiedler, J., J. Groll, E. Engelhardt, P. Gasteier, C. Dahmen, H. Kessler, M. Moeller, and R.E. Brenner. *NCO-sP(EO-stat-PO) surface coatings preserve biochemical properties of RGD peptides*. *International Journal of Molecular Medicine*, 2011. **27**(1): p. 139-145.
114. Bohm, G., Y. Ushakova, H.P. Alizai, T. Braunschweig, C. Lente, K.H. Heffels, J. Groll, U.P. Neumann, and K. Junge. *Biocompatibility of PLGA/sP(EO-stat-PO)-coated mesh surfaces under constant shearing stress*. *European Surgical Research.*, 2011. **47**(3): p. 118-129.
115. Rossi, A., L. Wistlich, K.H. Heffels, H. Walles, and J. Groll. *Isotropic Versus Bipolar Functionalized Biomimetic Artificial Basement Membranes and Their Evaluation in Long-Term Human Cell Co-Culture*. *Advanced Healthcare Materials*, 2016. **5**(15): p. 1939-1948.
116. Wistlich, L., J. Kums, A. Rossi, K.H. Heffels, H. Wajant, and J. Groll. *Multimodal Bioactivation of Hydrophilic Electrospun Nanofibers Enables Simultaneous Tuning of Cell Adhesivity and Immunomodulatory Effects*. *Advanced Functional Materials*, 2017. **27**(46): p. 1702903.
117. Hersel, U., C. Dahmen, and H. Kessler. *RGD modified polymers: biomaterials for stimulated cell adhesion and beyond*. *Biomaterials*, 2003. **24**(24): p. 4385-4415.
118. Beer, M.V., C. Rech, P. Gasteier, B. Sauerzapfe, J. Salber, A. Ewald, M. Möller, L. Elling, and J. Groll. *The Next Step in Biomimetic Material Design: Poly-LacNAc-Mediated Reversible Exposure of Extra Cellular Matrix Components*. *Advanced Healthcare Materials*, 2013. **2**(2): p. 306-311.
119. Beer, M.V., K. Hahn, S. Diederichs, M. Fabry, S. Singh, S.J. Spencer, J. Salber, M. Moller, A.G. Shard, and J. Groll. *Quantifying ligand-cell interactions and determination of the surface concentrations of ligands on hydrogel films: The measurement challenge*. *Biointerphases*, 2015. **10**(2): p. 021007.
120. Lin, C.-C. and K.S. Anseth. *PEG Hydrogels for the Controlled Release of Biomolecules in Regenerative Medicine*. *Pharmaceutical Research*, 2009. **26**(3): p. 631-643.

7. References

121. Neuerburg, C., S. Recknagel, J. Fiedler, J. Groll, M. Moeller, K. Bruellhoff, H. Reichel, A. Ignatius, and R.E. Brenner. *Ultrathin sP(EO-stat-PO) hydrogel coatings are biocompatible and preserve functionality of surface bound growth factors in vivo*. Journal of Materials Science. Materials in Medicine, 2013. **24**(10): p. 2417-2427.
122. Dhanasingh, A., J. Salber, M. Moeller, and J. Groll. *Tailored hyaluronic acid hydrogels through hydrophilic prepolymer cross-linkers*. Soft Matter, 2010. **6**(3): p. 618-629.
123. Dhanasingh, A. and J. Groll. *Polysaccharide based covalently linked multi-membrane hydrogels*. Soft Matter, 2012. **8**(5): p. 1643-1647.
124. Schulte, V.A., K. Hahn, A. Dhanasingh, K.H. Heffels, and J. Groll. *Hydrogel-fibre composites with independent control over cell adhesion to gel and fibres as an integral approach towards a biomimetic artificial ECM*. Biofabrication, 2014. **6**(2): p. 024106.
125. Goldstein, J. *Scanning electron microscopy and x-ray microanalysis* 2018. Springer (Heidelberg, Berlin). 550pp.
126. Schindelin, J., I. Arganda-Carreras, and E. Frise. *Fiji: an open-source platform for biological-image analysis*. Nature Methods, 2012. **9**(7): p. 676-682.
127. Hotaling, N.A., K. Bharti, H. Kriel, and C.G. Simon Jr. *DiameterJ: A validated open source nanofiber diameter measurement tool*. Biomaterials, 2015. **61**: p. 327-338.
128. Zeeh, B. *Infrarot- und Ramanspektren*, in Hesse, M., H. Meier, and B. Zeeh (Ed.). *Spektroskopische Methoden in der organischen Chemie*, 2005, Thieme (Stuttgart). p. 33-73.
129. Glassford, S.E., B. Byrne, and S.G. Kazarian. *Recent applications of ATR FTIR spectroscopy and imaging to proteins*. Biochim Biophys Acta, 2013. **1834**(12): p. 2849-2858.
130. Merly, L. and S.L. Smith. *Murine RAW 264.7 cell line as an immune target: are we missing something?* Immunopharmacology and Immunotoxicology, 2017. **39**(2): p. 55-58.
131. Topuz, F. and T. Uyar. *Electrospinning of gelatin with tunable fiber morphology from round to flat/ribbon*. Materials Science & Engineering C, Materials for Biological Applications, 2017. **80**: p. 371-378.
132. Klinkhammer, K., J. Bockelmann, C. Simitzis, G.A. Brook, D. Grafahrend, J. Groll, M. Moller, J. Mey, and D. Klee. *Functionalization of electrospun fibers of poly(epsilon-caprolactone) with star shaped NCO-poly(ethylene glycol)-stat-poly(propylene glycol) for neuronal cell guidance*. Journal of Materials Science. Materials in Medicine, 2010. **21**(9): p. 2637-2651.
133. Liu, H., E.B. Slamovich, and T.J. Webster. *Less harmful acidic degradation of poly(lactico-glycolic acid) bone tissue engineering scaffolds through titania nanoparticle addition*. International Journal of Nanomedicine, 2006. **1**(4): p. 541-545.
134. BaoLin, G. and P.X. Ma. *Synthetic biodegradable functional polymers for tissue engineering: a brief review*. Science China. Chemistry, 2014. **57**(4): p. 490-500.

7. References

135. Young, S., M. Wong, Y. Tabata, and A.G. Mikos. *Gelatin as a delivery vehicle for the controlled release of bioactive molecules*. Journal of Controlled Release, 2005. **109**(1-3): p. 256-274.
136. Choktaweessap, N., K. Arayanarakul, D. Aht-ong, C. Meechaisue, and P. Supaphol. *Electrospun Gelatin Fibers: Effect of Solvent System on Morphology and Fiber Diameters*. Polymer Journal, 2007. **39**: p. 622-631.
137. Li, J., A. He, J. Zheng, and C.C. Han. *Gelatin and gelatin-hyaluronic acid nanofibrous membranes produced by electrospinning of their aqueous solutions*. Biomacromolecules, 2006. **7**(7): p. 2243-2247.
138. Okutan, N., P. Terzi, and F. Altay. *Affecting parameters on electrospinning process and characterization of electrospun gelatin nanofibers*. Food Hydrocolloids, 2014. **39**: p. 19-26.
139. Yang, D., Y. Li, and J. Nie. *Preparation of gelatin/PVA nanofibers and their potential application in controlled release of drugs*. Carbohydrate Polymers, 2007. **69**(3): p. 538-543.
140. Hoveizi, E., M. Nabiuni, K. Parivar, S. Rajabi-Zeleti, and S. Tavakol. *Functionalisation and surface modification of electrospun polylactic acid scaffold for tissue engineering*. Cell Biology International, 2014. **38**(1): p. 41-49.
141. Liu, Y., L. Deng, C. Zhang, F. Feng, and H. Zhang. *Tunable Physical Properties of Ethylcellulose/Gelatin Composite Nanofibers by Electrospinning*. Journal of Agricultural and Food Chemistry, 2018. **66**(8): p. 1907-1915.
142. Marcolin, C. *Electrospinning of biopolymers for regenerative medicine*. Dipartimento di Chimica, Materiali e Ingegneria Chimica "G. Natta". 2009. Milan. 191pp.
143. Hudecki, A., J. Gola, S. Ghavami, M. Skonieczna, J. Markowski, W. Likus, M. Lewandowska, W. Maziarz, and M.J. Los. *Structure and properties of slow-resorbing nanofibers obtained by (co-axial) electrospinning as tissue scaffolds in regenerative medicine*. PeerJ, 2017. **5**: p. 1-27.
144. Hirota, N., K. Mizuno, and Y. Goto. *Cooperative alpha-helix formation of beta-lactoglobulin and melittin induced by hexafluoroisopropanol*. Protein Science, 1997. **6**(2): p. 416-421.
145. Lu, Q., X. Zhang, X. Hu, and D.L. Kaplan. *Green process to prepare silk fibroin/gelatin biomaterial scaffolds*. Macromolecular Bioscience, 2010. **10**(3): p. 289-298.
146. Grey, C.P., S.T. Newton, G.L. Bowlin, T.W. Haas, and D.G. Simpson. *Gradient fiber electrospinning of layered scaffolds using controlled transitions in fiber diameter*. Biomaterials, 2013. **34**(21): p. 4993-5006.
147. Reneker, D.H., A.L. Yarin, H. Fong, and S. Koombhongse. *Bending instability of electrically charged liquid jets of polymer solutions in electrospinning*. Journal of Applied Physics, 2000. **87**(9): p. 4531-4547.
148. Wang, C., Y.-W. Cheng, C.-H. Hsu, H.-S. Chien, and S.-Y. Tsou. *How to manipulate the electrospinning jet with controlled properties to obtain uniform fibers with the smallest diameter?—a brief discussion of solution electrospinning process*. Journal of Polymer Research, 2011. **18**(1): p. 111-123.

7. References

149. Carletti, E., A. Motta, and C. Migliaresi. *Scaffolds for tissue engineering and 3D cell culture*. *Methods in Molecular Biology*, 2011. **695**: p. 17-39.
150. Heydarkhan-Hagvall, S., K. Schenke-Layland, A.P. Dhanasopon, F. Rofail, H. Smith, B.M. Wu, R. Shemin, R.E. Beygui, and W.R. MacLellan. *Three-dimensional electrospun ECM-based hybrid scaffolds for cardiovascular tissue engineering*. *Biomaterials*, 2008. **29**(19): p. 2907-2914.
151. Zhang, Y., H. Ouyang, C.T. Lim, S. Ramakrishna, and Z.M. Huang. *Electrospinning of gelatin fibers and gelatin/PCL composite fibrous scaffolds*. *Journal of Biomedical Materials Research. Part B, Applied Biomaterials*, 2005. **72**(1): p. 156-165.
152. Thomas, V., X. Zhang, S.A. Catledge, and Y.K. Vohra. *Functionally graded electrospun scaffolds with tunable mechanical properties for vascular tissue regeneration*. *Biomedical Materials* 2007. **2**(4): p. 224-232.
153. Jaiswal, D., R. James, N.B. Shelke, M.D. Harmon, J.L. Brown, F. Hussain, and S.G. Kumbar. *Gelatin Nanofiber Matrices Derived from Schiff Base Derivative for Tissue Engineering Applications*. *Journal of Biomedical Nanotechnology*, 2015. **11**(11): p. 2067-2080.
154. Torricelli, P., M. Gioffre, A. Fiorani, S. Panzavolta, C. Gualandi, M. Fini, M.L. Focarete, and A. Bigi. *Co-electrospun gelatin-poly(L-lactic acid) scaffolds: modulation of mechanical properties and chondrocyte response as a function of composition*. *Materials Science & Engineering. C, Materials for Biological Applications*, 2014. **36**: p. 130-138.
155. Croisier, F., A.S. Duwez, C. Jerome, A.F. Leonard, K.O. van der Werf, P.J. Dijkstra, and M.L. Bennink. *Mechanical testing of electrospun PCL fibers*. *Acta Biomaterialia*, 2012. **8**(1): p. 218-224.
156. Baker, S.R., S. Banerjee, K. Bonin, and M. Guthold. *Determining the mechanical properties of electrospun poly- ϵ -caprolactone (PCL) nanofibers using AFM and a novel fiber anchoring technique*. *Materials Science and Engineering: C*, 2016. **59**: p. 203-212.
157. Yao, R., J. He, G. Meng, B. Jiang, and F. Wu. *Electrospun PCL/Gelatin composite fibrous scaffolds: mechanical properties and cellular responses*. *Journal of Biomaterials Science. Polymer Edition*, 2016. **27**(9): p. 824-838.
158. Vatankhah, E., D. Semnani, M.P. Prabhakaran, M. Tadayon, S. Razavi, and S. Ramakrishna. *Artificial neural network for modeling the elastic modulus of electrospun polycaprolactone/gelatin scaffolds*. *Acta Biomaterialia*, 2014. **10**(2): p. 709-721.
159. Soradech, S., J. Nunthanid, S. Limmatvapirat, and M. Luangtana-Anan. *An approach for the enhancement of the mechanical properties and film coating efficiency of shellac by the formation of composite films based on shellac and gelatin*. *Journal of Food Engineering*, 2012. **108**(1): p. 94-102.
160. Yu, X., A.H. Biedrzycki, A.S. Khalil, D. Hess, J.M. Umhoefer, M.D. Markel, and W.L. Murphy. *Nanostructured Mineral Coatings Stabilize Proteins for Therapeutic Delivery*. *Advanced Materials*, 2017. **29**(33): p. 1701255.

7. References

161. Heinemann, C., S. Heinemann, B. Kruppke, H. Worch, J. Thomas, H.P. Wiesmann, and T. Hanke. *Electric field-assisted formation of organically modified hydroxyapatite (ormoHAP) spheres in carboxymethylated gelatin gels*. *Acta Biomaterialia*, 2016. **44**: p. 135-143.
162. Haris, P.I. and F. Severcan. *FTIR spectroscopic characterization of protein structure in aqueous and non-aqueous media*. *Journal of Molecular Catalysis B: Enzymatic*, 1999. **7**(1): p. 207-221.
163. Cebi, N., M.Z. Durak, O.S. Toker, O. Sagdic, and M. Arici. *An evaluation of Fourier transforms infrared spectroscopy method for the classification and discrimination of bovine, porcine and fish gelatins*. *Food Chemistry*, 2016. **190**: p. 1109-1115.
164. Li, Y., X. Li, R. Zhao, C. Wang, F. Qiu, B. Sun, H. Ji, J. Qiu, and C. Wang. *Enhanced adhesion and proliferation of human umbilical vein endothelial cells on conductive PANI-PCL fiber scaffold by electrical stimulation*. *Materials Science & Engineering. C, Materials for Biological Applications*, 2017. **72**: p. 106-112.
165. Kai, D., G. Jin, M.P. Prabhakaran, and S. Ramakrishna. *Electrospun synthetic and natural nanofibers for regenerative medicine and stem cells*. *Biotechnology Journal*, 2013. **8**(1): p. 59-72.
166. Hu, J., D. Kai, H. Ye, L. Tian, X. Ding, S. Ramakrishna, and X.J. Loh. *Electrospinning of poly(glycerol sebacate)-based nanofibers for nerve tissue engineering*. *Materials Science & Engineering. C, Materials for Biological Applications*, 2017. **70**(Pt 2): p. 1089-1094.
167. Liu, T.L. and C.J. Kim. *Repellent surfaces. Turning a surface superrepellent even to completely wetting liquids*. *Science*, 2014. **346**(6213): p. 1096-1100.
168. Sang, Q., H. Li, G. Williams, H. Wu, and L.M. Zhu. *Core-shell poly(lactide-co-epsilon-caprolactone)-gelatin fiber scaffolds as pH-sensitive drug delivery systems*. *Journal of Biomaterials Applications*, 2018. **32**(8): p. 1105-1118.
169. Nadim, A., S.N. Khorasani, M. Kharaziha, and S.M. Davoodi. *Design and characterization of dexamethasone-loaded poly (glycerol sebacate)-poly caprolactone/gelatin scaffold by coaxial electro spinning for soft tissue engineering*. *Materials Science & Engineering. C, Materials for Biological Applications*, 2017. **78**: p. 47-58.
170. Ko, C.H., M.Y. Shie, J.H. Lin, Y.W. Chen, C.H. Yao, and Y.S. Chen. *Biodegradable Bisvinyl Sulfonemethyl-crosslinked Gelatin Conduit Promotes Regeneration after Peripheral Nerve Injury in Adult Rats*. *Scientific Reports*, 2017. **7**(1): p. 17489.
171. McWhorter, F.Y., T. Wang, P. Nguyen, T. Chung, and W.F. Liu. *Modulation of macrophage phenotype by cell shape*. *Proceedings of the National Academy of Sciences of the United States of America*, 2013. **110**(43): p. 17253.
172. Lin, W.H., J. Yu, G. Chen, and W.B. Tsai. *Fabrication of multi-biofunctional gelatin-based electrospun fibrous scaffolds for enhancement of osteogenesis of mesenchymal stem cells*. *Colloids and Surfaces. B, Biointerfaces*, 2016. **138**: p. 26-31.

7. References

173. Zhang, X., K. Tang, and X. Zheng. *Electrospinning and Crosslinking of COL/PVA Nanofiber-microsphere Containing Salicylic Acid for Drug Delivery*. Journal of Bionic Engineering, 2016. **13**(1): p. 143-149.
174. Tan, Z., H. Wang, X. Gao, T. Liu, and Y. Tan. *Composite vascular grafts with high cell infiltration by co-electrospinning*. Materials Science & Engineering. C, Materials for Biological Applications, 2016. **67**: p. 369-377.

8. Appendix

Table 1: EDX quantified element contents in pure gelatin and NCO-sP(EO-stat-PO).

Sample	Element	Content [% (w/w)]
Pure gelatin	C	67.2
	O	13.6
	N	19.2
Pure NCO-sP(EO-stat-PO)	C	76.9
	O	23.1
	N	0.0

Table 2: EDX measured element contents of different ratios of NCO-sP(EO-stat-PO) crosslinked meshes in % (w/w) before and after water incubation. Results are displayed for all measured batches.

NCO-sP(EO-stat-PO) : Gt = 3 : 2				NCO-sP(EO-stat-PO) : Gt = 1 : 1			
Batch	Element	Before	After	Batch	Element	Before	After
1	C	75,4	73,0	1	C	74,5	73,8
	O	18,0	19,2		O	16,1	16,9
	N	6,5	7,7		N	9,3	9,3
2	C	74,2	70,0	2	C	73,0	71,3
	O	18,8	21,8		O	17,2	17,4
	N	7,0	8,2		N	9,8	11,2
3	C	77,3	71,3	3	C	74,8	70,8
	O	14,8	21,0		O	15,1	17,4
	N	8,0	7,4		N	10,1	11,8

NCO-sP(EO-stat-PO) : Gt = 1:3			
Batch	Element	Before	After
1	C	72,5	70,3
	O	15,9	17,9
	N	11,7	11,8
2	C	70,6	65,3
	O	15,0	19,5
	N	14,3	15,3

Danksagung

Ich danke vielmals Herrn Prof. Dr. Groll für die Möglichkeit der Promotion an seinem Lehrstuhl sowie für die Übernahme des Referats.

Ebenso bedanke ich mich bei Herrn Prof. Dr. Dr. Kübler für die Übernahme des Korreferats.

Meinem Betreuer Dr. Berat Taşkin gilt mein besonderer Dank für die Bereitstellung des Themas, die hervorragende Einführung und Betreuung im Labor und seine kontinuierliche Hilfsbereitschaft und Unterstützung.

Vielen herzlichen Dank auch an Herrn Prof. Dr. Uwe Gbureck, der immer ein offenes Ohr für Fragen und Probleme hatte und viele gute Ratschläge.

Unverzichtbar waren Philipp Stahlhut und Judith Friedlein. Meinen allergrößten Dank für zahllose REM Aufnahmen und EDX Messungen, Eure unglaubliche Geduld, viele hilfreiche Tipps und gute Gespräche!

Ganz besonders danken möchte ich auch Carina Blum für ihre unkomplizierte Hilfsbereitschaft in allen Belangen.

Zum Gelingen der Arbeit haben mit Rat, Tat und unterhaltsamen Mittagspausen außerdem beigetragen: Manuel Roesener, Jan Weichhold, Willi Smolan, Isabell Biermann, Michaela Rödel, Ilona Paulus, Junwen Shan, Annika Seifert, Franziska Weigl, Jessica Brand, Viktoria Sokolowski, Florian Pinzner, Ib Holzmeister, Leo Förster, Johanna Lutz, Johannes Herbig und Christoph Böhm. Ein riesengroßes Dankeschön an Euch alle für die großartige Zeit am FMZ!!

Mein großer Dank gebührt auch allen Mitarbeitern der Biologieabteilung, insbesondere Simone Werner, Dr. Andrea Ewald und Dr. Tatjana Schilling für spontane Ratschläge ebenso wie die umfassende Unterstützung in der Zellkultur.

Zuletzt gilt mein größter Dank meiner Familie und Daniel, meinem Fels in der Brandung, die zu jeder Zeit für mich da waren und mich immer auf jegliche Art unterstützt haben. Ihr Lieben, DANKE für alles!

Lebenslauf

Persönliche Daten

Name: Christina Maria Wiesbeck

[REDACTED]

[REDACTED]

[REDACTED]

[REDACTED]

Staatsangehörigkeit: deutsch

Schulbildung und Studium

seit 02/2019	Vorbereitungsassistentin in zahnärztlicher Praxis
02/2018 – 12/2018	Promotionsbezogenes Projekt am Lehrstuhl für Funktionswerkstoffe der Medizin und der Zahnheilkunde (Universitätsklinikum Würzburg)
11/2017	Staatsexamen Zahnmedizin Approbation als Zahnärztin
2012 – 2017	Studium der Zahnmedizin (Universität Würzburg)
2003 – 2012	Doppelstudium der Geographie/Anglistik für Lehramt an Gymnasien und der Geographie, Mineralogie und Statistik (Universität Würzburg) Abschluss: Diplom-Geographin Univ.
07/2002	Allgemeine Hochschulreife (Augustinus Gymnasium Weiden i.d.Opf)

Würzburg, Februar 2019